Cleaning Process in High Density Plasma Chemical Vapor Deposition Reactor

A Thesis

Submitted to the Faculty

of

Drexel University

by

Kamilla Iskenderova

in partial fulfillment of the

requirements for the degree

of

Doctor of Philosophy

October 2003

ACKNOWLEGMENTS

First, I would like to express my profound gratitude to both my advisor Dr. Alexander Fridman and co-advisor Dr. Alexander Gutsol, whose constant support and valuable suggestions have been the principal force behind my work. For their expertise in plasma physics and plasma chemistry and their invaluable guidance and assistance to me in the research projects. They have expanded my understanding of plasma physics tremendously. I am thankful to all my committee members and other professors who thought me during my graduate study. Thanks must also go to all my fellow group mates, past and present.

Also, this work would not have been possible without the endless help and inspiration of my dearest husband Alexandre Chirokov who is also my group mate.

I am most indebted to my parents, friends and relatives for their constant support and encouragement throughout the course of my education.

TABLE OF CONTENTS

LIST OF TABLES v

LIST OF FIGURES vi

ABSTRACT viii

CHAPTER 1: INTRODUCTION 1

- 1.1 CVD in electronic application 1
- 1.2 In Situ Plasma Cleaning 2
- 1.3 Remote Cleaning Technology 4
- 1.4 Choice of the Cleaning Gas 5

CHAPTER 2: PLASMA-CHEMISTRY MODELING IN THE REMOTE PLASMA SOURCE 7

- 2.1 Introduction 7
- 2.2 Plasma Kinetic Model 8
- 2.3 Simulations and Results 11
- 2.4 Conclusions 20

CHAPTER 3: FLUORINE RADICALS RECOMBINATION IN A TRANSPORT TUBE 21

- 3.1 Introduction 21
- 3.2 Surface Kinetic Model 22
  - 3.2.1 Langmuir-Rideal Mechanism 22
  - 3.2.2 Rate Equation Components 23
  - 3.2.3 Sticking Coefficients 27
- 3.3 Volume Kinetic Model 36

3.4 Simulation Results 37

3.5 Discussion and Conclusions 44

CHAPTER 4: CLEANING OPTIMIZATION PROCESS IN HIGH DENSITY PLASMA CVD CHAMBER 46

4.1 Introduction 46

4.2 Modeling Plasma Chemistry for Microelectronics Manufacturing 48

4.3 HDP-CVD Reactor Model 52

4.3.1 Continuum Approach 53

4.3.2 Plasma Chemistry Module 56

4.4 Inductively Coupled Plasma 62

4.5 Capacitively Coupled Plasma 63

4.6 Estimation of Power Consumption 65

4.7 Estimation of Plasma Volume 68

4.8 Results and Discussion 69

CHAPTER 5: SUMMARY AND CONCLUSIONS 89

5.1 Conclusions 89

5.2 Recommendations for Future Work 90

LIST OF REFERENCES 92

APPENDIX A: PLASMA CHEMISTRY REACTIONS OF $NF_3/CF_4/C_2F_6$ 96

APPENDIX B: COMPUTATIONAL CODE FOR CHEMISTRY MODELING IN A TRANSPORT TUBE 101

APPENDIX C: COMPUTATIONAL CODE FOR HDP-CVD MODELING 107

VITA 109

LIST OF TABLES

1. Lifetime and global warming potential ... 6
2. Comparison of nitrogen-fluorine and carbon-fluorine bond strength for common PFC gases ... 6
3. F-yield in discharge with different parent molecules. ... 19
4. Computational parameters involved in surface kinetics. ... 38
5. Data requirements for different plasma modeling approaches. ... 50
6. Data from NIST database. Thermal dissociation of fluorine. ... 60
7. Three-body recombination reaction rate constants. ... 60
8. Inductively coupled plasma parameters. ... 63
9. Capacitively coupled plasma parameters. ... 65
10. Energy losses of the electron and corresponding rate coefficients in the fluorine gas ... 66
11. Intermediate film thickness for corresponding zone ... 70
12. Average etch rate and corresponding etch time for each zone. Side ICP only. ... 73
13. Average etch rate and corresponding etch time for each zone. Upper ICP only. ... 76
14. Average etch rate and corresponding etch time for each zone. Side and Upper ICPs. ... 78
15. Average etch rate and corresponding etch time for each zone. CCP discharge only. ... 82
16. STEP 1: both side and upper ICPs are turned on for 7 s ... 84
17. STEP 2: only CCP discharge is turned on for 30 s. ... 84
18. Etch gas utilization of C_2F_6, C_3F_8 and NF_3 during chamber cleaning. ... 86
19. Comparison of process and other factors for the various clean gases (highlighting potential advantages and concerns) ... 88

LIST OF FIGURES

1. Numerical simulation of NF_3 dissociation in discharge. Time dependence of the main species concentration. Initial Mixture: Ar=67%, N_2=0.4%, NF_3=35%. ... 12

2. Numerical simulation of NF_3/SiF_4 dissociation in discharge. Time dependence of the main species concentration. Initial Mixture: Ar=67%, N_2=3.9%, NF_3=24%, SiF_4=5.8%. ... 13

3. Numerical simulation of NF_3/O_2 dissociation in discharge. Time dependence of the main species concentration. Initial Mixture: Ar=67%, N_2=3%, NF_3=20%, O_2=5.3% ... 14

4. Numerical simulation of CF_4/O_2 dissociation. Time dependence of the main species concentration. Initial Mixture: Ar=67%, N_2=0.4%, O_2=4.2%, CF_4=28.3%. ... 15

5. Numerical simulation of C_2F_6/O_2 dissociation. Time dependence of the main species concentration. Initial Mixture: Ar=67%, N_2=0.4%, O_2=4.2%, C_2F_6=28.3%. ... 16

6. Demonstration of the Langmuir-Rideal heterogeneous mechanism. ... 23

7. Gas-wall collision model. ... 34

8. Initial sticking coefficient for F on Ni as a function of temperature. The curves show computed values for physical and chemical bonding. ... 35

9. Initial sticking coefficient for F_2 on Ni as a function of temperature. The curves show computed values for physical and chemical bonding. ... 35

10. Initial sticking coefficient for Ar on Ni as a function of temperature (physical bonding only). ... 36

11. Transport Tube. Computational Geometry. ... 38

12. Adsorption rate of atomic fluorine in transport tube length. The curves show computed values for three different pressures: 3, 5 and 8 Torr. ... 39

13. Mole fractions of F atoms in transport tube length. The curves show computed values for three different pressures: 3, 5 and 8 Torr. ... 40

14. Mole fractions of F_2 molecules in transport tube length. The curves show computed values for three different pressures: 3, 5 and 8 Torr. ... 40

15. The dependence of function *f* on a pressure. Simulated results for three pressures: 3, 5 and 8 Torr. Critical pressure is 4.5 Torr....................................... 42

16. F-atoms concentration after the transport zone as a function of pressure............. 43

17. Fluorine atom percentage versus pressure for different wall materials. A plot of percentage of total F atoms in plasma found as molecular F_2 vs. total pressure for different wall materials as indicated in the figure............................ 45

18. Schematic of HDP-CVD reactor.. 53

19. Velocity vectors in HDP-CVD reactor. 67

20. Zone numbering in HDP-CVD reactor. 70

21. Contours of static temperature, K. Side ICP only.. 74

22. Contours of mole fraction of F atoms. Side ICP only. 74

23. Contours of etch rate. Side ICP only. 75

24. Contours of mole fraction of F atoms. Upper ICP only....................................... 76

25. Contours of etch rate, kA/min. Upper ICP only. 77

26. Contours of temperature, K. Side and Upper ICPs.. 78

27. Contours of mole fraction of F atoms. Side and Upper ICPs. 79

28. Contours of etch rate, kA/min. Side and Upper ICPs.. 79

29. The dependence of average F-atoms concentration vs. residence time............... 81

30. Contours of mole fraction of F atoms. CCP discharge only................................ 82

31. Contours of etch rate, kA/min. CCP discharge only.. 83

32. The dependence of operating pressure and NF_3 flow rate on cleaning time (Air Products and Chemicals Inc.).. 85

33. Comparison of cleaning time for different cleaning gases (relative to standard C_3F_8 process = 1.0)... 87

ABSTRACT

Cleaning Process in High Density Plasma Chemical Vapor Deposition

Kamilla Iskenderova
Alexander Fridman, PhD.

One of the major emitters of perfluorocompounds (PFCs) in semiconductor manufacturing is the *in situ* plasma cleaning procedure performed after the chemical vapor deposition of dielectric thin films. The release of these man-made gases can contribute to the greenhouse effect. To reduce emissions of PFCs, it has developed a new plasma cleaning technology that uses a remote plasma source (RPS) to completely break down fluorine-containing gases into an effective cleaning chemical.

The downstream plasma reactor consists of a plasma source, where the inductive discharge occurs; a transport region, which connects the source to the chamber; and the actual chemical vapor deposition chamber, where the fluorine radicals react with the deposition residues to form non-global-warming volatile byproducts that are pumped through the exhaust. From environmental point of view the overall method has clear benefits, however, with the new technology several new optimization problems arise.

In recent years, semiconductor equipment manufacturers have put in a great effort to improve the production worthiness and the overall effectiveness of the tools. Equipment qualification procedures can be quite expensive and lengthy. The film deposition process stability is of great importance since it can be correlated to the final integrated circuit quality and yield. The chamber cleaning process can affect the stability of the film properties.

The objective of this work is to concern the main aspects of the problems that prevent the remote clean process for achieving both superior chamber cleaning performance and improved environmental friendliness.

In order to meet these significant technical challenges we have developed detailed numerical models of the systems involved in the downstream cleaning process. For the remote plasma source, the detailed plasma-kinetic model has been developed to describe the atomic fluorine production from NF_3, CF_4, and C_2F_6 and provided comparison of the effectiveness in decomposition of these parent molecules. In the transport tube the homogeneous and heterogeneous kinetic model was developed to analyze the recombination mechanism of atomic fluorine. To study the optimization process of gas and power consumption in the processing chamber, the numerical 2D modeling of complex plasma-chemical processes was performed.

CHAPTER 1: INTRODUCTION

1.1 CVD in electronic application

Chemical vapor deposition (CVD) is a widely used method for depositing thin films of a variety of materials. Applications of CVD range from the fabrication of microelectronic devices to the deposition of protective coatings. With CVD, it is possible to place a layer of most metals, many nonmetallic elements such as carbon and silicon, as well as, a large number of compounds including carbides, nitrides, oxides, intermetallics, and many others. This technology is now an essential factor in the manufacture of semiconductors and other electronic components, in the coating of tools, bearings, and other wearresistant parts and in many optical, optoelectronic and corrosion applications. Chemical vapor deposition may be defined as the deposition of a solid on a heated surface from a chemical reaction in the vapor phase. It belongs to the class of vapor-transfer processes which is atomistic in nature, that is the deposition species are atoms or molecules or a combination of these. Beside CVD, they include various physical-vapor deposition processes (PVD) such as evaporation, sputtering, molecular beam epitaxy, and ion plating.

A major development in semiconductor technology occurred in 1959 when several components were placed on a single chip for the first time at Texas Instruments, inaugurating the era of integrated circuits (IC’s) [1]. Since then, the number of components has increased to the point where, in the new ultra-large-scale-integration designs (ULSI), more than a million components can be put on a single chip. This has

been accompanied by a considerable increase in efficiency and reliability and a better understanding of the related physical and chemical phenomena. The result of these developments was a drastic price reduction in all aspects of solid-state circuitry. The cost per unit of information (bit) has dropped by an estimated three orders of magnitude in the last twenty years. Obviously, this dramatic progress has led to a considerable increase in the complexity of the manufacturing technology and the need for continuous efforts to develop new materials and processes in order to keep up with the ever-increasing demands of circuit designers. These advances are due in a large part to the development of thin-film technologies such as evaporation, sputtering, and CVD. The fabrication of semiconductor devices is a complicated and lengthy procedure which involves many steps including lithography, cleaning, etching, oxidation, and testing. For example, a 64 Mb DRAM, scheduled for 1997 production, requires 340 processing steps. Many of these steps include CVD, and CVD is now a major process in the fabrication of monolithic integrated circuits (IC), custom and semi-custom ASIC's, active discrete devices, transistors, diodes, passive devices and networks, hybrid IC's, opto-electronic devices, energy-conversion devices, and microwave devices.

1.2 In Situ Plasma Cleaning

One of the major emitters of PFCs in semiconductor manufacturing is the *in situ* plasma cleaning procedure performed after the chemical vapor deposition of dielectric thin films. This process typically represents 50% to 70% of the total PFC emission in a semiconductor fabrication plant. To effectively clean the process chambers of deposited

by-products, conventional cleans use CF_4 or C_2F_6 gases activated by a capacitively coupled RF plasma (usually 13.56 MHz) inside the process chamber. These PFC gases achieve a relatively low degree of dissociation and unreacted molecules are emitted in the process exhaust.

Significant PFC emissions reductions have been achieved through optimization of CVD chamber cleans. Over the past four years, semiconductor industry has continually reduced the MMTCE (million metric ton carbon equivalent) of its in situ CVD chamber cleaning [2]. It was demonstrated that the overall gas flow could be reduced, while the chamber cleaning time could be shortened. These improvements resulted from gains in source gas utilization, obtained by adjustment of the operating power, pressure, or the number of steps required to achieve complete residue removal. Optimization of the CVD chamber design is also of critical importance to improving the cleaning efficiency. The chamber can be designed with reduced chamber volume and surface area to limit the quantity of deposition residues to be cleaned. The use of ceramic materials (Al_2O_3, AlN) for the chamber components (liners, heater, electrostatic chuck, dome) is also preferable because the recombination rate of the reactive species (F radicals) injected in the chamber is much lower on ceramics than on metals. Moreover, these ceramic components present better resistance to fluorine corrosion, compared to conventional materials.

Although these advances have been considerable, they have not achieved the goal of near-complete destruction of the PFC gases. For example, efforts to continue increasing radio frequency power with fluorocarbon chemistries have resulted in the generation of other PFCs (i.e. CF_4 from C_2F_6 decomposition). Furthermore, increased *in*

situ plasma power density can lead to severe corrosion of the chamber components, and can induce process drifts and particulate contamination.

To overcome these limitations, it was suggested to use a new plasma cleaning technology that uses a remote RF inductively coupled plasma source to completely break down NF_3 gas into an effective cleaning chemical. This remote cleaning technology is introduced in the next section.

1.3 Remote Cleaning Technology

A fluorine-containing gas (NF_3) is introduced in a remote chamber, where plasma is sustained by application of microwave or RF energy. In the plasma, the clean gas is dissociated into charged and neutral species (F, F_2, N, N_2, NF_x, electron, ions and excited species). Because the plasma is confined inside the applicator, and since ions have a very short lifetime, mainly neutral species are injected in the main deposition chamber (CVD). The fluorine radicals react in the main chamber with the deposition residues (SiO_2, Si_3N_4, etc.) to form non-global-warming volatile byproducts (SiF_4, HF, F_2, N_2, O_2) that are pumped through the exhaust, and can be removed from the stream using conventional scrubbing technologies. The method has clear benefits: Due to the high efficiency of the microwave/RF excitation, the NF_3 gas utilization removal efficiency can be as high as 99% in standard operating conditions [2]. This ensures an extremely efficient source of fluorine, while virtually eliminating global warming emissions. With this “remote” technique, no plasma is sustained in the main deposition chamber and the cleaning is

much "softer" on the chamber components, compared to an *in situ* plasma cleaning technology.

1.4 Choice of the Cleaning Gas

PFC molecules have very long atmospheric lifetimes (see Table 1). This is a direct measure of their chemical stability. It is not surprising then that very high plasma power levels are required to achieve near-complete destruction efficiencies of these gases. After a survey of the commonly used fluorinated gas sources, nitrogen trifluoride (NF_3) was determined to be the best source gas. NF_3 has similar global warming potential (GWP) compared to most other PFCs (with a 100 years integrated time horizon – ITH). However, when considering the global warming potential of NF_3 over the life of the molecule it is much lower than CF_4, C_2F_6 and C_3F_8 due to a shorter lifetime (740 years vs. 50,000 for CF_4). This should be taken into consideration for estimating the long term impacts of PFC gas usage. One other reason why NF_3 is well suited to this application is the weaker nitrogen-fluorine bond as compared to the carbon-fluorine bonds in CF_4 or C_2F_6 (see Table 2). NF_3's relative ease of destruction results in an efficient use of the source gas.

Another advantage of the NF_3 chemistry is that it is a non-corrosive carbon-free source of fluorine. Indeed, the use of fluorocarbon molecules (CF_4, C_2F_6, etc.) requires dilution with an oxidizer (O_2, N_2O, etc.) to prevent formation of polymeric residues during the cleaning process [3]. Dilution of NF_3 by oxygen in this process enhances the

etch rate, but this solution was not chosen because of the formation of NOx by-products (another global warming molecule and a hazardous air pollutant, or HAP).

This clearly shows the advantage of a remote NF_3 discharge to achieve high etch rates at distances further downstream from the source, allowing for faster and mor complete chamber cleaning.

Table 1: Lifetime and global warming potential

Gas	Lifetime (years)	GWP (100 years ITH)	GWP ∞ (ITH)
CO_2	100	1	1
CF_4	50,000	6,500	850,000
C_2F_6	10,000	9,200	230,000
SF_6	3,200	23,900	230,000
C_3F_8	7,000	7,000	130,000
CHF_3	250	11,700	11,000
NF_3	740	8,000	18,000

Table 2: Comparison of nitrogen-fluorine and carbon-fluorine bond strength for common PFC gases

Source Gas	Elementary Reaction	Bond Strength (kcal/mole)
NF_3	NF_2+F	59
CF_4	CF_3+F	130
C_2F_6	C_2F_5+F	127

CHAPTER 2: PLASMA-CHEMISTRY MODELING IN THE REMOTE PLASMA SOURCE

2.1 Introduction

The ongoing improvement of the Remote Cleaning technology is based on recirculation and re-use of fluorine-rich products of the cleaning process, which are entirely exhausted in the traditional approach. This seemingly simple way of improving economical and environmental parameters depends on many assumptions, applicability of which we plan to assess in this study. In the production of integrated circuits the cleaning of treatment chambers is a very time consuming operation because deposits of silicon oxides are difficult to remove from surfaces of the treatment chamber. The cleaning is usually achieved by etching chamber surfaces by active particles, among which atomic fluorine is the most effective. Atomic fluorine can be conveniently produced from stock gases as NF_3, CF_4, C_2F_6 and SF_6 in low temperature discharge plasmas. Chemical downstream etch used in the integrated circuits manufacture is a system that generates etching atoms in a remote plasma chamber.

The numerical study intended to assess the robustness of the Remote Cleaning technology is presented in this chapter. From the practical standpoint, it is important to understand how significant perturbations of the cleaning process could be due to the presence of SiF_4 and O_2 (and possibly their fragments) in the remote plasma source and the deposition chamber. We have developed a plasma kinetic model to describe the atomic fluorine production from NF_3, CF_4, C_2F_6 in the remote plasma source (RPS) and provided a comparison of the effectiveness in decomposition of these parent molecules.

Dilution of the fluorine-based molecules with O_2 is also studied and found to be very important. The reaction mechanism containing 216 reactions includes reactions of neutrals, ionization, dissociation, excitation, relaxation, electron-ion recombination, ion-ion recombination, dissociative attachment and ion-molecular reactions (Appendix A).

2.2 Plasma Kinetic Model

The difficulty in the chemical kinetics simulation in a plasma environment is the strong interaction between the plasma electron kinetics and the chemistry of neutrals particles. To estimate the rate constants of electron-neutral reactions, the electron energy distribution function (EEDF) must be found. The Boltzman equation for EEDF was solved in [4], and the data obtained for the rate constants were presented in the Arrhenius expressions as a function of the electron temperature, while for neutral-neutral reactions only the dependence on gas temperature is considered. Avoiding undesirable complexity, we have undertaken a parametric study of the gas chemistry stimulated by reactions with inductive plasma electrons. The electron temperature and concentration are considered as parameters, and their values are in the ranges used in the present conditions. We assume that the surface coverage is proportional to the gas density. The time integration of the particle balance equations is performed for the plasma zone at constant values of particle flux (1 slpm).

For the plasma kinetic modeling the numerical simulation code was specially created using CHEMKIN gas-phase libraries. The reacting mixture is treated as a closed system with no mass crossing the boundary, so the total mass of the mixture $m = \sum_{k=1}^{K} m_k$

is constant, and $dm/dt = 0$. Here m_k is the mass of the k-th species and K is the total number of species in the mixture. The individual species are produced or destroyed according to

$$\frac{\mathbf{dm_k}}{\mathbf{dt}} = \mathbf{V} \cdot \omega_k \cdot \mathbf{W_k} \qquad \mathbf{k = 1, \ldots, K} \tag{2.1}$$

where t is time, ω_k is the molar production rate of the k-th species by elementary reaction, W_k is the molar mass of the k-th species, and V is the volume of the system, which may vary in time. Since the total mass is constant, this can be written in terms of the mass fractions as

$$\frac{\mathbf{dY_k}}{\mathbf{dt}} = \upsilon \cdot \omega_k \cdot \mathbf{W_k} \qquad \mathbf{k = 1, \ldots, K} \tag{2.2}$$

where $Y_k = m_k/m$ is the mass fraction of the k-th species and $\upsilon = V/m$ is the specific volume.

The first law of thermodynamics for a pure substance in an adiabatic, closed system states that

$$\mathbf{de + pd\upsilon = 0} \tag{2.3}$$

where e is the internal energy per mass and p is the pressure. This relation holds for an ideal mixture of gases, with the internal energy of the mixture given by

$$\mathbf{e = \sum_{k=1}^{K} e_k Y_k} \tag{2.4}$$

where e_k is the internal energy of the k-th species. Differentiating the internal energy of the mixture leads to the expression

$$\mathbf{de = \sum_{k=1}^{K} Y_k de_k + \sum_{k=1}^{K} e_k dY_k} \tag{2.5}$$

Assuming calorically perfect gases, we write $\mathbf{de_k = c_{v,k} dT}$, where T is the temperature of the mixture, and $c_{v,k}$ is the specific heat of the k-th species evaluated at constant volume. Defining the mean specific heat of the mixture, $\mathbf{c_v = \sum_{k=1}^{K} Y_k c_{v,k}}$ and differentiating equation (2.5) with respect to time and substituting in equation (2.3), the energy equation becomes

$$\mathbf{c_p \frac{dT}{dt} + p \frac{d\upsilon}{dt} + \upsilon \sum_{k=1}^{K} h_k \omega_k W_k = 0} \qquad \mathbf{(2.6)}$$

In the energy equation, c_p is the mean specific heat capacity at constant pressure and h_k is the specific enthalpy of the k-th species. As we solve the problem for constant pressure in each reactor, the energy equation for the constant pressure case becomes

$$\mathbf{c_p \frac{dT}{dt} + \upsilon \sum_{k=1}^{K} h_k \omega_k W_k = 0} \qquad \mathbf{(2.7)}$$

The net chemical production rate ω_k of each species results from a competition between all the chemical reactions involving that species. Each reaction proceeds according to the law of mass action and the forward rate coefficients are in the modified Arrhenius form

$$\mathbf{k_f = A \cdot T^{\beta} \cdot \exp\left(\frac{-E}{RT}\right)} \qquad \mathbf{(2.8)}$$

where the activation energy E, the temperature exponent β, and the pre-exponential constants A are parameters in the model formulation.

In plasma kinetics the electron concentration distribution and electron temperature should be specifying. In this model we assume that the electron concentration in fluorine-nitrogen plasma varies from 10^9 cm^{-3} (at walls) up to 10^{12} cm^{-3} (at the center) and does not depends on time. The electron temperature is found from the following fundamental formula

$$\mathbf{w(T_e) = \sum_i \sum_j k^i_{ej}(T_e) n_e n^i_0 \Delta E^i_j} \quad \textbf{(2.9)}$$

taking into account the specific power consumption and geometry of the reactor. Where w is the specific power per unit volume, T_e is an electron temperature, n_e is an electron concentration, n_0 is the gas concentration, i is the number of species, j is an excited state of the species i, k – coefficient rate of excited state of the species i, ΔE_j^i is an excitation energy of the species i in j excited state.

2.3 Simulations and Results

The focus of this part of the work was on analyzing several aspects of RPS operation including destruction of SiF_4 in NF_3/O_2 plasma, influence of O_2 on fluorine production, NO_x formation, and the efficiency of CF_4 and C_2F_6 in comparison with NF_3 in downstream chamber cleaning. The performance measures emphasized are the dissociation efficiency of the parent molecule in the discharge.

The plug flow reactor model was used. The gas residence time in the RPS is 0.5 seconds and the gas temperature reaches 2000 K. In this model the nature of the discharge is taken into account in calculation of electron temperature and concentration. The electron temperature in typical capacitively coupled plasma is 3 eV and electron concentration can be estimated from simplified equation of energy consumption:

$$\mathbf{W = k_{eV} \cdot n_e \cdot n_0 \cdot \varepsilon_0 \cdot V} \quad \textbf{(2.10)}$$

Where W is power of the source, V - plasma volume, n_e - electron concentration, n_0 - gas concentration, $\varepsilon_0 \approx 0.1$ eV - characteristic value of energy transfer from electron to

molecule in one collision, $k_{eV} \approx 3\times10^{-8}$ cm^3/s - rate coefficient of the electron-vibrational relaxation.

Figure 1-6 represent the results of plasma chemistry numerical modeling for NF_3 and C_xF_y contained gases.

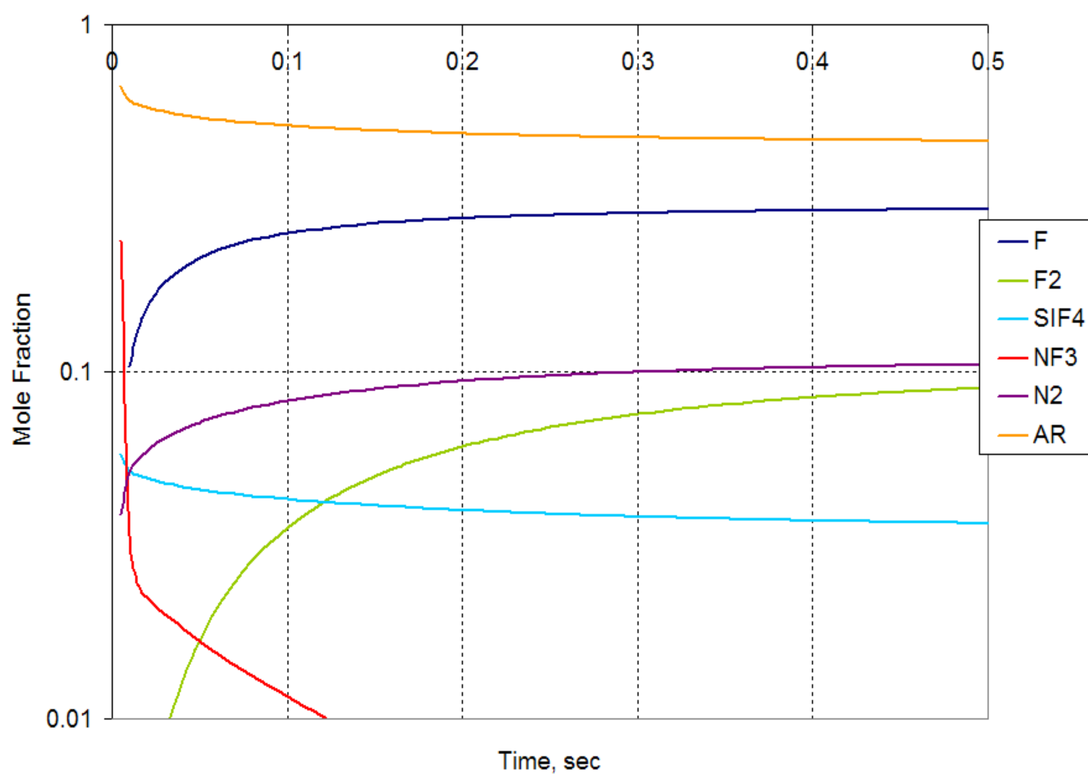

Figure 1: Numerical simulation of NF_3 dissociation in discharge. Time dependence of the main species concentration. Initial Mixture: Ar=67%, N_2=0.4%, NF_3=35%.

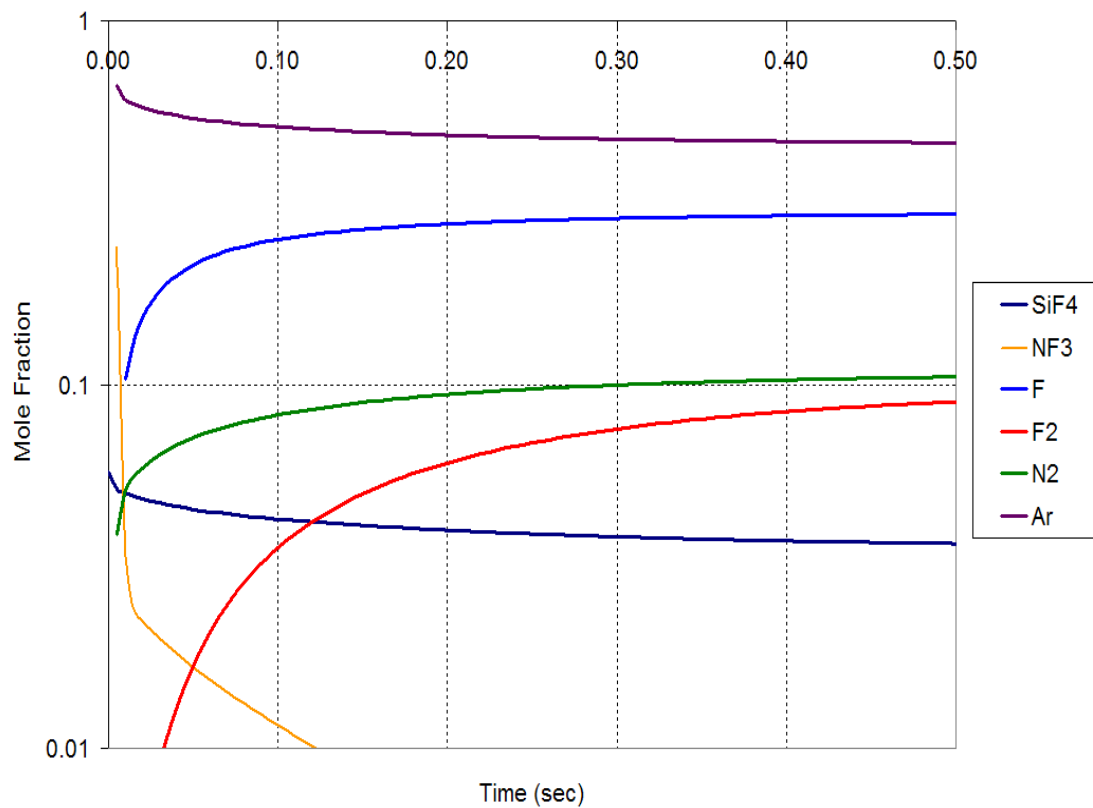

Figure 2: Numerical simulation of NF_3/SiF_4 dissociation in discharge. Time dependence of the main species concentration. Initial Mixture: Ar=67%, N_2=3.9%, NF_3=24%, SiF_4=5.8%.

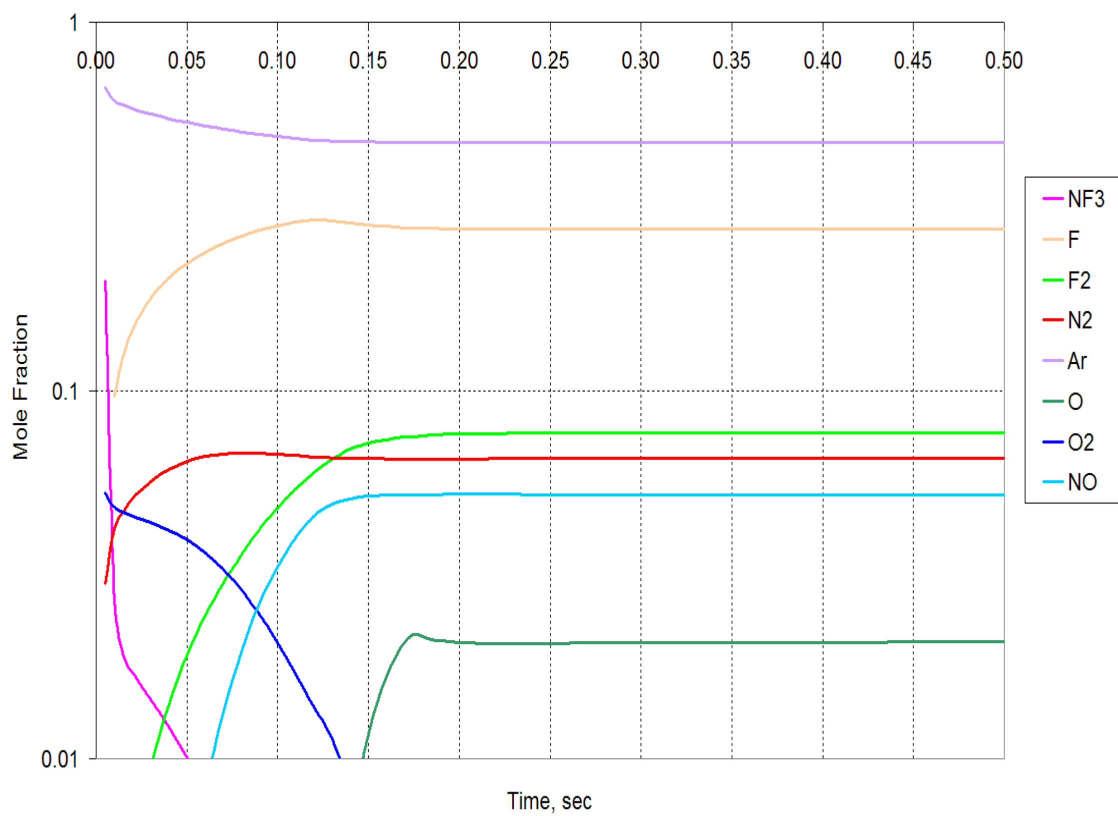

Figure 3: Numerical simulation of NF_3/O_2 dissociation in discharge. Time dependence of the main species concentration. Initial Mixture: Ar=67%, N_2=3%, NF_3=20%, O_2=5.3%

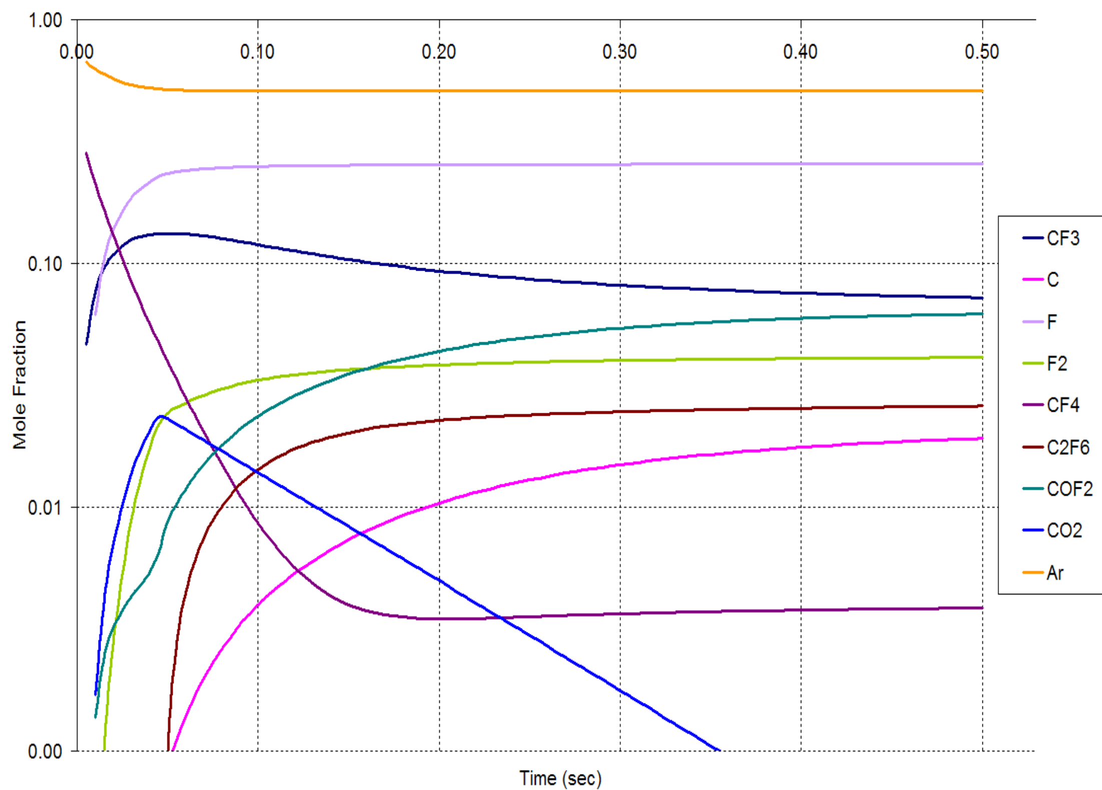

Figure 4: Numerical simulation of CF_4/O_2 dissociation. Time dependence of the main species concentration. Initial Mixture: Ar=67%, N_2=0.4%, O_2=4.2%, CF_4=28.3%.

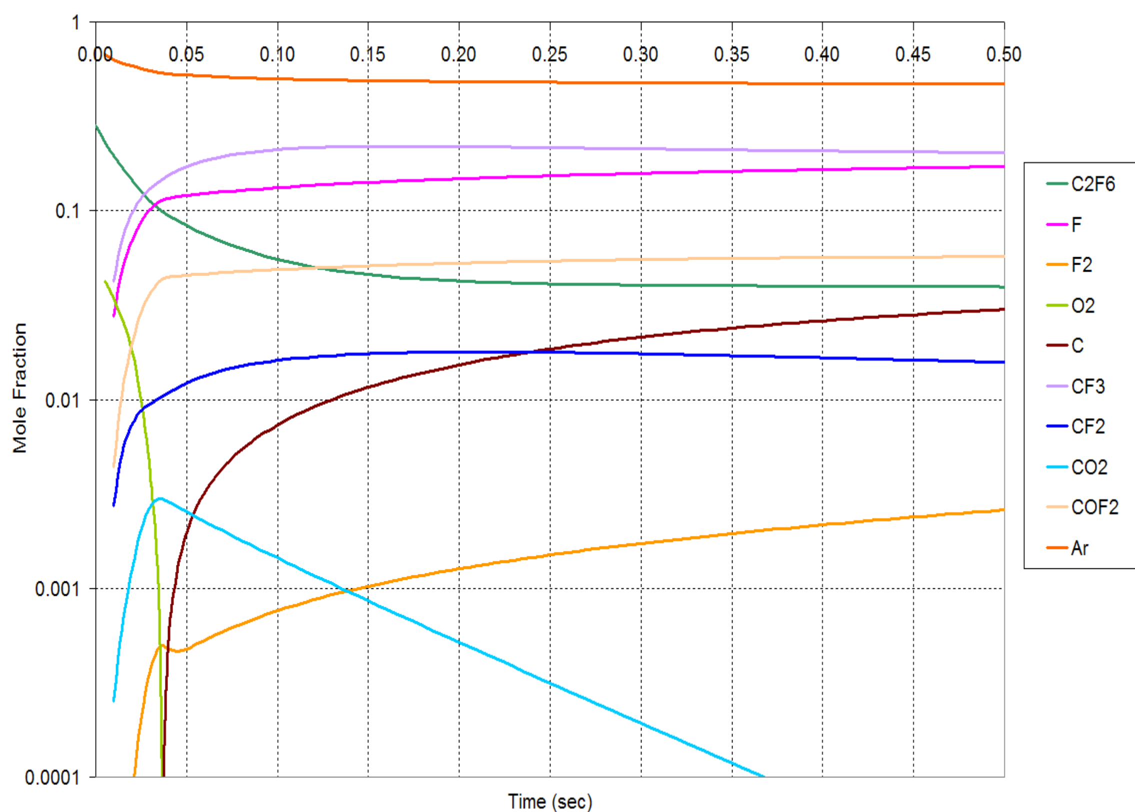

Figure 5: Numerical simulation of C_2F_6/O_2 dissociation. Time dependence of the main species concentration. Initial Mixture: Ar=67%, N_2=0.4%, O_2=4.2%, C_2F_6=28.3%.

The dissociation efficiency in pure NF_3 gas is presented in Figure 1. The atomic fluorine yield in this case is 0.4. Dissociation of NF_3 in discharge approaches 100%, resulting in higher F atom concentrations and higher etch rates in comparison with fluorocarbon gases, see Figures 4-5.

In the case of SiF_4 presents in initial gas mixture, the dissociation of these molecules can lead to the particulate Si_x formation. The simulation data with SiF_4 addition is presented in Figure 2. The dissociation degree (D.D.) of SiF_4 and Si_2 yield in plasma is very small: 5.8% and 7.4E-8 respectively. Dissociation degree and Si_2 yield are calculated according to the formulas:

$$\mathbf{D.D.} = 1 - \frac{(\mathbf{SiF_4})_{out}}{(\mathbf{SiF_4})_{in}} \cdot \frac{(\mathbf{Ar})_{in}}{(\mathbf{Ar})_{out}} \quad (2.11)$$

$$\mathbf{Si_2(yield)} = \frac{(\mathbf{2Si_2})_{out}}{(\mathbf{SiF_4})_{in}} \cdot \frac{(\mathbf{Ar})_{in}}{(\mathbf{Ar})_{out}} \quad (2.12)$$

As the total number of moles is changed, we use argon gas, which does not participate in mechanism of dissociation, as a norm factor in the equation above. Whatever the mechanism involving SiF_4, the final product formed in the system is likely to be the thermodynamically stable molecule SiF_4. However, reactions in RPS can lead to the formation of considerable amount of SiF_3 radicals.

The presence of O_2 in the discharge gives the various results showing in Figure 2. The dissociation of SiF_4 with addition of oxygen molecules decreases insignificantly from 5.8% to 5 % while the Si_2 yield increases considerably up to 2.7E-6. The appearance of NO molecules, which are known to be produced through several reaction pathways in discharges containing nitrogen and oxygen, is also observed in the simulation results. The main reaction of NO formation is the N-atom and O-atom three-body recombination

$$\mathbf{O + N + (M) \Rightarrow NO + (M)} \quad (2.13)$$

According to publication [5] some positive effects of the NO molecule could be observed for silicon etching. NO presence enhanced etch rate by reducing the thickness of the reactive layer that forms on the crystalline Si during the etch time. Apparently, O-atoms enhance production of atomic fluorine but the concentration of F is not increased as addition of O_2 essentially dilutes the system. This effect can be explained in terms of the following reactions. In the absence of O_2, the NF_x daughter species recombine according to

$$NF + NF \Rightarrow N_2 + 2F \qquad (2.14)$$

$$NF + NF_2 \Rightarrow N_2 + F_2 + F \qquad (2.15)$$

The recombination mechanism of the NF_x is different in the presence of oxygen atoms. Oxygen atoms react quickly with NF_x species

$$O + NF_2 \Rightarrow NF + OF \qquad (2.16)$$

$$O + NF \Rightarrow NO + F \qquad (2.17)$$

which leads to a reduced NF density. OF is very reactive and is lost in the discharge immediately to O_2 and F

$$2OF \Rightarrow 2F + O_2 \qquad (2.18)$$

$$O + OF \Rightarrow O_2 + F \qquad (2.19)$$

Therefore, in the presence of oxygen atoms at the discharge the occurrence of the recombination reactions (2.14) and (2.15) is reduced, the concentration of their products N_2 and F_2 is smaller, and production of atomic fluorine is enhanced by O atoms. The experiments showed that despite this higher F-atom production the presence of oxygen considerably reduces SiO_2 etching rate. This may be explained by an equilibrium shift for the next complex chemical reaction

$$SiO_2 + 4F \Rightarrow SiF_4 + O_2 \qquad (2.20)$$

In remote plasma source the fluorocarbon based gases (C_xF_y) should be mixed together with oxygen. The oxygen prevents the formation of polymeric residues. The dissociation of CF_4 and C_2F_6 in the gas discharge in presence of oxygen is shown in Figure 4 and Figure 5 correspondingly. The discharges of fluorocarbon gases produce significant amounts of molecules and radicals that do not contribute to etching reactions and even cause fluorocarbon deposition, such as CF_3, COF_2, and larger carbon chain molecules like C_2F_6. The O_2 addition into CF_4 discharge plays a significant role. It

increases the atomic fluorine concentration due to the oxidation of CF_x molecules. The dissociation of C_2F_6 is less dependent on the O_2 but more dependent on power consumption. Also, CF_4 molecule dissociates faster then the C_2F_6. Such tendency is observed in the systems with the high-energy input (200 J/cm^3) [6]. Similar results are also observed in our simulations, shown in Figure 4 and Figure 5. The dissociation degree of CF_4 molecules reaches 97 % and the dissociation degree of C_2F_6 molecules reaches 80 %. In a remote plasma source the dissociation degree of fluorocarbon molecules is much higher than in CVD chamber with *in situ* capacitively coupled plasma. It happens due to the ability of generation of high plasma density which results in higher destruction efficiency.

The summary of F yield in discharge for different parent molecules is presented in Table 3. The F yields for different parent molecules were calculated as following:

$$\begin{aligned}
&\textbf{For } (Ar/NF_3\ /N_2): && F_{yield} = \frac{(F)_{out}}{3(NF_3)_{in}} \times \frac{(Ar)_{in}}{(Ar)_{out}} \\
&\textbf{For } (Ar/CF_4/N_2): && F_{yield} = \frac{(F)_{out}}{4(CF_4)_{in}} \times \frac{(Ar)_{in}}{(Ar)_{out}} \qquad (2.21) \\
&\textbf{For } (Ar/C_2F_6/N_2): && F_{yield} = \frac{(F)_{out}}{6(C_2F_6)_{in}} \times \frac{(Ar)_{in}}{(Ar)_{out}}
\end{aligned}$$

Table 3: F-yield in discharge with different parent molecules.

	NF_3	CF_4	C_2F_6
Ar/ N_2	0.4	0.27	0.1
Ar/ N_2/ SiF_4	0.6	-	-
Ar/ N_2/ O_2	0.68	0.34	0.15

2.4 Conclusions

The important issues of the plasma source performance have been addressed in this study. The NF_3-based CVD chamber cleaning process using a remote RF plasma achieves near complete destruction (> 99%) of the NF_3 source gas, resulting in extremely low emission of global warming compounds, higher F atom concentrations and higher etch yields as compared to fluorocarbon gases. The NF_3 gas is clearly preferable to CF_4 and C_2F_6 gases. The SiF_4 decomposition degree is very low ~8% which assess the feasibility of recirculation scheme combined with the Remote Clean technology.

The remote cleaning technology takes advantage of the unique properties of NF_3 to achieve high residue removal rates. The NF_3 gas, which is in widespread used by the semiconductor industry, can be safely and effectively delivered to the tool by using the proper engineering and operational safeguards. The remote inductive plasma cleaning technology has the unique capability of reducing emissions of PFC gases from the CVD chamber cleaning processes while increasing tool productivity. It was demonstrated that excellent process stability can be obtained over thousands of processed wafers, and that the tool throughput can be increased, due to shorter cleaning times. In addition, the cost of consumables is reduced, due to reduction of corrosion (i.e., a soft cleaning) in the main deposition chamber. Using this process the semiconductor industry has the opportunity to implement significant reductions in PFC emissions and, at the same time, improve tool throughput and uptime, thus lowering the cost of ownership.

CHAPTER 3: FLUORINE RADICALS RECOMBINATION IN A TRANSPORT TUBE

3.1 Introduction

Plasmas are used extensively to generate F atoms for various processing and cleaning applications in the semi-conductor industry. The reaction (called recombination) of the F atoms to form F_2 molecules decreases the effectiveness and efficiency of these applications. Little is known about the mechanism of recombination, and the effect of various environmental factors such as wall material, pressure, flow rate, residence time, etc. on this reaction. Also, the relative importance of different possible mechanisms for the reaction, such as wall recombination and gas phase recombination, is not known.

Our work is aimed toward increasing knowledge of the basic chemistry and physics involving the transport of fluorine containing plasma in order to manipulate such plasma to maximize chamber cleaning and etching efficiency, and to minimize hazardous waste products. In order to gain this understanding a detailed two-dimensional model for fluorine atoms recombination in a transport tube was developed based on the Langmuir-Rideal heterogeneous reaction mechanism [7]. The model is able to predict fluorine recombination as a function of temperature, pressure and other influencing conditions. The model proposed herein is capable of qualitatively explaining the nature of steady-state heterogeneous fluorine recombination on the surface. The sequence of the steps in model development are:

- Detailed consideration of Langmuir-Rideal surface recombination mechanism.

- Creating rate equations (ODE's) for the change in the surface concentration of atomic fluorine based on the Langmuir-Rideal mechanism.
- Creating of steady-state laminar flow model with a species transport in a gas-phase mode using Fluent CFD software.
- Writing a numerical code solving ODE's and compiling it with Fluent CFD software.

3.2 Surface Kinetic Model

3.2.1 Langmuir-Rideal Mechanism

A kinetic theory for atomic and molecular recombination on solid surfaces employing Langmuir-Rideal mechanism is used in our modeling, Figure 6. Langmuir-Rideal surface recombination mechanism can be described as two-step process. A gas-phase atom, *A*, must first collide with the surface and stick at an empty surface site, *s*. Another gas-phase atom may strike the adhered atom and recombine, leaving the site again empty. The mechanism may be written as follows:

1-st Reaction (Adsorption)

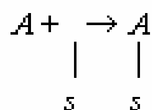

2-nd Reaction (Recombination)

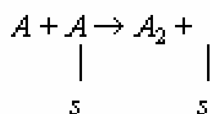

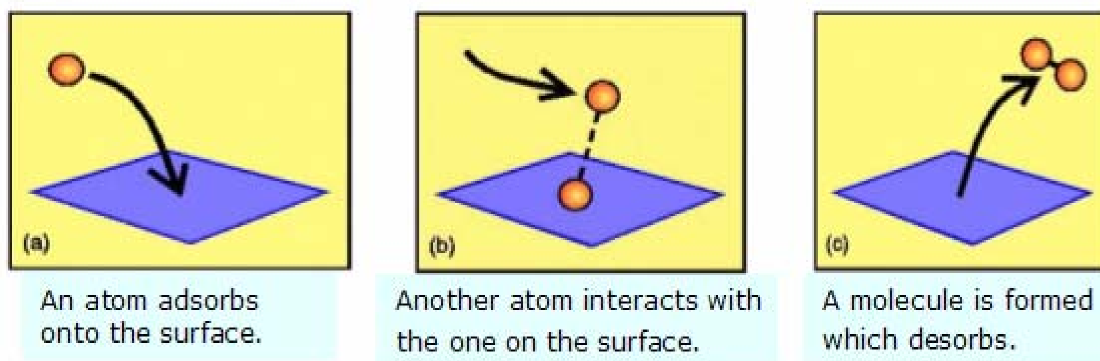

Figure 6: Demonstration of the Langmuir-Rideal heterogeneous mechanism.

Adsorption reaction shows the necessary direction for the Langmuir-Rideal mechanism to proceed; the reaction is further complicated, however, by the fact that the reverse reaction does exist and cannot be neglected at elevated temperatures. The choice of surface site of either being empty or filled with a reacting atom is a naive one in dealing with fluorine recombination since any recombination of fluorine leads to a concentration of molecular fluorine near the wall. We must, therefore, deal with the possibility of surface sites being filled with other than the reacting atoms. Finally, the type of bonding process should be addressed in forming the most general set of rate equations.

3.2.2 Rate Equation Components

Species. In order to properly write the rate equations, a cursory component overview is given here. Of course, plasma products contain various amounts of neutral species as well as excited species, but nevertheless, the dominant concentrations carry the species as F, F_2 and Ar. We will limit ourselves to these three main gas-phase species. Each of these species will be allowed to occupy a surface site. The fraction of the total

surface sites available taken up by a given species will be given by θ with the appropriate subscript to denote the type species occupying that fraction. Here we are not specifying the type of the surface. The surface recombination coefficient or steric factor implemented into the equations will denote the type of surface; these parameters will be discussed later.

Surface Bonding. The surface bonding can take one of two forms, physical bonding due to Van der Waals forces, and chemical bonding requiring certain activation energy in the collision process. Both forms of bonding will be permitted for the F and F_2 species but, because the diluent (Ar) is assumed inert, only physical bonding will be allowed for the diluent. The fractional surface concentration, θ, will be further subscripted p for physical and c for chemical on the F and F_2 species to indicate the type of surface bonding.

Adsorption Equation. The equation for an adsorption (physical or chemical) of a given species can be represented as follows:

$$\textbf{adsorption rate} = \mathbf{N} \cdot \mathbf{S} \tag{3.1}$$

where N is the rate of surface impingement per unit area and S is the sticking coefficient, a function of temperature and surface–site coverage. The rate of impingement is given by the well-known kinetic equation [8]

$$\mathbf{N} = \mathbf{n} \cdot \frac{\mathbf{c}}{\mathbf{4}} \qquad \textbf{and} \qquad \mathbf{c} = \sqrt{\frac{3\kappa \mathbf{T}}{\mathbf{m}}} \tag{3.2}$$

where n is the number density of particles in the gas, κ is the Boltzmann constant and c is the average velocity of the particles which is found from the expression of average molecular kinetic energy.

If the clean surface or initial sticking coefficient is given by S_0, a function of temperature, T, the form of S, as experimentally verified by Christman [9] is given by

$$\mathbf{S(T,\theta_T) = (1-\theta_T)S_0(T)} \tag{3.3}$$

where the subscript T on θ indicates the total fractional surface concentration (i.e., the sum of the fractional surface concentrations of all species present). The initial sticking coefficient is defined as the statistical probability that any given collision of a gas-phase particle with the clean surface at the temperature T would cause the particle to be trapped by the surface. The gas and the surface are assumed to be in thermal equilibrium. The initial sticking coefficients as a function of temperature were calculated for both physical surface bonding and chemical surface bonding (see section 3.2.3).

Thermal Desorption Equation. The equation for thermal desorption is given by

$$\textbf{thermal desorption rate} = \delta \cdot \theta \tag{3.4}$$

where δ is the thermal desorption rate per unit area for a given species, and θ the fractional surface concentration of that species [11]. The thermal desorption rate is given by Glasstone, Laidler, and Eyring [12] as

$$\delta = \mathbf{C_A \frac{\kappa T}{h} \exp(-E_D / \kappa T)} \tag{3.5}$$

where C_A is the number of surface sites per unit area (for a monolayer of adhered atoms this is taken to be approximately equal to the metal surface atom packing [11]; any experimental surface will undoubtedly be polycrystalline but, for the purpose of analysis, it will be taken to be a face centered cubic [13]), h the Planck constant, and E_D the desorption energy, which is taken to be the well depth for the particular bonding process (ΔE_w for the physical and E_0 for the chemical well).

Recombination Desorption Equation. The desorption by recombination is applicable only for the surface-bonded atomic fluorine and is given by the kinetic equation

$$\textbf{recombination desorption rate} = \mathbf{P_S N_F \theta_F} \qquad \textbf{(3.6)}$$

where and θ_F the fractional surface concentration of F atoms and P_s is a steric factor. The steric factor is less than 1.0 and takes into account the effectiveness for reaction of the gas-phase/surface-adhered atom collision. Since the reaction is an atom-atom recombination, the steric factor may reasonably be assumed to be independent of temperature. The possibility of temperature dependence does, of course, exist because of the added complexity of the surface. However, the gas temperature in our transport tube is assumed to be constant and equal to the room temperature. In our simulations we used a steric factor of 0.018 as determined experimentally for a nickel surface [10].

Relying on the equations given above, the rate equation for the change in surface concentration of atomic fluorine bonded in physical wells is given by

$$\left(\frac{dn_F^{sur}}{dt}\right)_p = (S_{0F})_p(1-\theta_T)N_F - (\delta_F)_p(\theta_F)_p - P_S N_F(\theta_F)_p \qquad (3.7)$$

where n_F^{sur} is the surface concentration of F per unit area. All the F subscripts refer to atom fluorine, and the *p* subscripts to physical bonding.

Similar rate equations can be written for chemically surface-bonded atomic fluorine, physically surface-bonded and chemically surface-bonded molecular fluorine, subscripted F_2, and the physically surface-bonded Ar, subscribed Ar.

$$\left(\frac{dn_F^{sur}}{dt}\right)_c = (S_{0F})_c(1-\theta_T)N_F - (\delta_F)_c(\theta_F)_c - P_S N_F(\theta_F)_c \qquad (3.8)$$

$$\left(\frac{dn_{F_2}^{sur}}{dt}\right)_p = (S_{0F_2})_p(1-\theta_T)N_{F_2} - (\delta_{F_2})_p(\theta_{F_2})_p \tag{3.9}$$

$$\left(\frac{dn_{F_2}^{sur}}{dt}\right)_c = (S_{0F_2})_c(1-\theta_T)N_{F_2} - (\delta_{F_2})_c(\theta_{F_2})_c \tag{3.10}$$

$$\left(\frac{dn_{Ar}^{sur}}{dt}\right) = S_{0Ar}(1-\theta_T)N_{Ar} - \delta_{Ar}\theta_{Ar} \tag{3.11}$$

The *c* subscripts indicate chemical bonding. The θ_T is the total fractional surface concentration which is limited by $0 \le \theta_T \le 1$.

$$\theta_T = (\theta_F)_p + (\theta_F)_c + (\theta_{F_2})_p + (\theta_{F_2})_c + \theta_{Ar} \tag{3.12}$$

The above equations completely describe the surface reaction mechanism for $F/F_2/Ar$ mixture. In the region above 100 K, physically surface-bound species, in our case Ar, can no longer play a role in the catalytic process since they are incapable of occupying surface sites.

3.2.3 Sticking Coefficients

To determine the sticking coefficients, the atom-wall inelastic collision process must be addressed. This will not only involve modeling of the collision process but also require some knowledge of the well depths associated with the various types of particle-surface bonds: $(F\text{-}Ni)_p$, $(F\text{-}Ni)_c$, $(F_2\text{-}Ni)_c$, and (Ar-Ni). The justification for including chemically surface-bonded F_2 and the need for chemically surface-bonded F is implicit in the Langmuir-Rideal mechanism at room temperature and above. Neither the well depth for physical or chemical surface bonding is known for fluorine.

Physical Surface Bonding. A simple model for physical surface bonding can be constructed for the potential well near a surface based upon an adsorption (attractive)

potential and a repulsive potential as suggested by Lennard-Jones [15]. The construction is described by example. The closest distance of approach of nickel atomes in metal is 2.48×10^{-8} cm, while that for fluorine atoms is 1.28×10^{-8} cm. The equilibrium distance of approach, R_E, for nickel and fluorine can be taken as the mean of these two distances or 1.88×10^{-10} cm. At this equilibrium distance the repulsive forces are from 1/3 to 1/2 that due to the attractive forces. Thus, by letting the repulsive force be 40% that of the attractive force, a well depth can be determined by algebraically summing the two potentials. Thus, an attractive potential, assumed to be $W(r)$, where r is the distance of separation, will yield a well depth, ΔE_W, at the equilibrium position, R_E, of

$$\mathbf{\Delta E_w = 0.6 \cdot W(R_E)} \tag{3.13}$$

No reference is made to activation energy and in fact no activation energy is experimentally observed for physical adsorption [11]. Several authors have described the functional relationship of the attractive potential for physical bonding, $W(r)$. The earliest of these descriptions [14] was the simplest and yielded fair results. This relationship served as an upper limit on the physical attractive force. In a more recent paper, Mavroyannis [15] derived a formula for $W(r)$ and compared the results of his relationship with four previously derived relationships, those of Lennard-Jones [14], Bardeen [16] and Pollard [17]. The results of this comparison showed that the Mavroyannis formulation compared as well as, or better than, the previous relationships when compared with data for several atom-surface systems. In addition, the Mavroyannis relationship makes use of readily available material properties. For these reasons the Mavroyannis potential was adopted here for use in approximating the attractive potential for physical surface bonding. The formula for this potential is given by

$$\mathbf{W(r)} = -\frac{\langle \mathbf{q}^2 \rangle}{\mathbf{12r}^3} \frac{\hbar \mathbf{W_p} / \mathbf{2}^{1/2}}{\frac{3}{2} \frac{\mathbf{N}}{\langle \mathbf{q}^2 \rangle} + \hbar \mathbf{W_p} / \mathbf{2}^{1/2}} \tag{3.14}$$

where $\langle q^2 \rangle$ is the sum of the electronic charge of each electron in the adsorbed particle times the expectation value of its orbital radius, $\hbar W_p$ is the work function of the metal surface, and N is the number of electrons in the adsorbed atom. The results obtained by use of equation (1) and (2) are listed in Table 4 for those atom-surface systems of interest. The values of these well depths are consistent with those to be expected for van der Waals adsorption [11].

Chemical Surface Bonding. The well depth in chemical surface bonding is not as easily modeled as that for physical surface bonding; this parameter is usually experimentally determined. The values for chemical bonding, E_0, given in Table 4 were obtained by an optimization process discussed in reference [10].

Atom-wall Inelastic Collision. In order to model an inelastic collision process, the soft cube model by Logan and Keck was used [18]. As dictated by the soft cube model, the surface of the wall is pictured as made up of wall atoms vibrating at a frequency consistent with the bulk Debye temperature (i.e., at the Debye frequency, ω_s) in a direction normal to the plane of the surface. During a surface interaction only the velocity component of the gas-phase atom normal to the surface was considered. The use of the normal velocity component enabled data correlation which was not able to be made by using the total velocity in the case of low incident angle particle-surface collisions. The gas-phase atom was further assumed to interact with only one surface atom (i.e. each surface atom was treated as a surface site). The various frequencies and potentials were then modeled as shown in Figure 7. The shape of the well beyond the interaction position

was of no importance; the incoming particle was simply given additional velocity consistent with the well depth above its Boltzmann-predicted gas-phase velocity. In the case of physical surface bonding, this presented no problem since no activation energy is required to enter the well. Pagni [10] makes no distinction between chemical and physical bonding except for the well depth. It is, however, possible to formulate a cutoff energy (activation energy) required to enter the chemical-bonding well and to incorporate it into Logan's model. Very little is available on theoretical or experimental determination of the activation energies required for the present application. A reasonable estimate of the activation energies for chemical bonding was taken to be 10% of the well depth. Based on this estimate, sticking coefficient curves were obtained by Emmett. A collision of a gas-phase atom (or molecule) with the wall can have only one of three possible outcomes, adherence to the wall in a physical well (physical adsorption), adherence to the wall in a chemical well (chemical adsorption), or avoidance of trapping (scattering). By including an activation energy barrier, we allowed gas-phase atoms (or molecules) below the barrier to interact solely with a physical well and those above the barrier to interact with only a chemical well. If the particle never overcomes the activation barrier it cannot be chemically bonded, and if the energy of the reflected particle is sufficient to overcome the chemical well plus the activation barrier, it could not be expected to be trapped in the somewhat smaller physical well.

Having entered the appropriate well, the atom (or molecule) encountered an interacting spring of spring constant k_g. The spring, following the discussion of Modak and Pagni [19], represented an exponential repulsive potential, which led to a spring constant of

$$\mathbf{k_g = 0.2 \cdot D^{1.17} / \kappa^2} \tag{3.15}$$

where D is well depth (ΔE_w for the physical and E_0 for the chemical well), and κ the distance over which the interaction takes place. The spring constant for the surface atom mass m_s was

$$\mathbf{k_g = \omega_s^{\,2} \cdot m_s} \tag{3.16}$$

A collision began when a gas phase particle of mass m_g came in contact with the moving end of the spring with constant k_g. From this point until the collision ended, the system was treated as a simple undamped two mass system. The collision then took place with a gas-phase particle of velocity υ

$$\mathbf{\upsilon = V_3 + (2D / m_g)^{1/2}} \tag{3.17}$$

representing a combination of the Boltzmann-predicted random surface-normal component of velocity, V_3, the probability for which is given by [8]

$$\mathbf{p\left[\frac{V_3}{\left(\frac{2kT}{m_g}\right)^{1/2}}\right] = \frac{2V_3}{\left(\frac{2kT}{m_g}\right)^{1/2}} \exp\left\{-\left[\frac{V_3}{\left(\frac{2kT}{m_g}\right)^{1/2}}\right]^2\right\}} \tag{3.18}$$

where T is the gas temperature at the wall, and the additional kinetic velocity gained from entering the well. The position of the spring at the moment of the collision, Y(0), was also random but equal in magnitude to the position of the wall atom at that moment, Z(0). The initial conditions were

$$\mathbf{Z(0) = Y(0)} \tag{3.19}$$

$$\mathbf{\upsilon > \dot{Y}(0)} \tag{3.20}$$

Equation (3) is interpreted to mean that if the velocity, υ, were less than $\dot{Y}(0)$, there would have been no collision at that initial condition.

The collision ended at time t_c when the magnitude of colliding-particle position, $Y(t_c)$, again equaled the magnitude of the wall-atom position, $Z(t_c)$. At that point, if

$$\frac{1}{2}\mathbf{m_g}\cdot\left[\dot{\mathbf{Y}}(\mathbf{t_c})^2\right] < \mathbf{D} \tag{3.21}$$

(or D plus the activation energy in the case of chemical surface bonding) the gas particle was trapped, and if

$$\frac{1}{2}\mathbf{m_g}\cdot\left[\dot{\mathbf{Y}}(\mathbf{t_c})^2\right] \geq \mathbf{D} \tag{3.22}$$

(or D plus the activation energy in the case of chemical surface bonding) the gas particle escaped the well and avoided trapping.

Referring to Figure 7, the equations of motion for the collision process are

$$\mathbf{m_g\ddot{Z} + (k_g + k_s)Z - k_gY = 0} \tag{3.23}$$

$$\mathbf{m_g\ddot{Y} - k_gZ + k_gY = 0} \tag{3.24}$$

The solution for equations 38 and 39 then gave analytic expression for $Y(t)$, $Z(t)$, and $\dot{Y}(t)$ which could be used to find t_c. Having t_c, the collision criteria, equation 36 and 37, were used to make decisions of either a stick (trapped) or no stick (escape) for each of initial conditions. Since the model assumed that the surface site represented by the surface atom was clean, the results of the solutions of equations (38) and (39) was used to calculate the initial sticking coefficient of equation (3.3) for the specific set of initial conditions.

Initial Sticking Coefficient. The stick or no stick decisions from above were made for 40 initial conditions of surface-atom phase angle for each of 26 initial non-

dimensional velocity conditions for each temperature. These in turn were weighted by the probability of that velocity condition occurring according to the probability density function, equation (33). This was done for 20 temperatures between 0 and 800 K for each of the gas-metal systems of interest. The result of this process yielded the initial or clean surface sticking coefficient, $S_0(T)$, defined as the statistical probability that any given collision of a gas-phase particle with the clean surface at the temperature T would cause the particle to be trapped by the surface. The gas and surface were assumed to be in thermal equilibrium. The initial sticking coefficients were calculated for both physical surface bonding and, where applicable, for chemical surface bonding. The results of the calculations for atomic and molecular fluorine, and for argon diluents on a nickel surface, are given in Figures 8-10. The constants for intermediate calculations of the physical well depth by use of equation (29) were taken from the literature [20] for F and Ar. In the case of F_2, $\langle q^2 \rangle$ was obtained from initial calculations [21] which solved the time-independent Schrödinger equation by using a configuration-interaction method.

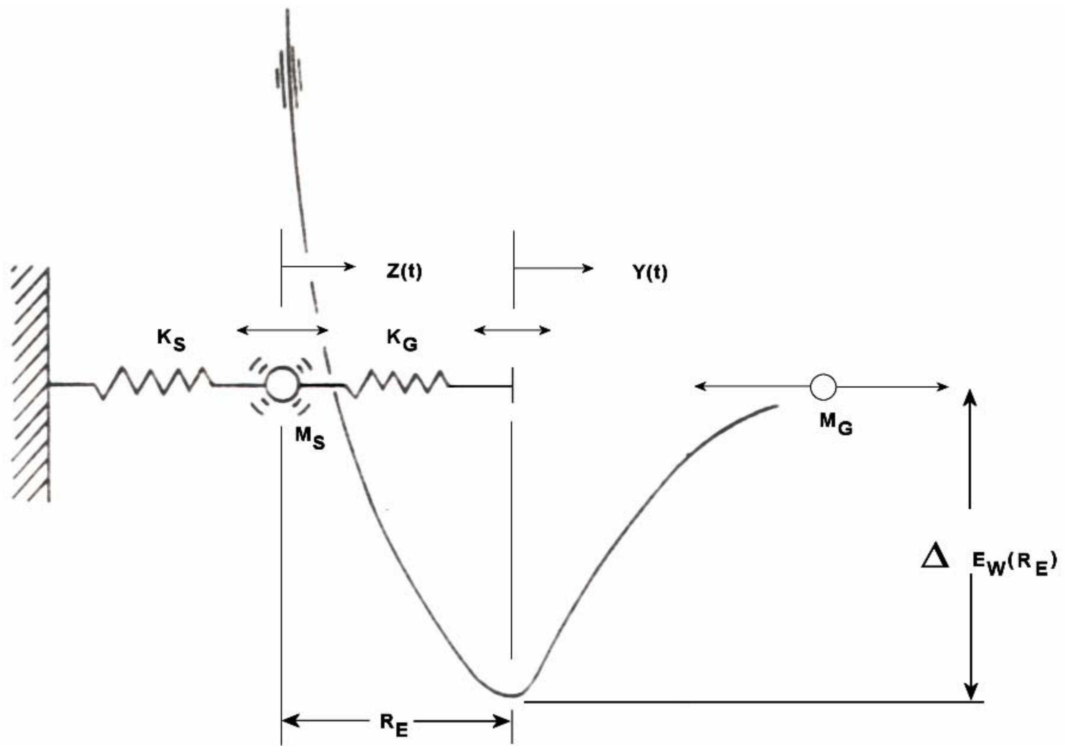

Figure 7: Gas-wall collision model.

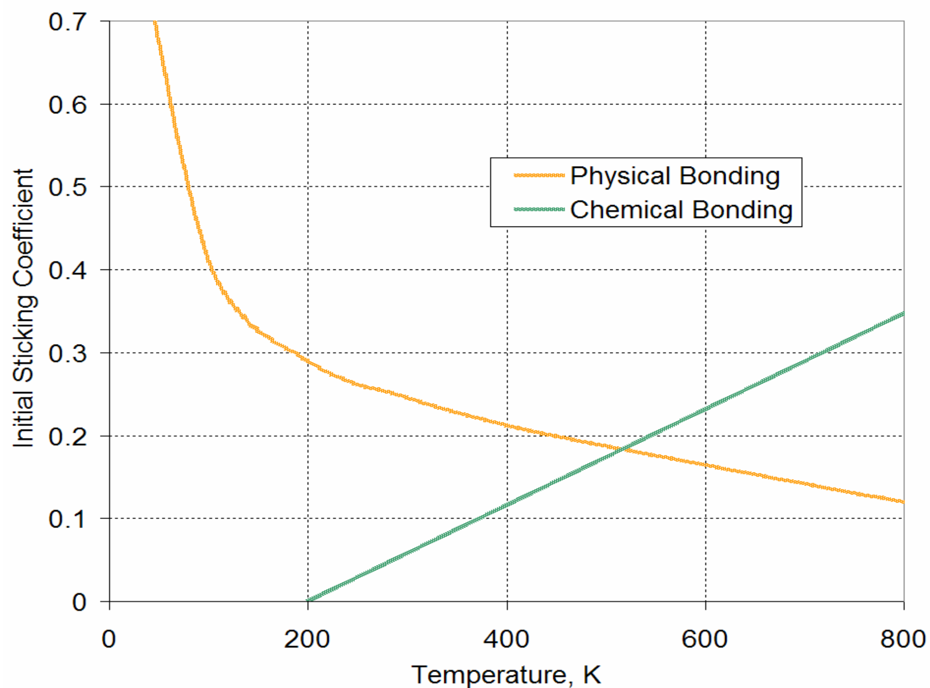

Figure 8: Initial sticking coefficient for F on Ni as a function of temperature. The curves show computed values for physical and chemical bonding.

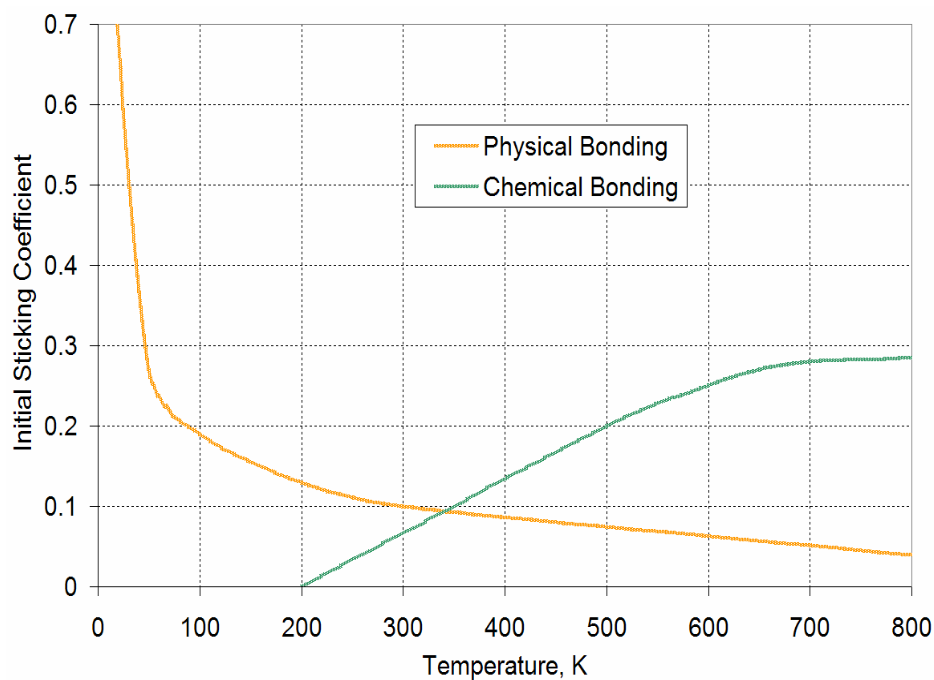

Figure 9: Initial sticking coefficient for F_2 on Ni as a function of temperature. The curves show computed values for physical and chemical bonding.

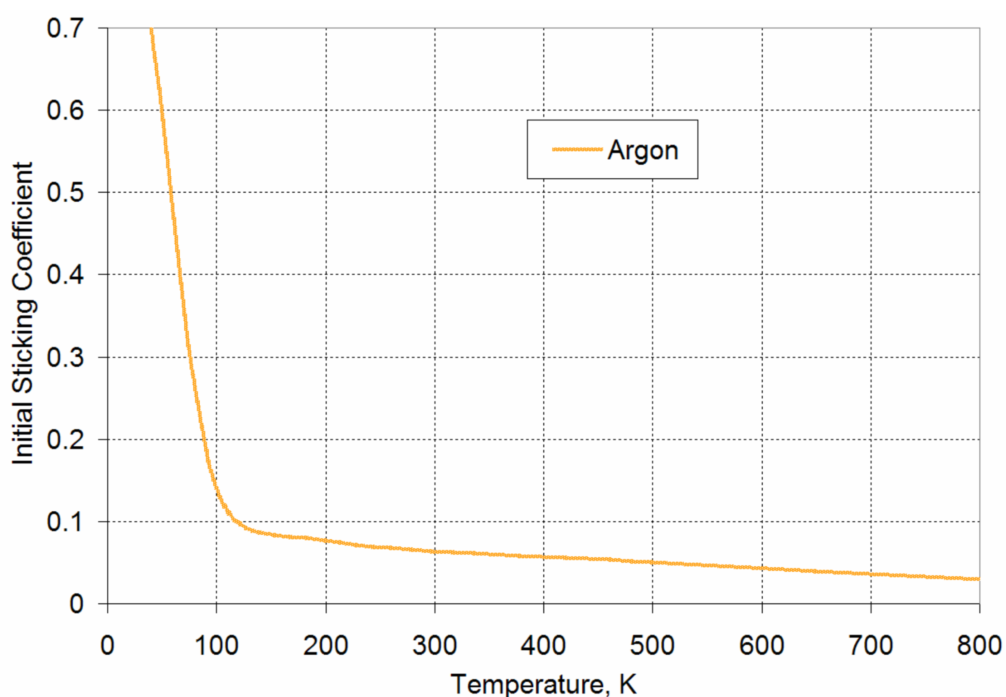

Figure 10: Initial sticking coefficient for Ar on Ni as a function of temperature (physical bonding only).

3.3 Volume Kinetic Model

Because both F_2 and Ar do not react with each other in the gas-phase and on the surface (at room temperature) and F-atoms do not react with F_2 and Ar either, the only homogeneous reaction considered is the third-body recombination reaction of fluorine atoms

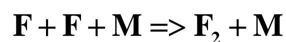

$$\mathbf{F + F + M => F_2 + M}$$

where *M* represents a collision partner usually referred to as third body. A typical rate expression for this reaction was used to model kinetics in a volume:

$$\frac{dn_F}{dt} = -2 \cdot k \cdot (n_F)^2 \cdot n_M$$

where the n_F and n_M are the volume concentration of the fluorine and the third body respectively. Reaction rate, *k*, is defined by the Arrhenius expression:

$$k = k_0 \exp\left(-\frac{E_a}{RT} \right)$$

where k_0 reaction rate constant, E_a activation energy, *T* gas temperature and *R* universal gas constant. The recombination rate constant is taken from [22]:

$$k_0 = 2.21 \times 10^{14} \quad \left[\frac{cm^6}{mol^2 \cdot s} \right]$$

This constant was obtained for temperature 300 K and pressure range from 1 Torr to 35 Torr. The reverse reaction is not relevant due to low temperature in the tube (300 K). Dissociation of F_2 takes place only at temperatures higher than 1300 K.

3.4 Simulation Results

The simulation was performed using Fluent CFD software. The flow model describing gas motion in a transport tube was developed and solved for the following equations: conservation equations for mass and momentum for laminar flow, energy conservation (for heat transfer) and species conservation equations.

The rate equations describing surface chemistry were introduced as a user-defined source code and are coupled together with the flow model and gas-phase chemistry. The different parameters involved in the modeling of surface kinetics appear in Table 4.

Table 4: Computational parameters involved in surface kinetics.

Parameter	Numerical Value
Steric Factor, P	0.018
ΔE_{WF}	1.571×10^{-13} erg/atom
E_{0F}	1.261×10^{-12} erg/atom
ΔE_{WF2}	1.328×10^{-13} erg/atom
E_{0F2}	1.215×10^{-12} erg/atom
ΔE_{WAr}	1.448×10^{-13} erg/atom
$C_a(k/h)$	3.3878×10^{25} particles/(K-s-cm^2)

The computational geometry of the transport tube is presented in Figure 11. A 30 cm long tube with inner diameter of 3.4 cm is mounted to the source exit connecting the RPS and the CVD chamber. Feed gas with composition F = 60 %, F_2 = 10%, Ar = 30% flows into the tube with the flow rate of 250 sccm. The temperature of the tube walls is room temperature (300 K). The pressure range we considered varies from 1 to 8 Torr. The tube material is nickel.

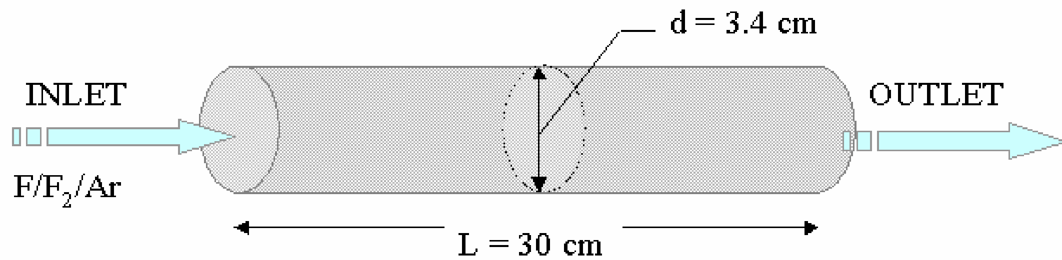

Figure 11: Transport Tube. Computational Geometry.

Simulation results showing adsorption rates as a function of the transport tube length for the different pressures are presented in Figure 12. The pressures considered are: 3, 5 and 8 Torr. The actual difference between lines representing the different

pressures lies near the beginning, where gas enters the transport tube. At the inlet section of the tube the adsorption of F-atoms goes faster when the pressure raises, Figure 12. Figure 13 shows lose of fluorine radicals for different pressures as a function of tube length. The higher the pressure the faster the fluorine radicals are lost. The similar picture, Figure 14, shows the production of fluorine radicals. At higher the pressures the production of fluorine molecules is faster. It is clear, both surface and volume reactions contribute to the overall F atom loss mechanism in the gas flow from the plasma source.

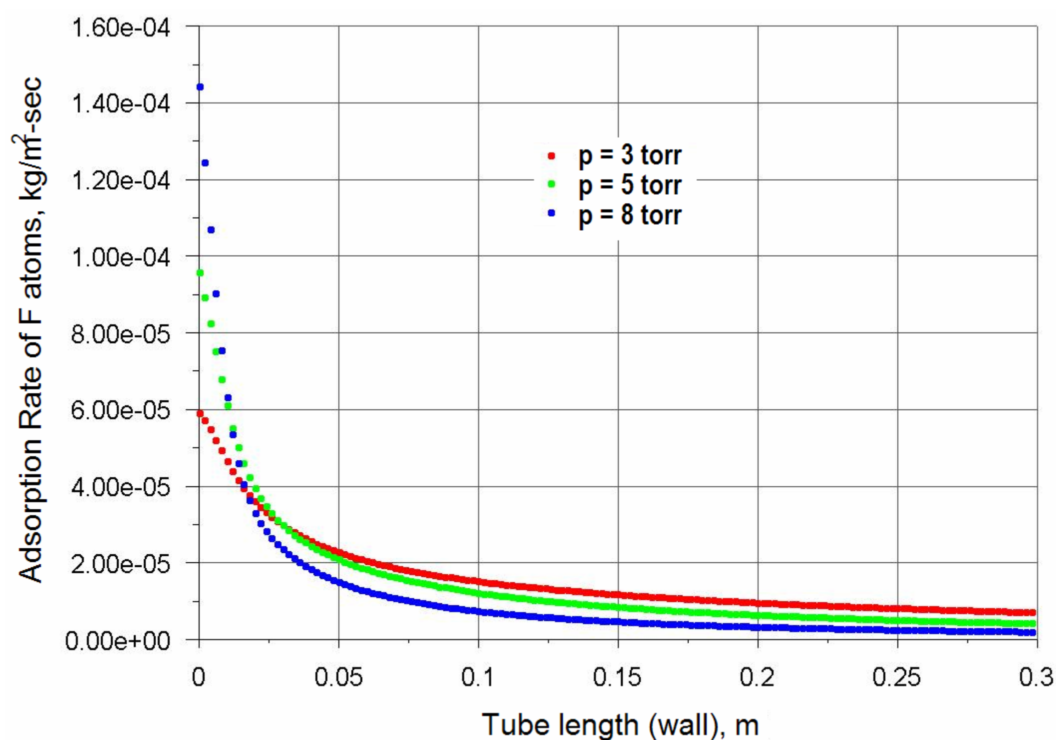

Figure 12: Adsorption rate of atomic fluorine in transport tube length. The curves show computed values for three different pressures: 3, 5 and 8 Torr.

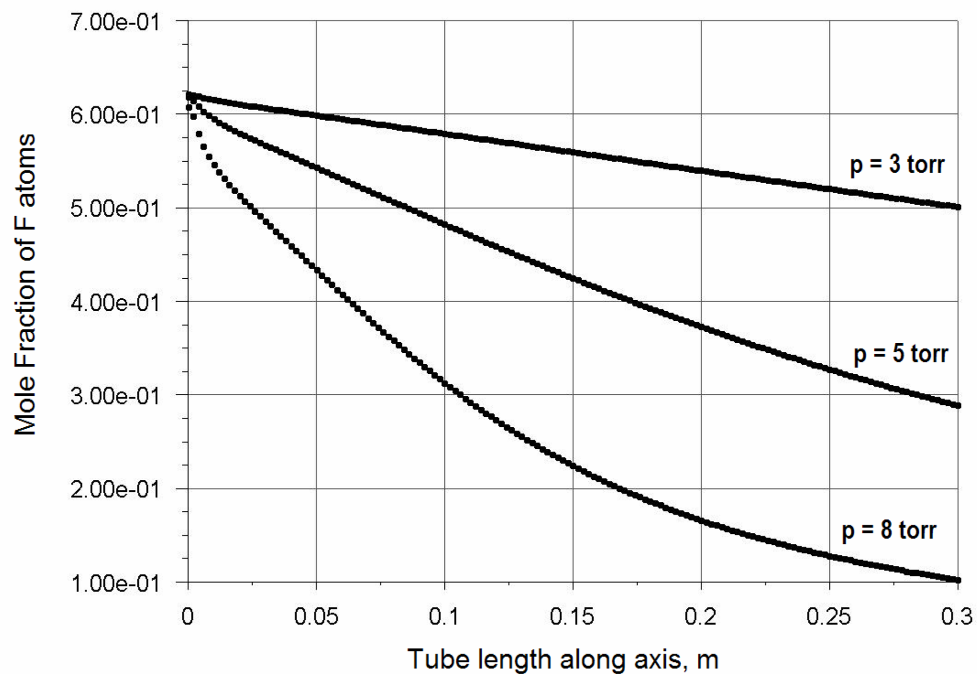

Figure 13: Mole fractions of F atoms in transport tube length. The curves show computed values for three different pressures: 3, 5 and 8 Torr.

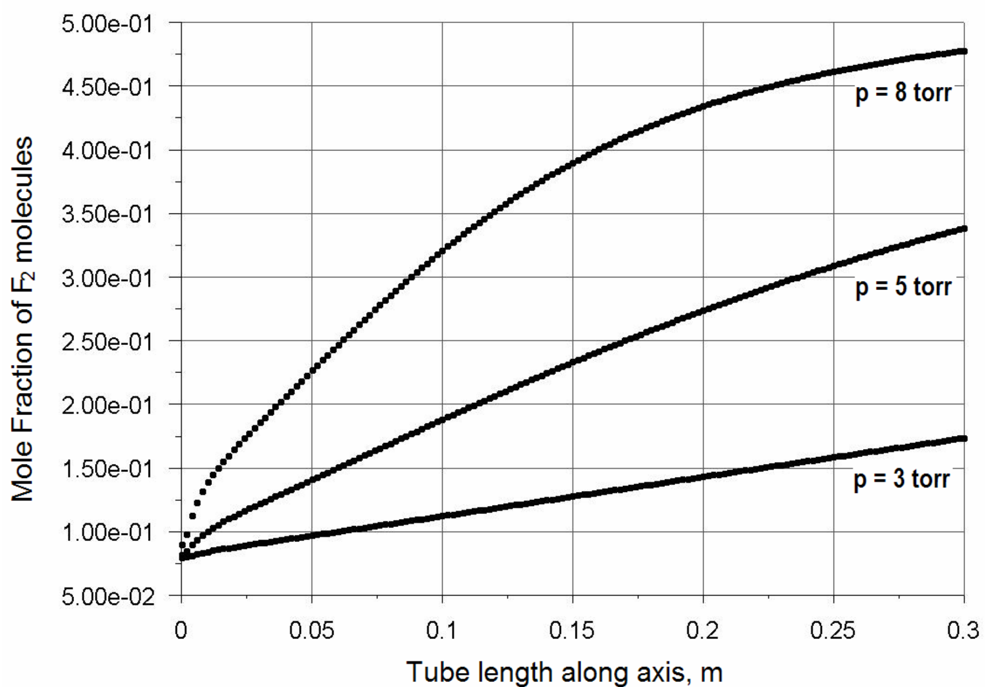

Figure 14: Mole fractions of F_2 molecules in transport tube length. The curves show computed values for three different pressures: 3, 5 and 8 Torr.

Figure 13 and Figure 14 show the lose of fluorine radicals in the transport zone. We know that the loss of radicals takes place in the volume (volume recombination) and on the surface (surface recombination) due to low operating pressures and such parameters as flow rate, tube material and pressure have an influence on these two mechanisms of recombination. Some experimental work has been made toward understanding these influences [23] but nothing was done in this direction in the area of theoretical analysis and numerical modeling. There is no sense to study numerically the dependence of recombination processes as a function of the tube material, if only for validation purpose. The results will strictly depend on the sticking coefficients of the given materials which in return can be found only experimentally. One main aspect in this study is still of concern to the technological sector: dependence of volume and surface recombination on pressure changes. It is clear that with higher pressures the volume recombination will dominate the surface recombination. The contribution of the volume recombination increases with pressure (the volume recombination rate constant behaves as p^3). There is some critical pressure which differ these both mechanisms. But what is the critical pressure in our system? A logical selection is pressure at which the contribution in lost process of fluorine radicals from both channels is equal. To find this pressure the graph representing the dependence of some function *f* on pressure *P* must be built. This function *f* is the difference between integral over the surface of the recombination desorption rate and integral over the volume of the volume recombination rate

$$\frac{\textbf{Recombination Desorption Rate}}{\textbf{Volume Recombination Rate}} = \frac{\int_S \mathbf{R}_{\text{surface}}}{\int_V \mathbf{R}_{\text{volume}}} = \mathbf{f(P)}$$

As we are solving the steady-state problem and thermal desorption can be neglected because of low temperature (300 K), one can assume that the adsorption rate is equal to the recombination desorption rate and therefore the equation above is true. The graph showing the dependence of function *f* on pressure in the transport tube is presented in Figure 15. The simulations were made for three different pressures: 3, 5 and 8 Torr. From the Figure 15, the critical pressure is 4.5 Torr (at the intersection of curve and line $f = 1$). This means that in the region below this critical pressure (i.e., 4.5 Torr) the surface recombination of atomic fluorine is dominant and in the region above 4.5 Torr the volume recombination of atomic fluorine is dominant.

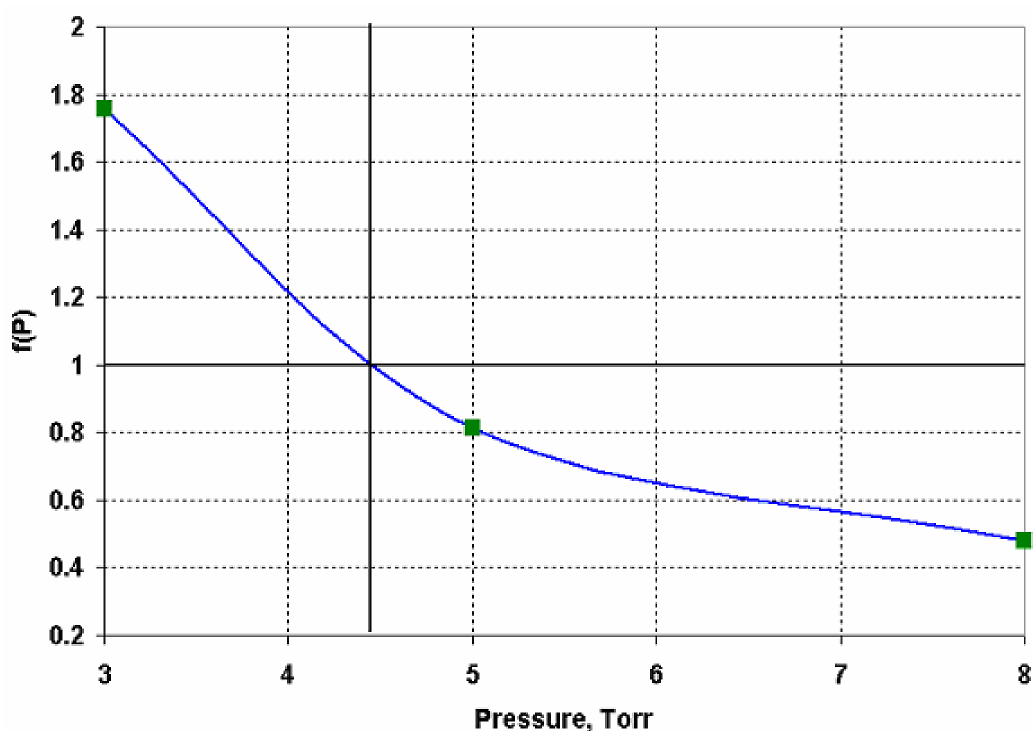

Figure 15: The dependence of function *f* on a pressure. Simulated results for three pressures: 3, 5 and 8 Torr. Critical pressure is 4.5 Torr.

Another important issue we have to study concerns finding the optimum operating pressure for the transport tube. However, it is clear that with the high pressures the lost of fluorine radicals would be exponential and, thus, there is no optimal solution for pressure at its high values. In order to find the optimal pressure we considered the low values pressure range (from 1 Torr to 10 Torr). The dependence of average fluorine atoms concentration as a function of pressure is presented in Figure 16. These simulation results can also be compared with the recent experimental results [23]. The agreement between predicted and experimental data is reasonably good, specifically the position of maximum of F-atoms concentration at 3 Torr is accurately predicted, while the deviation between the experimental and numerical data is within 30%. Referring to the obtained results the optimal pressure value in transport tube could also be 2 Torr.

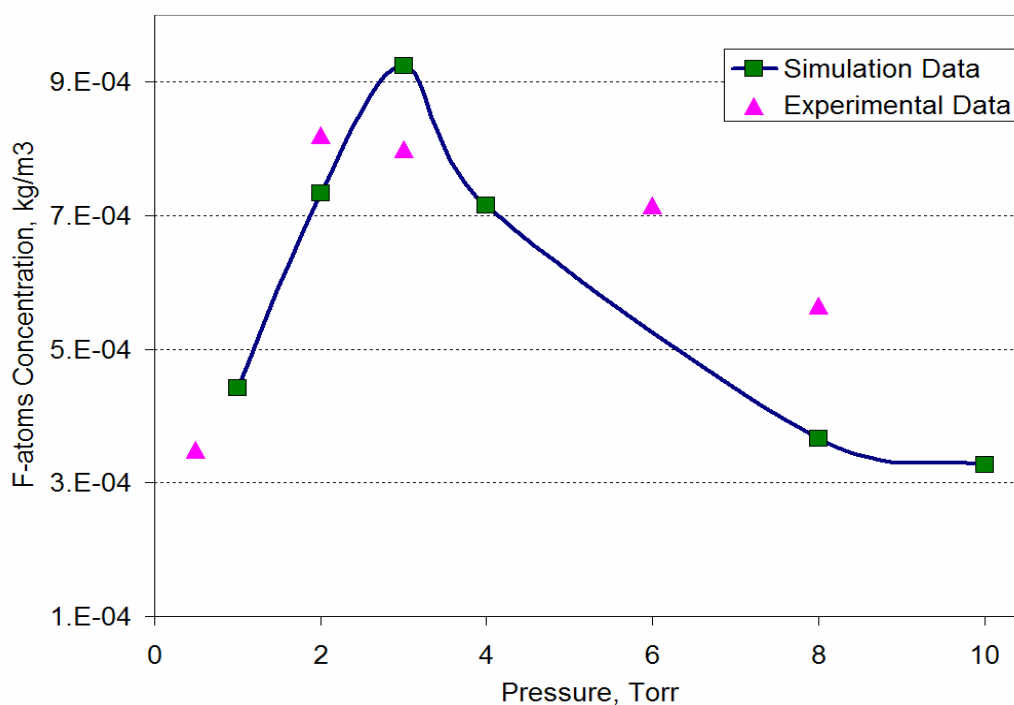

Figure 16: F-atoms concentration after the transport zone as a function of pressure.

3.5 Discussion and Conclusions

For validation of the given model we used the experimental results of Bernstein [23] who also worked toward understanding the recombination mechanism of F-atoms in a transport tube. These experimental results showed that in the pressure range $1 \leq P \leq 10$ Torr the concentrations of species F and F_2 do not, in general, depend on the wall material, see Figure 17. The only variations F and F_2 ratios with respect to wall material are found under low pressure conditions (below ~5 Torr). This means that at the low pressures below 5 Torr the tube material is essential and so surface recombination reaction, and at the pressures above 5 Torr the tube material is no longer essential and volume recombination reaction dominates in the production fluorine molecules (F_2). These experimental results have a good correlation with our modeling, Figure 15. Where we showed that at the pressure 4.5 Torr the surface reaction rate is equal to the volume reaction rate.

The obtained simulation results also showed some optimal solution for the operating pressure in transport tube which lays somewhere in the pressure range of 2-3 Torr. Indeed, the optimal pressure value could be only in the pressure range where the surface recombination is dominant.

The described approach to modeling the recombination of fluorine on a surface has attempted to identify the key microscopic phenomena involved. The comparison with the experimental data corroborates this statement. Experiments addressing just the sticking coefficients, or addressing the question of the number of surface sites per unit

area for polycrystalline nickel or other tested material, could be helpful in removing some of the uncertainties introduced by the theoretical approach.

This specific model is capable of modeling not only the surface chemistry of F, F_2 and Ar but the surface chemistry of any atoms and molecules. For modeling the dependence of tube material on recombination processes the appropriate data for recombination coefficients (i.e., recombination probabilities) should be considered. Unfortunately, this continuum approach has a pressure limit and because of this the lowest pressure we considered was 1 Torr. To obtain a true modeling in low pressure regime (< 1 Torr), a separate study is required that focuses specifically on this pressure range. To better describe system behavior at low pressures (low densities) the Monte Carlo simulation approach is usually used.

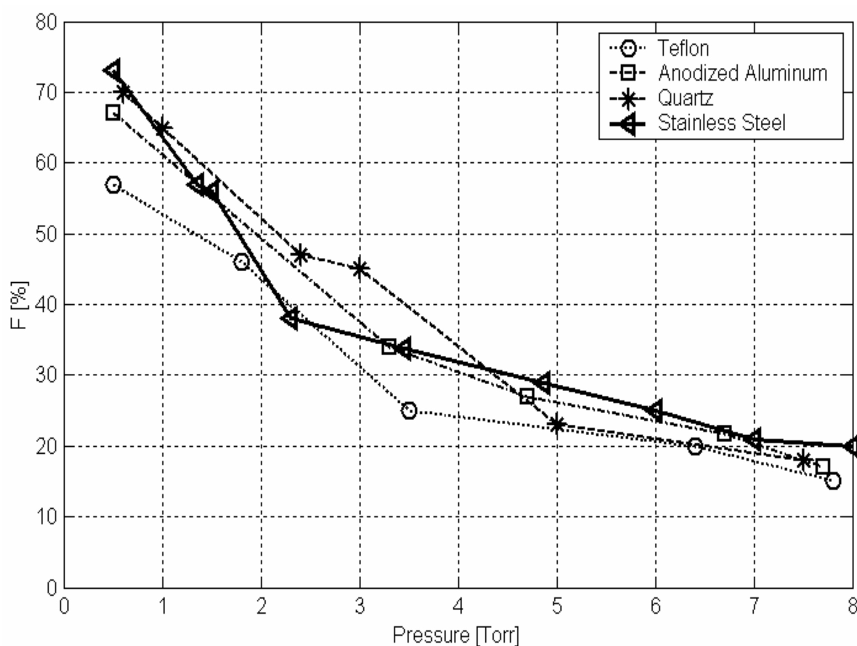

Figure 17: Fluorine atom percentage versus pressure for different wall materials. A plot of percentage of total F atoms in plasma found as molecular F_2 vs. total pressure for different wall materials as indicated in the figure.

CHAPTER 4: CLEANING OPTIMIZATION PROCESS IN HIGH DENSITY PLASMA CVD CHAMBER

4.1 Introduction

The specific CVD chamber studied in this work is used in microelectronics and is called a High Density Plasma CVD or HDP-CVD chamber. HDP-CVD reactor, targeted for advanced intermetal dielectric (IMD), shallow trench isolation (STI) and pre-metal dielectric (PMD) applications, can deposit both undoped and doped films for numerous processes including SiN, and "low k" films. The chamber's hardware set is also extendible to < 0.18-micron process applications, including ultra-low k < 3.0 materials. The fundamental difference between conventional dielectric CVD and HDP-CVD is the ability of the latter to provide void-free gap fill of a high-aspect ratio (as high as 3:1) metal structure with a film of excellent quality. This gap fill capability is the direct result of two simultaneous processes: deposition and sputter etch. Physical sputter etching with argon ions is extremely effective at low pressure (< 5 mTorr) on a biased substrate, a wafer clamped on an electrostatic chuck for heat removal purposes. Simultaneously, by using a high-density plasma source, it is possible to provide a high-deposition rate for the oxide while maintaining this low pressure. As a result, a deposition "from the bottom up" takes place to provide high-aspect ratio gap fill, with the sputtering responsible for keeping open the gap in the structure.

In an HDP-CVD reactor, the high plasma density combined with low pressure guarantees that the silane gas is present everywhere in the chamber, and is decomposed to silicon dioxide (SiO_2) everywhere. In addition, about 30% of the deposited film is

sputtered off of the wafer and migrates towards the walls. In consequence the reactor inevitably has a lot of deposition on all the exposed surfaces. If this unwanted deposited film should spall off as flakes, due to thermal expansion, stress, or abrasion, particles are generated that will fall onto the wafers. So periodic cleaning of the chamber walls is essential for semiconductor applications. To maximize the amount of film that can be tolerated before a chamber clean, the wall temperature is typically actively controlled. Without such control, the huge heat load encountered when the plasma is on would cause expansion of the chamber walls, stressing the film and probably leading to spalling from sharp corners and other surfaces.

Film removal is accomplished with an *in situ* RF high density plasma source which produce fluorine radicals' by dissociating cleaning gases such as CF_4 and C_2F_6. Most high density plasma sources have a plasma potential of only a few 10's of volts. In addition, many source types, such as an inductive source, require an insulating wall of for example ceramic material, which would tend to float to the chamber potential even if it were large. The result is that there is very little ion bombardment to assist cleaning at the walls. It is well-known in plasma etching that etching of SiO_2 with typical etchants (CF_4, C_2F_6) requires ion bombardment to proceed at a reasonable rate. Usage of C_2F_6 also causes environmental problems (see chapter 1.4). To obtain high cleaning rates in the absence of ion assistance and eliminate PFC emission, one is forced to use NF_3 as the fluorine precursor and operate at high pressures (e.g. 1 Torr). In this regime, the generation of copious amounts of monatomic fluorine allows for a reasonably fast purely chemical removal of the silica. However, other problems arise: at high pressures, the inductive plasma is strongly confined to the region near the walls, and in fact tends to be

localized near the center of the inductive coil. The resulting intense heating in that region can stress the ceramic casing and even cause cracking: a catastrophically expensive way to ensure a clean chamber. A further problem with HDP-CVD chamber cleans is that gas-flow levels have not been optimized adequately. Typically, cleaning recipes call for a higher gas-flow rate than is necessary for efficient film removal. Excess, unreacted NF_3 (relatively expensive gas) is wasted, resulting in unnecessary gas costs. Also, the fluorine molecules (recombined in transport tube) should be reactivated (dissociated) *in situ* with help of all (or combination) of available plasma sources in order to increase the effectiveness of gas utilization. All of these problems demand a detailed optimization of cleaning conditions to achieve maximum utilization for cleaning gas and high cleaning rates with minimal danger to the hardware.

A comprehensive model has been developed to study the optimization processes in a low-pressure high density plasma CVD reactor. The model couples plasma chemistry and transport self-consistently to fluid flow and gas energy equations. The model and the commercial simulation software Fluent CFD have been used to analyze fluorine-based plasma used in reactor cleaning.

4.2 Modeling Plasma Chemistry for Microelectronics Manufacturing

Plasma processing has become increasingly important in the microelectronics industry. The kinetics of the competing chemical reactions that occur within the CVD chamber affects almost every metric of the wafer process. Especially in low pressure (2-20 mTorr) plasma reactors, where transport processes are fast, gas-phase and surface

kinetics dominate the determination of etch rates, etch uniformity, etch selectivity, and profile evolution. Modeling and simulation, together with experimentation, can provide necessary information about the competing processes in a plasma reactor and allow better control of the process performance. In order for plasma reactor modeling to provide relevant information to reactor and process designers, however, the model must capture the kinetic phenomena. Although the literature contains a great deal of information on fundamental plasma phenomena, insufficient attention has been paid to methods for using this fundamental data in simulating real reactor conditions with complex gas mixtures and surface processes.

Successful numerical simulations of real plasma processing systems require compromises between the level of detail included in the model and the computational resources required. Such compromises often involve trade-offs between the descriptions of transport and chemistry. A simulation that treats transport issues in two or three dimensions will generally include simplified chemistry, while simulations that focus on a detailed description of the reaction kinetics generally use a simplified description of the transport in the reactor. There are several comprehensive reviews of plasma reactor models and modeling techniques [24], so only a brief discussion is included here, with an emphasis on the different data requirements for different approaches to plasma modeling summarized in Table 5.

Table 5: Data requirements for different plasma modeling approaches.

	Well mixed reactor models	**Continuum models**	**Models with Monte Carlo neutrals and ions, and continuum electrons**	**Models with continuum neutrals and ions, and Monte Carlo electrons**
Electron-impact cross sections				×
Electron-impact reaction-rate coefficients	×	×	×	
Neutral and ion rate coefficients	×	×	×	×
Fundamental transport parameters (e.g. Lennard-Jones parameters)			×	
Transport-properties (e.g. thermal conductivity, viscosity, diffusion coefficients)		×	× (electrons)	× (neutrals and ions)
Thermodynamic data	×	×	×	×
Surface reaction rates and probabilities	×	×	×	×

The simplest treatment of the transport in a plasma reactor is the use of ‘global’ or well-mixed-reactor approaches [25]. The formulation is similar to that of a perfectly stirred reactor (PSR) or continuously stirred tank reactor (CSTR), commonly used in chemical engineering. These compact models assume fast transport and focus instead on information about etching or deposition uniformity, but are computationally very fast. Such models are useful in providing first-cut understanding of plasma behavior and as tools for developing and testing reaction mechanisms. They require rate coefficients and thermodynamic data for the electron-impact, neutral and ion reactions of interest both in the gas-phase and at the surface.

Continuum models have been successfully applied to the plasma used for microelectronics processing [26], even though the pressures are below the range where continuum models of transport are generally considered reliable. In view of the fact that

transport processes are typically not rate limiting for either etching or deposition in an HDP reactor, the approximate description of the transport phenomena provided by the continuum models often suffices, despite large Knudsen numbers that characterize the reactor. In addition to the description of the chemistry, these models require transport properties for all the gas-phase species of interest.

Despite the success of the continuum models, the very low pressures (~2-20 mTorr) suggest that a non-continuum approach more accurately describes the transport phenomena in the reactor. To this end, several groups have developed direct-simulation Monte Carlo (DSMC) models for plasma-reactor simulation [27]. Although a Monte Carlo or other particle approach to transport modeling implies the direct use of collision cross sections, such detailed information for heavy-body collisions is often difficult to find. In practical DSMC implementations, therefore, cross sections are often derived from reaction-rate coefficients [28]. In this way, the input data requirements are not substantially different from those of a continuum model.

For models that include a kinetic description of the electrons, such as [25], electron cross sections are employed directly in the model. Such models typically solve the Boltzmann equation, either directly or through Monte Carlo techniques, to determine local electron-energy distribution functions. This information, together with the energy-dependent cross sections, allows determination of local reaction rates that depend not only on the mean electron energy but also on the local field and gas composition.

4.3 HDP-CVD Reactor Model

The schematic of HDP-CVD reactor is presented in Figure 18. The chamber is roughly cylindrical with diameter of 50 cm and the height of 20 cm. The diameter of the substrate is 35 cm while the diameter of the wafer is 30 cm. The dome of the chamber is made from the dielectric material (ceramic) while the substrate and the outlet walls are made from the non-dielectric material. The gas enters the chamber with the temperature of 300 K through 72 nozzles (ID = 0.057 cm) and has the following proportion: NF_3/Ar = 1/2, where NF_3 can vary from 0.7 slm to 1.5 slm and Ar can vary from 0.35 to 0.7 slm. The system operating pressure is constant and equals 2 Torr. The walls of the reactor, wafer region and the substrate are covered with the silicon (Si) deposits with the film thickness of up to 0.6 mkm. At the beginning of the cleaning process the temperature of the wafer reaches 400 K. There are two types of radio frequency (RF) discharges that could be ignited inside the system: inductively coupled plasma (ICP) and capacitively coupled plasma (CCP). The first ICP discharge can be ignited at the top of the reactor from the flat antenna located at the top. The flat antenna generates a plasma power up to 5 kW with the frequency up to 2 MHz. The second ICP is toroidal-like discharge generated by the RF coils surrounding the chamber wall. The second ICP can also generate a plasma power up to 5 kW and frequency up to 2 MHz. The capacitively coupled discharge could be ignited at the region close to the substrate and the outlet zone of the chamber. The CCP discharge operates at the frequency of 13.65 MHz and can generate a power up to 10 kW.

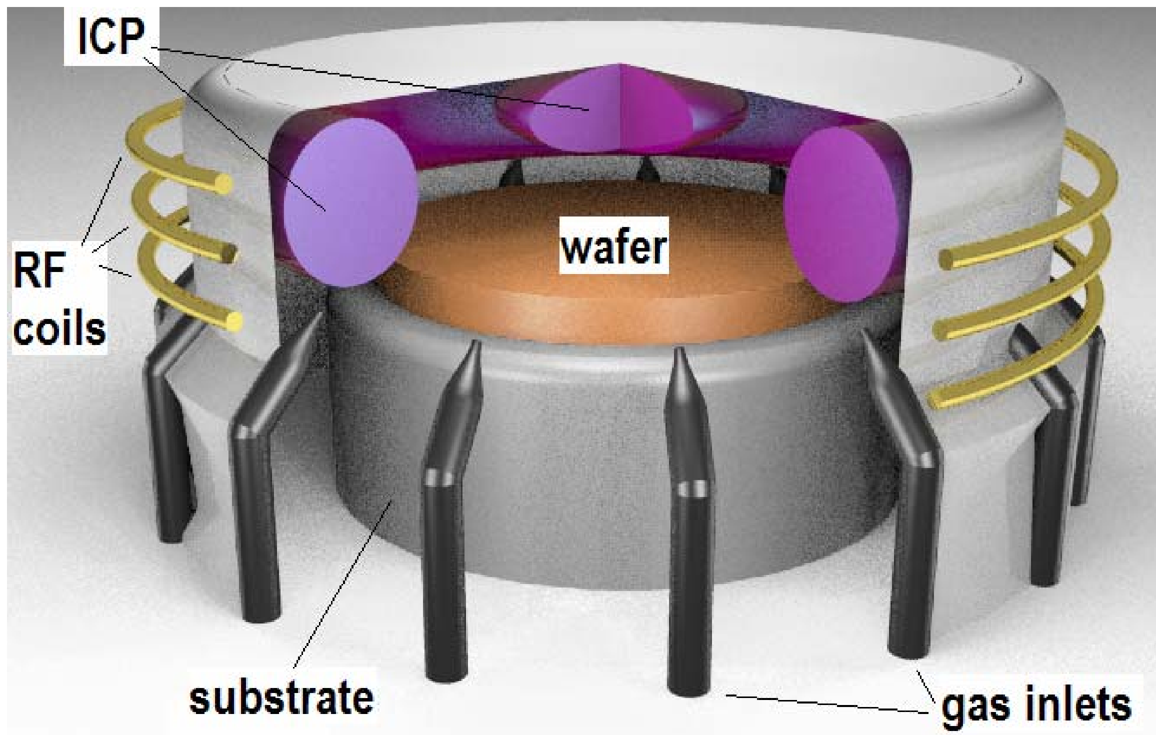

Figure 18: Schematic of HDP-CVD reactor.

4.3.1 Continuum Approach

Analyzing all possible models used for transport modeling in plasma reactors, the choice was given to the continuum model which works well at low Knudsen numbers (K_n<0.2). The Knudsen number is defined as the ratio of free mean path λ to the characteristic length L:

$$\mathbf{K_n = \frac{\lambda}{L}}$$

The free mean path of the fluorine is 3×10^{-3} cm [29] and the characteristic length of the chamber is 25 cm. The corresponding Knudsen number is 1.2×10^{-4} which is much smaller than the critical value 0.2. In two-dimensional geometry with steady-state

conditions the continuum model couples Navier-Stokes equations, gas energy equation and mass conservation equations for neutrals and charged species. The continuum model was built and the described equations were solved using commercial Fluent CFD software (www.fluent.com).

Continuity Equation. For two-dimensional (2D) axisymmetric geometries, the equation for conservation of mass, or continuity equation, as follows

$$\frac{\partial \rho}{\partial t}+\frac{\partial}{\partial x}(\rho u)+\frac{\partial}{\partial r}(\rho \upsilon)+\frac{\rho \upsilon}{r}=S_m$$

where x is the axial coordinate, r is the radial coordinate, u is the axial velocity, and υ is the radial velocity. The source S_m is the mass added to the continuous phase from the user-defined source (plasma mode).

Momentum Conservation Equations. For 2D axisymmetric geometries, the axial and radial momentum conservation equations are given by

$$\frac{\partial}{\partial t}(\rho u)+\frac{1}{r}\frac{\partial}{\partial x}(r\rho uu)+\frac{1}{r}\frac{\partial}{\partial r}(r\rho \upsilon u)=-\frac{\partial p}{\partial x}+\frac{1}{r}\frac{\partial}{\partial x}\left[r\mu\left(2\frac{\partial u}{\partial x}-\frac{2}{3}(\nabla\cdot\vec{\upsilon})\right)\right]+ \\ +\frac{1}{r}\frac{\partial}{\partial r}\left[r\mu\left(\frac{\partial u}{\partial r}+\frac{\partial \upsilon}{\partial x}\right)\right]$$

and

$$\frac{\partial}{\partial t}(\rho \upsilon)+\frac{1}{r}\frac{\partial}{\partial x}(r\rho u\upsilon)+\frac{1}{r}\frac{\partial}{\partial r}(r\rho \upsilon\upsilon)=-\frac{\partial p}{\partial r}+\frac{1}{r}\frac{\partial}{\partial x}\left[r\mu\left(2\frac{\partial \upsilon}{\partial x}+\frac{\partial u}{\partial r}\right)\right]+ \\ +\frac{1}{r}\frac{\partial}{\partial r}\left[r\mu\left(2\frac{\partial u}{\partial r}-\frac{2}{3}(\nabla\cdot\vec{\upsilon})\right)\right]-2\mu\frac{\upsilon}{r^2}+\frac{2}{3}\frac{\mu}{r}(\nabla\cdot\vec{\upsilon})+\rho\frac{w^2}{r}$$

where

$$\left(\nabla\cdot\vec{\upsilon}\right)=\frac{\partial\mathbf{u}}{\partial\mathbf{x}}+\frac{\partial\upsilon}{\partial\mathbf{r}}+\frac{\upsilon}{\mathbf{r}}$$

and *w* is the swirl velocity.

Energy Equation. Fluent CFD solves the energy equation in the following form

$$\frac{\partial}{\partial\mathbf{t}}\left(\rho\mathbf{E}\right)+\frac{\partial}{\partial\mathbf{x_i}}\left(\mathbf{u_i}\left(\rho\mathbf{E}+\mathbf{p}\right)\right)=\frac{\partial}{\partial\mathbf{x_i}}\left(\mathbf{k_{eff}}\frac{\partial\mathbf{T}}{\partial\mathbf{x_i}}-\sum_{j'}\mathbf{h}_{j'}\mathbf{J}_{j'}+\mathbf{u_j}(\tau_{ij})_{eff}\right)+\mathbf{S_h}$$

where k_{eff} is the effective conductivity and $J_{j'}$ is the diffusion flux of species j'. S_h includes heat of chemical reactions

$$\mathbf{S_h}=\sum_{j'}\left[\frac{\mathbf{h}^{\circ}_{j'}}{\mathbf{M}_{j'}}+\int_{\mathbf{T}_{ref_{j'}}}^{\mathbf{T_{ref}}}\mathbf{c}_{p,j'}\mathbf{dT}\right]\cdot\mathbf{R}_{j'}$$

where h_j° is the enthalpy of formation of species j' and R_j' is the volumetric rate of creation of species j',

and

$$\mathbf{E}=\mathbf{h}-\frac{\mathbf{p}}{\rho}+\frac{\mathbf{u_i^2}}{\mathbf{2}}$$

where sensible enthalpy *h* is defined for ideal gases as

$$\mathbf{h}=\sum_{j'}\mathbf{m}_{j'}\mathbf{h}_{j'}$$

and for incompressible flows as

$$\mathbf{h}=\sum_{j'}\mathbf{m}_{j'}\mathbf{h}_{j'}+\frac{\mathbf{p}}{\rho}$$

$m_{j'}$ is the mass fraction of the species j' and

$$\mathbf{h_{j'}} = \int_{T_{ref}}^{T} \mathbf{c_{p,j'} dT}$$

where T_{ref} is 298.15 K.

4.3.2 Plasma Chemistry Module

To describe plasma processes in the reactor we built a Plasma Chemistry Module (PCM) which coupled together with Fluent CFD as user-defined source code. The plasma models that have a continuum treatment of the electron and energy employ reaction rates that depend on the mean electron energy. Electron-collision cross sections $\sigma(\varepsilon)$ are converted to reaction rate coefficients through the following integration

$$\mathbf{k} = \int_0^\infty \mathbf{f}(\varepsilon)\left(\frac{2\varepsilon}{\mathbf{m_e}}\right)^{1/2} \sigma(\varepsilon)\mathbf{d}\varepsilon \qquad \mathbf{(4.1)}$$

where k is the reaction-rate coefficient, $f(\varepsilon)$ is the electron energy distribution function (EEDF), and m_e is the electron mass. This integration is straightforward, provided that one knows the form of the EEDF. In that case, the mean electron temperature is determined as

$$\mathbf{T_e} = \frac{2}{3}\frac{\varepsilon}{\mathbf{k_B}} = \frac{2}{3\mathbf{k_B}}\int_0^\infty \varepsilon \cdot \mathbf{f}(\varepsilon)\mathbf{d}\varepsilon \qquad \mathbf{(3.2)}$$

where k_B is the Boltzmann constant. However, an accurate determination of the local EEDF requires a spatially dependent kinetic simulation, either through particle treatment of the electrons or through direct solution of the Boltzmann equation. Ideally such treatment could couple the determination of local plasma conditions (e.g. composition,

percent ionization) and electrodynamics with the calculations of kinetic rates. This approach is computationally prohibited in most practical cases, and many modelers instead use a form of the EEDF that will allow an a priori determination of $k(T_e)$, where T_e is found through solution of an electron energy equation.

The simplest approach to treating the electron kinetics is to assume a Maxwellian distribution function that is related directly to the mean electron temperature. The use of a Maxwellian distribution assumes steady-state equilibrium conditions and neglects effects of inelastic collisions on the distribution function. The inaccuracies of this approach are generally overwhelmed by the uncertainties in the reaction cross sections, expect for a few special cases, such as rare gases. For this reason, because the computational efficiency and simplicity of the approach provides a path for achieving fast engineering results, Maxwellian distribution functions have been used extensively in modeling of high density plasma systems [24]. Assuming a Maxwellian EEDF, equation (4.1) becomes

$$\mathbf{k} = \left(\frac{8}{\pi m_e}\right)^{1/2} \left(\frac{1}{k_B T_e}\right)^{3/2} \int_0^\infty \varepsilon \cdot \sigma(\varepsilon) \cdot e^{-\varepsilon / k_B T_e} d\varepsilon \qquad (4.3)$$

Once the relationship between k and T_e is established, use of the Fluent CFD software suite of software requires this function to be reduced to a set of fit coefficients. The default for fitting coefficients in Fluent is the modified Arrhenius form

$$\mathbf{k}(T_e) = A \cdot T_e^B \cdot \exp\left(\frac{C}{T_e}\right) \qquad (4.4)$$

Alternatively, the fit to the Arrhenius form could be made more accurately by limiting it to a smaller temperature range based on knowledge of the targeted reactor process.

Reactions Considered. Because our studies targeted only the optimization of the cleaning process inside of HDP-CVD we are limiting ourselves to the consideration of only the major reactions involved in the cleaning process such as

- reaction of direct electron-impact dissociative collision;
- thermal dissociation reaction;
- volume recombination reaction;
- etching reaction.

The species involved in the modeling are: F, F_2 and Ar. The electron concentration and temperature are assumed to be constant and corresponds to the typical values of the given plasma source.

Electron-Impact Dissociation. Electron collisions are the driving mechanism behind the plasma processes employed in the semiconductor industry. Gas discharges are maintained by electron-neutral ionization, and energy is lost in part by collisional energy losses such as ionization, excitation and elastic scattering. In molecular gases, electron impact dissociation is the key player in much of the chemistry; as well as being an energy-loss-mechanism. The only electron-impact dissociation reaction, which takes place in considered reactor, is the reaction of dissociation of molecular fluorine (F_2)

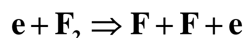

$$\mathbf{e + F_2 \Rightarrow F + F + e}$$

Fluorine is a shell-closed molecule with a ${}^{1}\sum_{g}^{+}$ ground state. The fluorine molecule is known to dissociate into neutral fluorine atoms (F) via various electronic state excitations. Electron-impact dissociation of the fluorine molecule is considered to take place via two classes of excited electronic states, purely repulsive or strongly perturbed by Rydberg valence-ionic potential energy curve crossing [31]. The first class

consists of all the 11 valence states of molecular fluorine that dissociate into two ground state fluorine atoms. The 11 valence excitation processes can be divided into one-electron molecular orbital transition that characterize the five valence states, $^{1,3}\Pi_u$, $^{1,3}\Pi_g$, $^3\Sigma_u^+$, and two-electron molecular orbital transitions, $^3\Sigma_g^-$, $^3\Sigma_u^-$, $^1\Sigma_g^+$, $^1\Sigma_u^-$, $^1\Delta_g$, $^3\Sigma_u^+(2)$. The rate coefficient for the dissociation of the fluorine molecule (k_d) was calculated from the excitation cross sections for one-electron molecular orbital transitions, $\alpha^3\Pi_u$ (threshold 3.21 eV), $A^1\Pi_u$ (threshold 4.34 eV), $^3\Pi_g$ (threshold 7.0 eV), $^1\Pi_g$ (threshold 7.5 eV) and $^3\Sigma_u^+$ (threshold 7.6 eV) [32]:

$$k_d = 1.18\times10^{-14}\exp\left(-\frac{6.88}{T_e}+\frac{1.11}{T_e^2}\right) \qquad [m^3/sec]$$

Thermal Dissociation: Table 8 shows that the gas temperature inside of inductive coupled plasma is very high and reaches 10^4 K. However, with the gas temperatures > 1300 K the molecular fluorine starts to dissociate in a thermal process

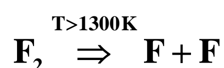

$$F_2 \overset{T>1300K}{\Rightarrow} F+F$$

Different data for the thermal reaction rate coefficients (k) were taken from the NIST (National Institute of Standards and Technology) chemical kinetics database (www.nist.gov) and gathered in Table 6. The data are given in Arrhenius form. For simulations the average value of thermal reaction rate coefficient was chosen, k = 4.8×10^{13} (cm^3/mole-s).

Table 6: Data from NIST database. Thermal dissociation of fluorine.

Gas Temperature, K	A, cm^3/mole-s	E_a / R, K
1400-2600	2.12×10^{13}	16970
1400-2600	9.84×10^{13}	17510
1400-2000	2.00×10^{13}	17610
1400-1600	3.59×10^{13}	19977
1400-1600	9.84×10^{13}	17512
1000-2000	4.57×10^{12}	14340
2200-3600	1.52×10^{12}	12038
1400-2000	2.00×10^{13}	17612
1300-1600	3.09×10^{12}	13737
1300-1600	7.08×10^{12}	15096

Volume Recombination. The three-body recombination reaction between fluorine atoms is important and present in the model:

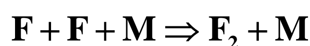

$$\mathbf{F + F + M \Rightarrow F_2 + M}$$

The rate constants for three-body recombination reactions are found in the literature and shown in Table 7. From the data presented in Table 7 the latest obtained rate coefficient (k_2 = 2.8E-34 cm^6/s) was chosen for simulations. This rate coefficient is also an average value among the others.

Table 7: Three-body recombination reaction rate constants.

k, cm^6/s	References:	Year of Publication
$k_1 = 8.0\times10^{-35}$	[33]	1974
$k_2 = 2.8\times10^{-34}$	[34]	1997
$k_3 = 6.0\times10^{-34}$	[32]	1977
$k_4 = 2.0\times10^{-33}$	[35]	1976
$k_5 = 2.4\times10^{-33}$	[36]	1987

Etching reaction. A broad understanding of the rates and mechanisms by which free radicals react with various substrates is important for the development and selection of plasma-etching techniques. Although fluorine atoms are the principal gaseous reactant

in many common etching processes, relatively little information is available on the reaction of these radicals with common semiconductor materials. Several investigators [37] have shown that an apparent continuum centered at 632 nm accompanies the etching of silicon by fluorine. Donnelly and Flamm [38] studied the spectrum of the chemiluminescence and compared it with spectra from species in the discharge and afterglow regions of an SiF_4 discharge. In other work the reaction probability for etching of silicon dioxide by F atoms and the etch ratio of Si and SiO_2 at room temperature was reported [39]. In [40] the etching of silicon by F atoms and intensity of the concomitant luminescence were measured as a function of temperature (223-403 K) and F atom concentration ($n_F \approx 5.5\times10^{15}$ cm^{-3}). The etching of SiO_2 was also measured in order to determine simultaneously the ratio of Si and SiO_2 etch rates. According to [40], the etch rate of SiO_2 by F atoms is

$$\mathbf{R_{F(SiO_2)} = 6.14 \pm 0.49 \times 10^{-13} n_F T^{1/2} \exp\left(-\frac{0.163}{k_b T}\right) \qquad [\mathring{A}/min]}$$

where T is the gas temperature and k_b is the Boltzmann constant (k_b = 1.3807×10^{-23} JK^{-1}). The reaction probability for SiO_2 is

$$\mathbf{\xi_{F(SiO_2)} = 0.0112 \pm 0.0009 \cdot \exp\left(-\frac{0.163}{kT}\right)}$$

where it is assumed that the final reaction product formed on the surface of SiO_2 by F atoms is SiF_4. The etch rate of Si by F atoms is

$$\mathbf{R_{F(Si)} = 2.91 \pm 0.20 \times 10^{-12} n_F T^{1/2} \exp\left(-\frac{0.108}{kT}\right) \qquad [\mathring{A}/min]}$$

The present rates and activation energies are also consistent with those reported for *in situ* etching of Si and SiO_2 in F atoms containing plasmas at pressures of 1 Torr (CF_4, SiF_6,

NF_3) [41]; consequently the F atom solid reaction alone can generally account for these data. It appears that ion or electron bombardment does not play an essential role in the etching of Si or SiO_2 by F-atom-containing plasmas in the few-tenths of a Torr pressure range, consistent with the isotropic nature of these etchants.

In current work only the etching of Si deposits by atomic fluorine was considered. The corresponding surface reaction describing this process is

$$\mathbf{Si_{(surface)} + 4F_{(gas)} \Rightarrow SiF_{4(gas)}}$$

and the etch rate for this reaction is chosen as above.

4.4 Inductively Coupled Plasma

The inductively-coupled plasma (ICP) is one type of electrodeless discharge that has recently being applied in microfabrication processes due to its relative simplicity, efficient use of power, long lifetime using reactive gases, and low process contamination.

The inductively coupled plasma ignited inside of dielectric chamber by applying the RF voltage on the solenoid coils surrounding the chamber. The current flow in the coil generates a magnetic field in the direction perpendicular to the plane of the coils. This time-varying magnetic field creates a time-varying electric field (wrapping around the axis of the solenoid). The field strength is proportional to the radial distance and the frequency. The electric field induces a circumferential current in the plasma. The electrons thereby accelerated gain energy, creating enough hot electrons to sustain the plasma through ionization. Once the plasma forms, the magnetic fields are screened by the induced currents, just as in a metal: in operation, the magnetic field penetrates into the

chamber to a depth determined by the magnetic skin depth, which is in turn set by the plasma conductivity and thus by the plasma density and the pressure.

Inductive plasma is high-density plasma and generates electrons and ions more efficiently than capacitive plasma, and can achieve electron densities of 10^{12} cm^{-3} at pressures of a few mTorr, as much as 100 times higher than comparable capacitive plasma. The inductive plasma has relatively low plasma potential, and results in little ion bombardment of surfaces. The electron temperature in ICP with the pressure range of 1-2 Torr is approximately 3 eV. The inductively coupled plasma parameters summary is presented in Table 8.

Table 8: Inductively coupled plasma parameters.

Parameters	Typical Values
Frequency	10 - 100 MHz
Gas Pressure	1 Torr - 10 Atm
Power Level	1 kW - 1 MW
Gas Temperature	10^3 K - 10^4 K

4.5 Capacitively Coupled Plasma

Capacitive radio frequency discharges (CRF or sometimes CCRF Capacitively Couple Radio Frequency) are widely used discharges for industrial applications. The choice of the radio frequency is mostly dictated by practical considerations. In fact the usual industrial frequency is 13.56 MHz, which is in the radio frequency range. The great majority of publications are devoted to this particular frequency for different gases (He,

N_2 and Ar). Another reason is that the electrical apparatus for the plasma radio frequency generator is simpler if compared with for example a microwave system.

The capacitive coupled plasma is excited and sustained by applying a RF voltage between two electrodes. The “capacitive” moniker arises from the nature of the coupling to the plasma. The plasma forms “sheaths”, regions of very low electron density, with solid surfaces: the RF voltage appears mostly across these sheaths as if they were the dielectric region of a capacitor, with the electrode and the plasma forming the two plates. In practice, the system pressure is typically between about 100 mTorr and 10 Torr and electron temperatures are around 5 eV. Electron temperature varies weakly with other parameters: it is dominated by the requirement that the electrons provide enough ions to keep the plasma going. The ions are mainly lost by diffusion to the walls in low-pressure plasma. The ion density is set by the balance between the input power, which heats the electrons and provides energy to ionize, and the loss of ions to the walls. Plasma density in capacitive plasmas is low: the fractional ionization is only about 0.01 % (1 molecule in 10,000 is ionized). Fractional excitation can be much higher, since excitation and dissociation usually require less energy than ionization. The electrons are distributed in a vaguely Maxwellian fashion, as $\exp(-E/k_bT_e)$. The typical values for the CCP parameters are presented in Table 9.

Table 9: Capacitively coupled plasma parameters.

Parameters	Typical Values
Frequency	13.56 MHz
Gas Pressure	3 mTorr - 5 Torr
Power Level	50 W - 500 W
Electrode Voltage	100 V - 1000 V
Current Density	0.1 - 10 mA/cm^2
Electron Temperature	3 eV - 8 eV
Electron density	10^{15} - 10^{17} m^{-3}
Ion Energy	5 eV - 100 eV

4.6 Estimation of Power Consumption

The estimation of power consumption is the important step in the modeling involving the detailed consideration of many fundamental aspects. Here, we consider the power consumption necessary only for dissociation of fluorine molecules. The dissociation can be performed by both plasmas CCP and ICP. However, because the high-density ICP discharge has low plasma potential resulting in relatively low ion bombardment it considered as a primary plasma discharge used in fluorine dissociation. The CCP discharge is considered to be as a secondary or auxiliary discharge which helps to sustain the ICP discharge and to dissociate fluorine remains.

The fundamental formula for estimation of power consumption in discharge as following

$$\mathbf{W_0 = Q_0 n_0 \varepsilon_0}$$

where n_0 is the gas concentration, Q_0 is the gas flow rate, ε_0 is energy cost of dissociation per one molecular fluorine. It is not necessary for electron to dissociate a

molecule of fluorine from the first electron-impact collision. In discharge the electron loses his energy on a variety of processes such as excitation, ionization and attachment before it comes to dissociation of F_2. Thus, the energy cost of fluorine dissociation (ε_0) has to take into account the energy losses for all these processes. Considering this fact, the energy cost of fluorine dissociation can be represented in the following expression

$$\varepsilon_0 = \frac{k_{diss} \cdot \varepsilon_{diss} + k_{ioniz} \cdot \varepsilon_{ioniz} + k_{attach} \cdot \varepsilon_{attach} + \sum_i (k_{excit} \cdot \varepsilon_{excit})_i}{k_{diss}}$$

where k is rate coefficient of the corresponding reaction and ε is the energy loss on the corresponding process. For all reactions (dissociation, attachment, etc.) containing an interaction with an electrons, the rate coefficients depend on average electron temperature. The typical (average) electron temperature for different type of the discharge is different. Thus, the typical electron temperature of ICP discharge is 3 eV while the typical electron temperature for CCP discharge is 5 eV. The data on the energy losses in the corresponding processes in fluorine plasma are taken from the paper of Jon Tomas Gudmundsson [42] and summarized in Table 10.

Table 10: Energy losses of the electron and corresponding rate coefficients in the fluorine gas.

Process (reaction)	Energy Loss, eV	ICP: k, m^3s^{-1}	CCP: k, m^3s^{-1}
Dissociation	4.7	0.11×10^{-15}	1.30×10^{-15}
Attachment	0.5	0.15×10^{-15}	0.46×10^{-15}
Ionization (F^+)	15.5	0.05×10^{-15}	0.52×10^{-15}
Ionization (F_2^+)	15.7	0.01×10^{-15}	0.20×10^{-15}
Excitation ($\sum_i$)	13.0	0.27×10^{-15}	2.57×10^{-15}

Referring to Table 10 and the equation above the energy cost of fluorine dissociation in inductively coupled plasma is

$$\varepsilon_{ICP} = \frac{k_{diss} \cdot \varepsilon_{diss} + k_{ioniz} \cdot \varepsilon_{ioniz} + k_{attach} \cdot \varepsilon_{attach} + k_{excit} \cdot \varepsilon_{excit}}{k_{diss}} \approx 40 \quad eV$$

In high temperature plasma (ICP), however, the cost of dissociation of molecular fluorine would be lower because in this case the reaction of thermal dissociation becomes effective. It was discussed previously that the thermal dissociation reaction takes place when the gas temperature is high (> 1300 K).

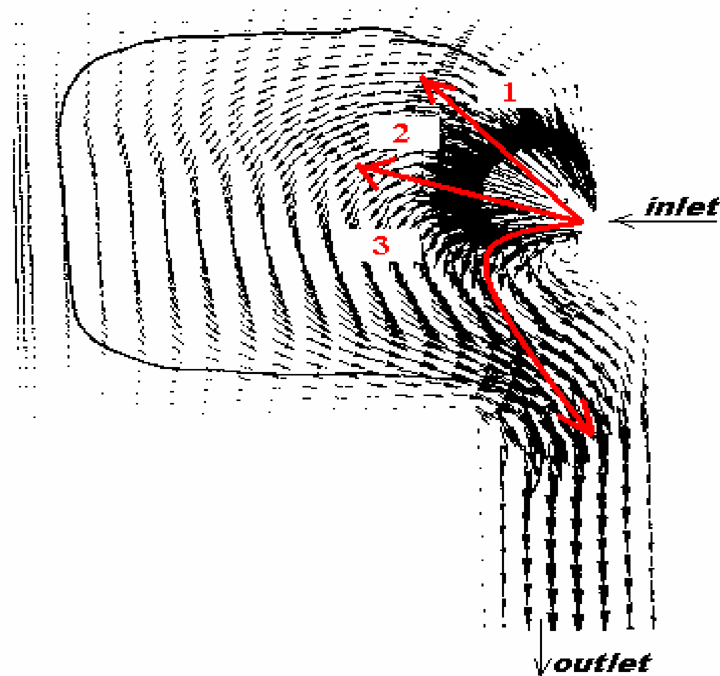

Figure 19: Velocity vectors in HDP-CVD reactor.

Analyzing the picture of velocity vectors in HDP-CVD, Figure 19, one can assume that only 2/3 of all inlet gas passes the ICP zone, therefore the equation for power consumption in ICP discharge becomes

$$\mathbf{W_0 = \frac{2}{3} Q_0 n_0 \varepsilon_0}$$

Knowing gas concentration, gas flow rate and energy cost of fluorine dissociation the power consumption in ICP discharge can be easily estimated and it's equal to 0.25 kW.

The electron with higher energy (capacitive coupled plasma, where T_e = 5 eV) dissociates more easily then the one with the lower energy (inductively coupled plasma, where T_e = 3 eV), i.e. it does not spend his energy on an intermediate processes as an attachment, excitation or ionization. Therefore, neglecting all these processes, the energy cost of fluorine dissociation in capacitively coupled plasma becomes

$$\varepsilon_{CCP} = \frac{k_{diss} \cdot \varepsilon_{diss} + k_{ioniz} \cdot \varepsilon_{ioniz} + k_{attach} \cdot \varepsilon_{attach} + k_{excit} \cdot \varepsilon_{excit}}{k_{diss}} \approx \frac{k_{diss} \cdot \varepsilon_{diss}}{k_{diss}} \approx 5 \quad eV$$

Because the CCP discharge in our system is ignited in the outlet area (near the wafer and inlets) all gas will pass this discharge region. In this case, by analogy with ICP discharge, the power consumption in CCP is 0.4 kW.

4.7 Estimation of Plasma Volume

The plasma volume can be estimated using the equation from gas discharge theory [29]:

$$\mathbf{W = \frac{\sigma \cdot E^2}{2} \cdot V}$$

where W is an applied power, E is an electric field, V is the plasma volume and σ is the plasma conductivity. The equation for plasma conductivity as following

$$\sigma = n_e \cdot e \cdot \mu_e$$

where n_e is an electron concentration (each plasma type has its own typical electron concentration range), e is an electron charge 1.6×10^{-19} C and μ_e is an electron mobility. The equation for electron mobility as following

$$\mu_e = \frac{e}{m_e \cdot \nu}$$

where ν is an electron collision frequency and m_e is an electron mass. The electron collision frequency is also depends on the discharge nature. For example, in case of capacitive coupled plasma in fluorine gas with low pressure (p = 2 Torr) the electron collision frequency is approximately 100 times exceed the driving frequency $\omega = 2\pi f$, where f =13.65 MHz (for CCP). Thus, the electron driving frequency is 0.86×10^{8} s^{-1} and the electron collision frequency is 0.86×10^{10} s^{-1}. In CCP plasma with the average electron concentration of 10^{10} cm^{-3} the ratio of electric field to the operating pressure is 10 $Vcm^{-1}Torr^{-1}$, therefore, for pressure 2 Torr the electric field will be 20 Vcm^{-1}. Finally, knowing the applied power (see the estimation of power consumption in previous section) the estimated volume for the capacitive coupled plasma is 0.005 m^3. The plasma volume of inductively coupled plasma can be estimated by analogy.

4.8 Results and Discussion

The estimated energies and plasma volumes were implemented into the Fluent CFD as the source terms. In the simulation results, first of all, we are interested in an etch

rates in different chamber zones and corresponding etch times for these zones and the total etch time. The species balance is also has to be calculated after each simulation process in order to track the outgoing amount of unprocessed fluorine. To consider the worst case scenario it was assumed that atomic fluorine does not enter the CVD chamber, i.e. all F-atoms recombine in a transport tube. Because of the problem complexity and difficulties in data analysis the chamber walls were virtually divided on seven zones. Each zone corresponds an intermediate film thickness (i.e. the Si residuals which have to be cleaned), Table 11.

Table 11: Intermediate film thickness for corresponding zone.

Zone, #	3	1	7(axis)	2	5	4	6
Film Thickness, mkm	0.6	0.4	-	0.3	0.3	0.35	0.35

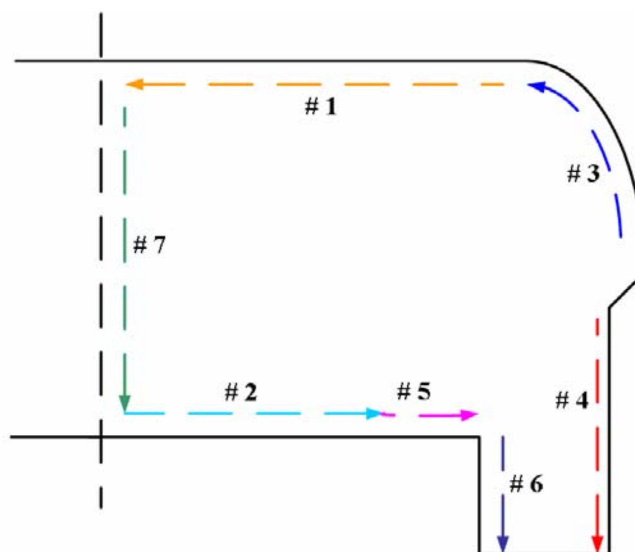

Figure 20: Zone numbering in HDP-CVD reactor.

Side Inductively Coupled Plasma. First simulation results were obtained for the side ICP (toroidal-like) discharge only (i.e. the regime where the only side RF coils are generate an electromagnetic field) and directed to NF_3 gas flow optimization. Typically, cleaning recipes call for a higher gas-flow rate than is necessary for efficient film removal. Excess, unreacted NF_3 is wasted, resulting in unnecessary gas cost. However, different CVD chambers require different analysis in gas flow optimization. In our HDP-CVD reactor we study the simulation results within available flow rates range (0.7 slm - 1.5 slm). The simulation results show that with an increasing the flow rates the corresponding etching rates do not increase. It actually means that within the given flow rates range our etching mechanism is limited to the surface recombination reaction and thus, there is no reason to increase the flow rate higher than 0.7 slm. With the flow rates lower than 0.7 slm the etching mechanism is limited by diffusion resulting in lower etch rates. Thus, the NF_3 flow rate of 0.7 slm is seems to be reasonable for ICP regime and is used in further analysis of simulation results.

In Figure 21 the temperature distribution inside of the chamber is shown. The red zone representing the highest temperature (2440 K) is an actually the discharge zone. The Figure 22 shows the contours of mole fraction of fluorine atoms producing in side ICP discharge. The maximum mole fraction of F atoms is in the discharge zone where it's produced. Because fluorine radicals are lost in surface and volume recombination process there is no atomic fluorine at the outlet. The Figure 23 shows the corresponding etch rates. The side ICP regime has the maximum etch rates are at the top of the chamber. The etch rates at the outlet walls (zones 4 and 6) is almost zero because of the shortage of reactive gas. The summaries of average etch rates and corresponding residence times are

presented in Table 12. The average etch rate of the corresponding zone is the ratio of the integral of the etch rate of the zone over the surface of this zone and the integral of the corresponding surface

$$\mathbf{R}_{\mathbf{average}} = \frac{\int\limits_{\mathbf{surf}} \mathbf{R\,dS}}{\int \mathbf{dS}}$$

As seen in Table 12 the etch rates at the top of the reactor (zones 3, 1) have the highest value, and the etch time necessary to clean these zones is 50.7 s. The time necessary for cleaning the lower zones (2, 5, 4 and 6) is 87.5 s which is also a total cleaning time. Thus, the reacting gas will flow for about 36.8 s over the top zones which have already been cleaned. This can cause substantial overetching of chamber and kit hardware. Given the high costs of NF_3 gas, process tool time, and chamber kits, the overetching would quickly result in essential losses.

Because of the high temperature in ICP discharge zone the volume recombination reaction rate of fluorine is very low having no effect on plasma volume kinetics and etching. The dilution gas such as argon (Ar) or helium (He) is always added to the plasma systems. Argon is probably the most favored primary plasma gas and sometimes is used with a secondary plasma gas (hydrogen, helium and nitrogen) to increase its energy. Argon is the easiest of these gases to form plasma and tends to less aggressive towards electrode and nozzle hardware. Most plasmas are started up using pure argon. Argon is a noble gas and is completely inert to all spray materials. Helium is mainly used as a secondary gas with argon. Helium is a noble gas and is completely inert to all spray materials and is used when hydrogen or nitrogen secondary gases have deleterious effects. It is commonly used for high velocity plasma spraying of high quality carbide

coatings where process conditions are critical. Because helium imparts good heat transfer properties it is not recommended to use it in ICP plasma.

The simulation results show that the highest etch rates comes with the minimum of dilution gas (Ar). From the other side, the power consumption will increase dramatically without the presence of Ar. It was shown in [7] that for the reasonable result the ratio of etching gas (NF_3) and dilutant (Ar) should be 1/2. Therefore, for 0.7 slm of NF_3 the flow rate of Ar should be 0.35 slm.

Table 12: Average etch rate and corresponding etch time for each zone. Side ICP only.

Zone #	Intermediate Film Thickness, mkm	Average Etch Rate, kA/min	Etch Time, s
3	0.6	7.1	50.7
1	0.4	7.0	33.8
7	-	-	-
2	0.3	4.0	45.0
5	0.3	2.4	75.0
4	0.35	2.4	87.5
6	0.35	2.8	75.0

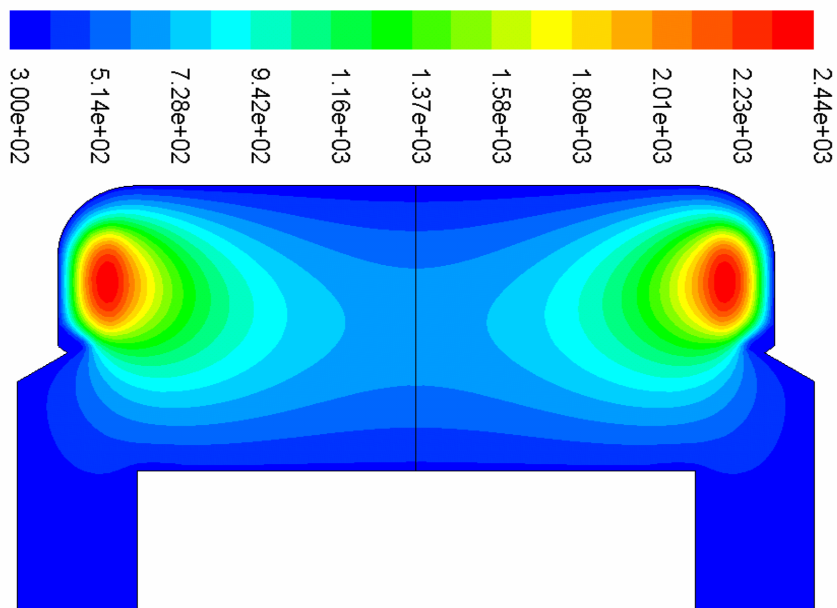

Figure 21: Contours of static temperature, K. Side ICP only.

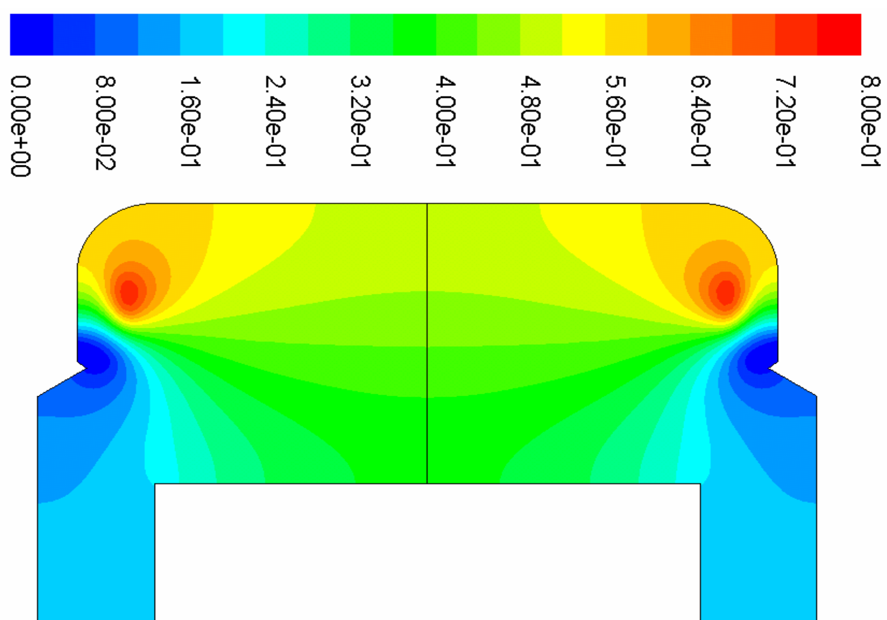

Figure 22: Contours of mole fraction of F atoms. Side ICP only.

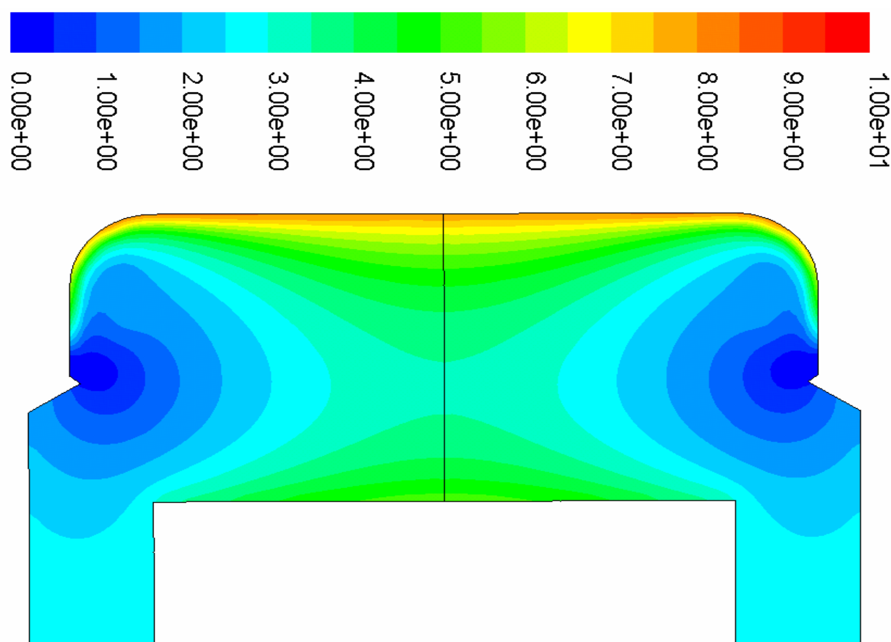

Figure 23: Contours of etch rate. Side ICP only.

Because the argon does not react with any other species and hardly stick to the surface its concentration remains constant during the all cleaning process. Nitrogen (N_2) has high bond energy (10 eV) and hardly dissociates in low energy plasma. The intermediate species formed by nitrogen atoms such as NF, NF_2 are very unstable and quickly decompose in a high temperature environment. The nitrogen itself also does not react with other species. The atomic fluorine mainly participates in the formation of SiF_4 molecules but still some amounts of it recombine in the gas-phase producing F_2 molecules. The cleaning products outgoing from the system are F_2, N_2, Ar and SiF_4.

Upper Inductively Coupled Plasma. The abilities of secondary (upper) inductively coupled plasma are also explored in this study. The flow rates for the inlet gases are the same as is used for side ICP discharge. The contours of mole fraction of fluorine atoms are shown in Figure 24 and corresponding contours of etch rates are shown in Figure 25.

As seen from both figures the upper ICP discharge is very local. The fluorine atoms produced in discharge do not propagate further through the system resulting in extremely low etching rates and overall cleaning efficiency, Table 13. The low values of the flow rates in the middle of the chamber result in discharge localization and low etch rates. In this regime plasma could not be thoroughly sustained by upcoming gas. The valuable result in etch rate is obtained only in zone #1, Table 13.

Table 13: Average etch rate and corresponding etch time for each zone. Upper ICP only.

Zone #	Intermediate Film Thickness, mkm	Average Etch Rate, kA/min	Etch Time, s
3	0.6	1.0	360
1	0.4	5.0	48
7	-	-	-
2	0.3	0.81	225
5	0.3	0.42	428
4	0.35	0.50	420
6	0.35	0.54	389

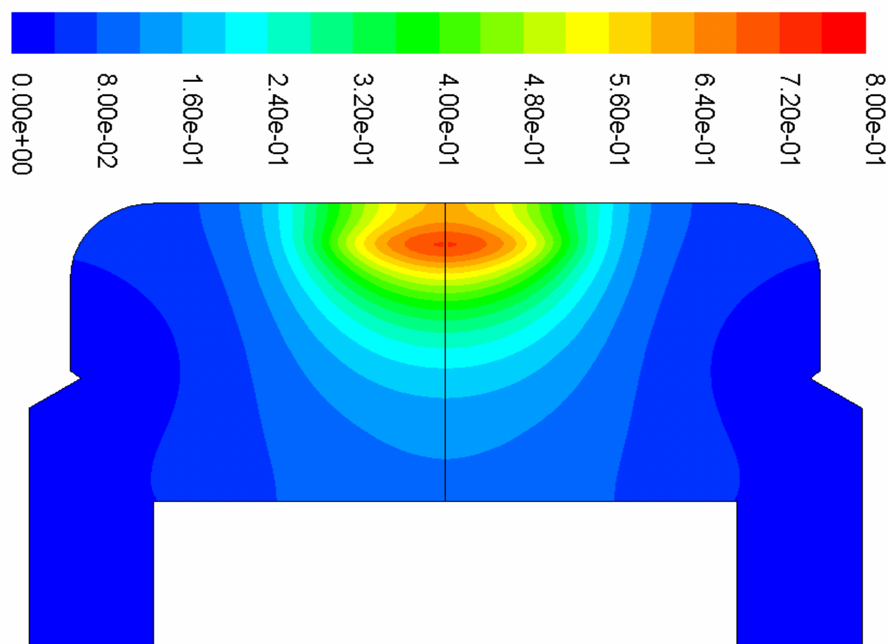

Figure 24: Contours of mole fraction of F atoms. Upper ICP only.

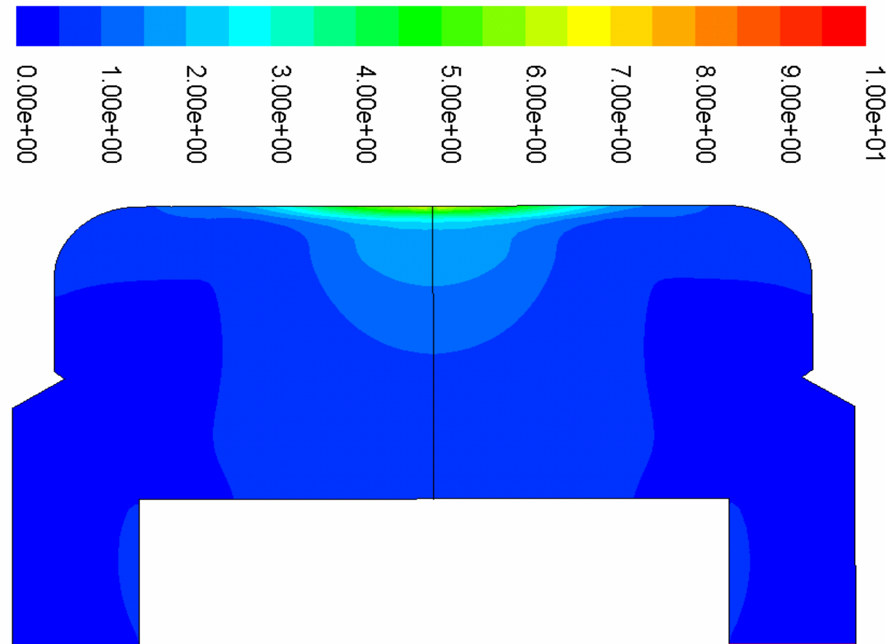

Figure 25: Contours of etch rate, kA/min. Upper ICP only.

Side & Upper Inductively Coupled Plasmas. The results obtained from single side and upper ICP discharges (Table 12 and Table 13) show the upper ICP can be used to increase the etch rates in upper zones only. For this reason the simulation with both side and upper ICPs was performed. The corresponding contours of temperature, mole fraction of F atoms and etch rates are presented in Figure 26, Figure 27 and Figure 28 accordingly. With both operational ICPs the etch time of upper chamber region could be essentially decreased from 50.7 s (Table 12) to 37.0 s (Table 14). Although the upper ICP helps to decrease the etch time in upper it has no effect on etch rates of lower zones. The established overetch time is 49.1 s.

Table 14: Average etch rate and corresponding etch time for each zone. Side and Upper ICPs.

Zone #	Intermediate Film Thickness, mkm	Average Etch Rate, kA/min	Etch Time, s
3	0.6	9.0	37.0
1	0.4	8.0	30.0
7	-	-	-
2	0.3	2.7	65.7
5	0.3	2.2	82.9
4	0.35	2.4	86.1
6	0.35	3.0	69.6

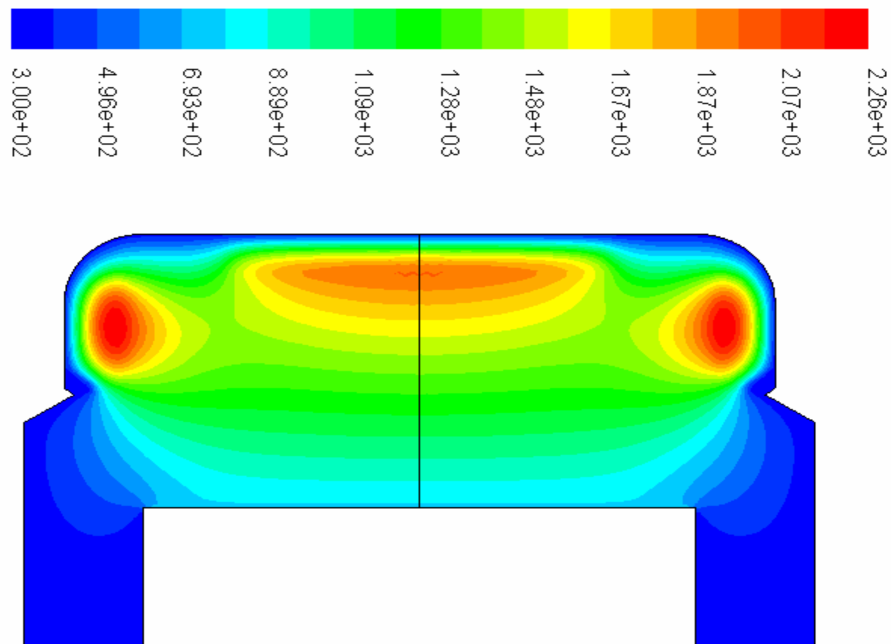

Figure 26: Contours of temperature, K. Side and Upper ICPs.

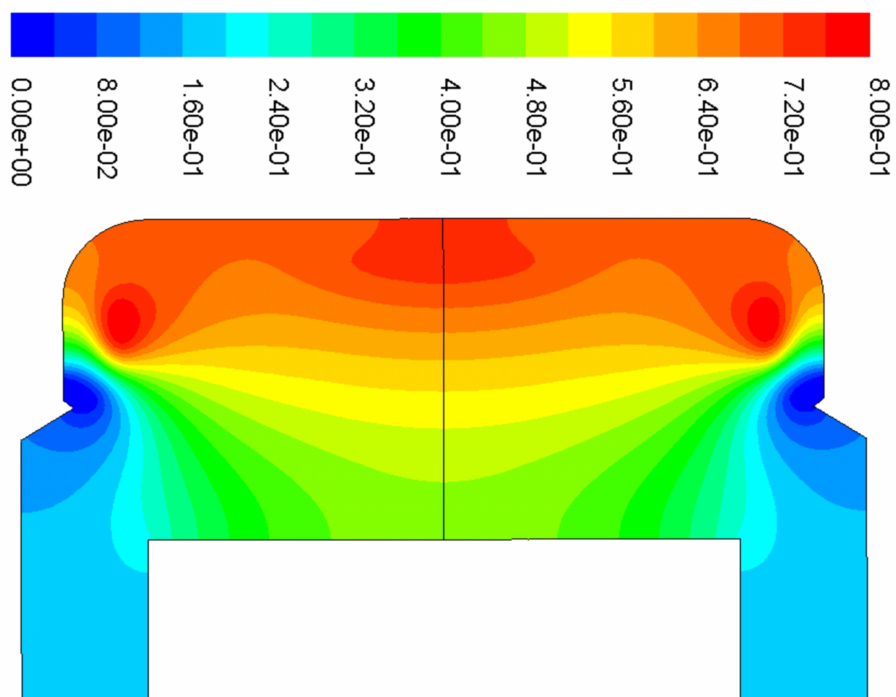

Figure 27: Contours of mole fraction of F atoms. Side and Upper ICPs.

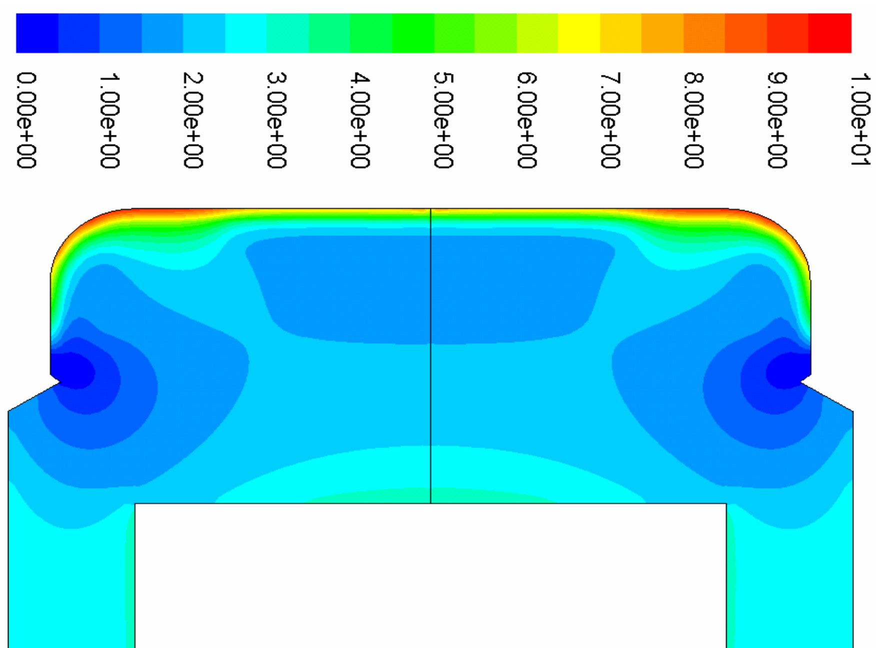

Figure 28: Contours of etch rate, kA/min. Side and Upper ICPs.

Capacitively Coupled Plasma. The capacitive coupled plasma discharge is considered as low density (n_e = 10^8-10^9 cm^{-3}) and high frequency (f = 13.56 MHz) discharge, used as a secondary discharge to increase etch rates in the lower zones of the chamber. The discharge is non-equilibrium. The temperature of the gas in the discharge reaches 600 K which means that thermal dissociation reaction of molecular fluorine will not occur in this type of plasma. However, the fluorine recombination reaction is important here and affects the etching process. Due to strong influence of volume recombination reaction the optimal value for the flow rate should be investigated. For example, if we try to decrease the flow rate the gas flows through the discharge slowly giving the time for proper dissociation, but once it passed the discharge zone it is also given a time for proper volume recombination. If we try to increase the flow rate the gas flows through the discharge quickly not having a time for proper dissociation, but once it passed the discharge zone it is also not given a time for proper volume recombination. In this situation there is some optimal solution for the gas flow rate and this solution is the maximum of some function depending on the flow rate or residence time. This function we are looking for is representation of the etch rates along the flow path. The highest value of the etch rate will give us the most optimal value for the gas flow rate. The Fluent modeling gives us F-atoms concentration along the path line. The integral of F-atoms concentration basically represents the average value of the etch rate. The Figure 29 shows the integral of F-atoms over the flow path (etch rates) as a function of residence time (flow rates). The wide spectrum of flow rates was considered. The highest value of the residence time represents the lowest value of the flow rate and vise versa. The obtained

function has the maximum value of the etch rate at the residence time of 5 s. For the residence time of 5 s the estimated flow rate is 0.7 slm.

Figure 30 shows the contours of mole fraction of fluorine atoms and Figure 31 shows the contours of etch rates for capacitively coupled plasma discharge. Because of CCP discharge location it affects only the lower zones of the chamber. Accordingly, the etch rates at the upper zones are very low while the etch rates at the lower zones have relatively high values, Table 15. The corresponding etching time is 47 s.

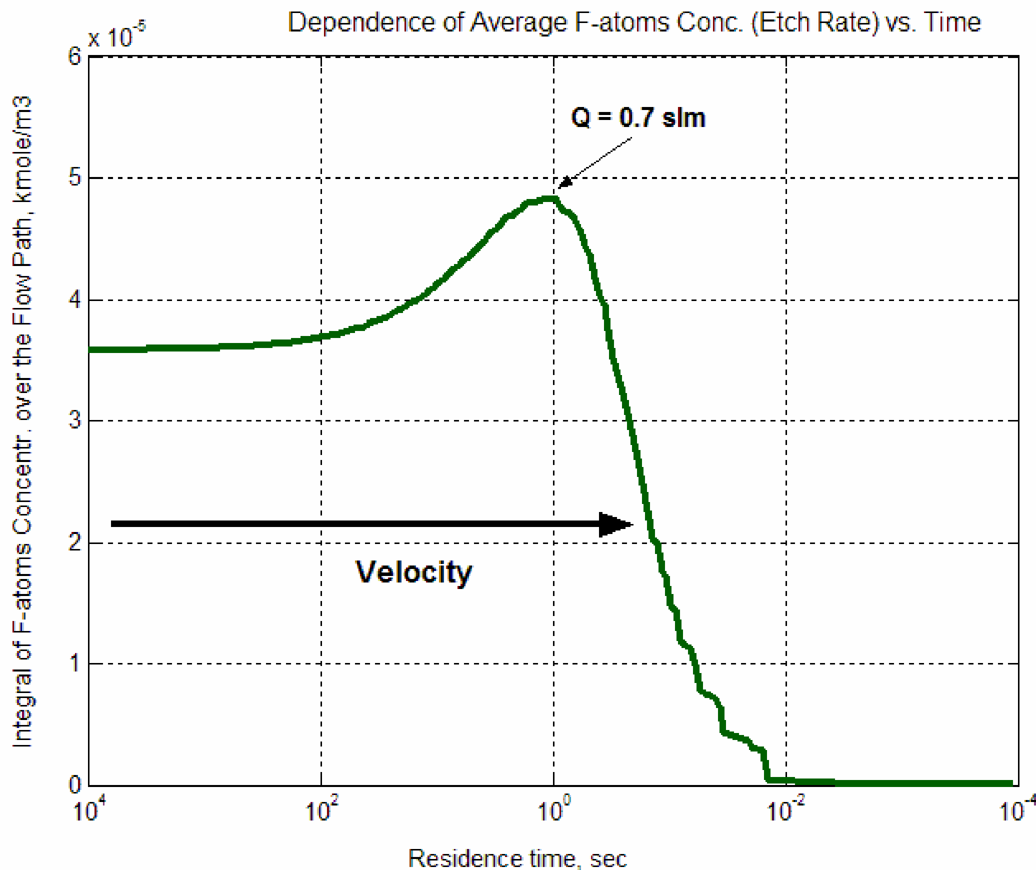

Figure 29: The dependence of average F-atoms concentration vs. residence time.

Table 15: Average etch rate and corresponding etch time for each zone. CCP discharge only.

Zone #	Intermediate Film Thickness, mkm	Average Etch Rate, kA/min	Etch Time, s
3	0.6	-	-
1	0.4	-	-
7	-	-	-
2	0.3	3.8	47.0
5	0.3	7.2	25.0
4	0.35	6.9	30.2
6	0.35	6.4	32.7

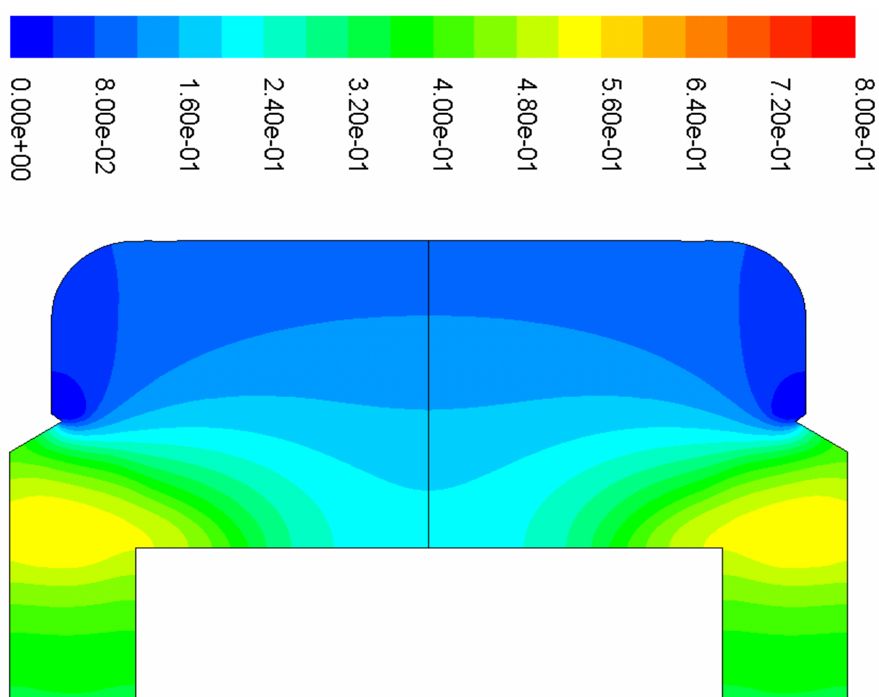

Figure 30: Contours of mole fraction of F atoms. CCP discharge only.

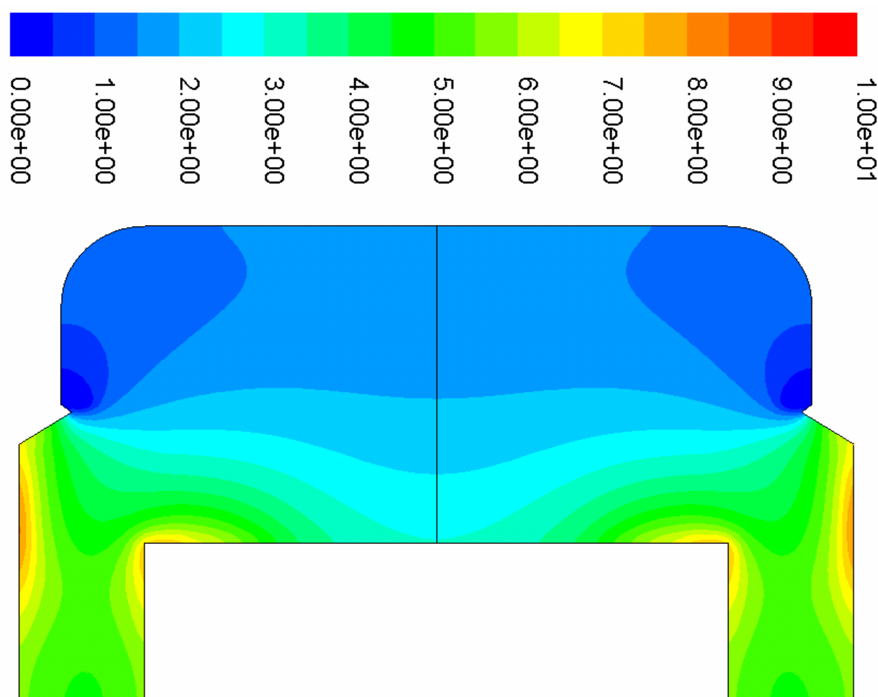

Figure 31: Contours of etch rate, kA/min. CCP discharge only.

The Optimal Solution. The control and manipulation of all considered discharges will give us the optimal solution in overall cleaning time. We propose to perform a cleaning process in two time steps. In a first time step which lasts 7 s both side and upper inductively coupled discharges are in a working regime, Table 16. In a 7 s the both inductive coupled discharges are turned off and the capacitive coupled discharge is turned on for 30 s, Table 17. Thus, the overall cleaning time of this process is 37 s. In the scope of the proposed method this can be the minimum time which could be achieved in remote cleaning technology with supported by *in situ* plasma.

Nowadays using NF_3-based remote cleaning technology without supported by *in situ* plasma the duration of cleaning time of HDP-CVD reactor performed usually reaches 2 min (for deposition time of 5 min). The proposed herein cleaning plasma technology

method with two-step cleaning mechanism can save as much as 80 s for each cleaning cycle.

Table 16: STEP 1: both side and upper ICPs are turned on for 7 s.

Zone #	Interm. Film Thickness, mkm	Average Etch Rate (Step 1), kA/min	Remaining Film Thickness after 7 s of etching, mkm
3	0.6	9.0	0.48
1	0.4	8.0	0.31
7	0	0	0
2	0.3	2.7	0.26
5	0.3	2.2	0.27
4	0.35	2.4	0.32
6	0.35	3.0	0.31

Table 17: STEP 2: only CCP discharge is turned on for 30 s.

Zone #	Remaining Film Thickness after 7 s of etching, mkm	Average Etch Rate (Step 2), kA/min	Etch Time, s
3	0.48	9.0	30.0
1	0.31	7.5	24.8
7	0	0	0
2	0.26	7.6	20.5
5	0.27	7.8	20.7
4	0.32	7.0	27.4
6	0.31	6.9	27.0

In a cleaning systems featuring NF_3-based remote clean technology the cleaning time varies from 60 to 180 s depending on operational pressure and gas flow rate, Figure 32. The results on Figure 32 were obtained according to advanced research conducted by an Air Products and Chemicals Inc. Electronics Division [43]. From Figure 32, the cleaning time of CVD chamber is 100 s for operating pressure of 2 Torr and the NF_3 flow

rate of 1000 sccm (which is similar to our simulation conditions: p = 2 Torr and NF_3 flow rate is 700 sccm).

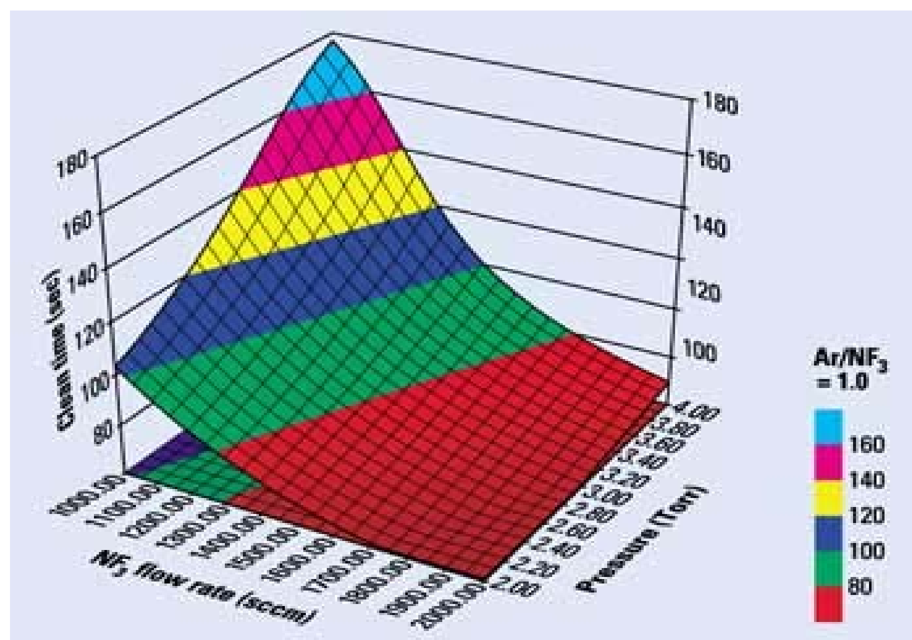

Figure 32: The dependence of operating pressure and NF_3 flow rate on cleaning time (Air Products and Chemicals Inc.).

Gas Utilization. The utilization (destruction efficiency) refers to the percentage of the etch gas which reacts during the plasma clean to form other products. The utilization is determined by measuring the etch gas concentration with RF power off and on, and was calculated using the following equation

$$\eta = \frac{[F_2]_{RF-OFF} - [F_2]_{RF-ON}}{[F_2]_{RF-OFF}} \cdot 100\%$$

The estimated utilization efficiency for two step cleaning regime reaches 95 %. The comparison of etch gas utilization with different etching gases and cleaning methods is

presented in Table 18. The data corresponding to the *in situ* RF capacitively coupled plasma cleaning are taken from [45]. Higher gas utilization leads to decreasing gas consumption and PFC emissions as well as in combination with other process parameters (e.g. pressure, oxygen concentration) to better clean performance due to increasing etch rates. NF_3 based chamber cleans, however, have no PFC emissions not only because of high gas utilization, but also because other PFC by-products are not generated.

Table 18: Etch gas utilization of C_2F_6, C_3F_8 and NF_3 during chamber cleaning.

	***In Situ* Capacitively Coupled Plasma Cleaning**		**Remote Cleaning Technology by Supported by *In Situ* ICP and CCP**
Deposited Film	C_2F_6	C_3F_8	NF_3
Silicon Oxide	33 %	61 %	Not considered
Silicon	33 %	60 %	95 %
Silicon Nitride	31 %	54 %	Not considered

Overall Comparison for Different Gases. Charles Allgood and Michael Mocella from DuPont Zyron® in their technical paper made a comparison of productivity (clean time) for different cleaning gases, Figure 33. In the obtained results they claim that the NF_3-based cleaning has the smallest cleaning time in compare with the other cleans. However, among the carbon-based gases the c-C_4F_8 shows the most favorable result.

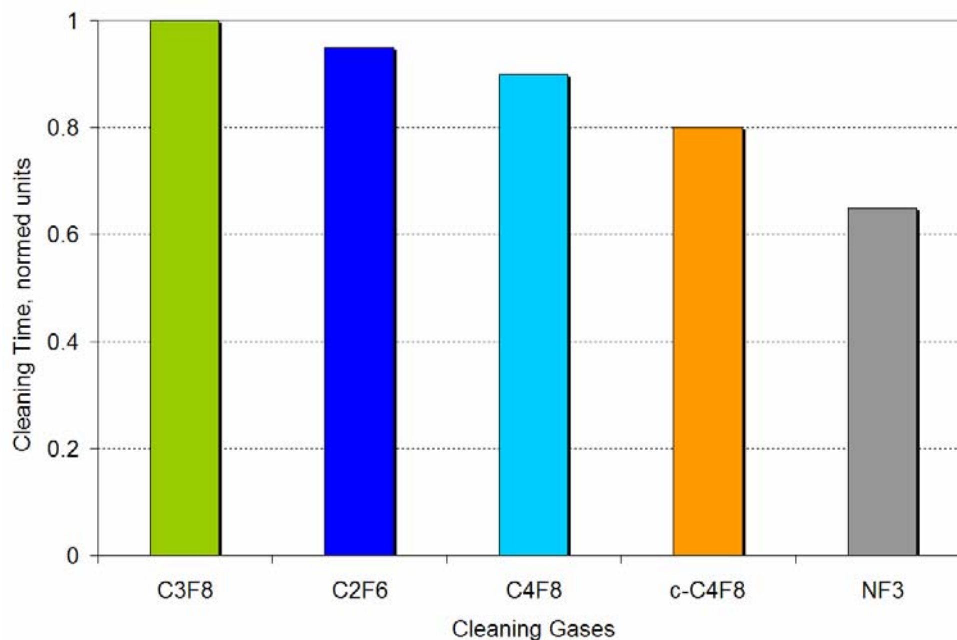

Figure 33: Comparison of cleaning time for different cleaning gases (relative to standard C_3F_8 process = 1.0)

As another means to compare the relative merits of the various cleaning gases, key performance data, as well as several other important process-related factors, have been assembled in the Table 19. These data were taken from recent works [45-52]. From this table, the following conclusions can be drawn.

- PFC emissions reduction: the largest benefit is found with NF_3. However, the four-carbon compounds are the most beneficial among the other carbon containing gases, and significant reductions from the standard C_2F_6 process are obtained with either C_2F_6 or C_3F_8 (which are essentially equivalent in PFC emissions, gas use, and clean time performance).
- Gas cost per clean: the largest benefit is available with c-C_4F_8 if it can be obtained for a price comparable to the other fluorocarbon gases. This is not presently the case, as the cost for very high purity grades for HDP

oxide etching (the current application) is about 2-3x the cost of the other commercially available carbon-based gases. However, with the proper optimization NF_3 has a good potential to further reduction in gas cost per clean.

- Gas availability: multiple producers provide the best assurance of adequate gas supply, as is presently the case for C_2F_6. This is not an absolute guarantee, however, as shown by the current supply concerns for NF_3 (which we believe will persist for the entire current industry expansion). The supply situation is good for c-C_4F_8; an issue is how many producers will offer a grade which is attractively priced for chamber cleaning.
- Health & safety factors and issues: the situation is the best for the three C_xF_y compounds, where there is an extensive data showing minimal concern with these gases.

Table 19: Comparison of process and other factors for the various clean gases (highlighting potential advantages and concerns)

Issue	C_2F_6	C_3F_8	c-C_4F_8	C_4F_8O	NF_3
PFC Emissions Reduction (vs. standard C_2F_6)	Not Significant	Not Significant	Large	Large	No PFCs
Gas Cost (per clean)	Average	Average	Low	Unknown	Average to High
Gas Availability	Good, Multiple producers	Limited, Few producers	Good, Multiple producers	Limited, Few producers	Average
Health & Safety Factors Known	Yes	Yes	Yes	Incomplete	Incomplete
Health and Safety Issues	Low	Low	Low	Unknown	Medium

CHAPTER 5: SUMMARY AND CONCLUSIONS

5.1 Conclusions

Substantial achievement has been made through a combination of substituting NF_3 for traditional *in situ* cleaning gases (C_2F_6, CF_4, C_3F_8 and others), and implementing the remote NF_3 cleaning technology. The success of this approach for most of the CVD tools has been described. For installed CVD tools presently being used for production, it is less feasible to change the chemistry of the cleaning process. Adjusting the process parameters so as to eliminate PFC emission and minimize the cleaning time is an effective strategy. In addition to eliminating PFC emissions, process optimization provided a reduction of gas costs and power consumption. It is accepted that most new CVD equipment will be cleaned using NF_3 remote clean technology with supported *in situ* plasma. Another advantage in using NF_3 instead of C_xF_y is the high conversion rates of NF_3 in process and abatement, lower energy consumption in abatement (therefore less CO_2 emission) and possibly positive influence on environmental assessment from longer tool lifetime. The major disadvantage is the toxicity and higher reactivity of NF_3, but this will not be a significant problem in semiconductor manufacturing. For the costs an overall reduction is expected from: (a) longer tool lifetime; (b) lower operating cost for the abatement and (c) reduced cost for process gases, if NF_3 prices will drop.

During the HDP-CVD chamber-clean optimization investigation described in this thesis, it was determined that the use of the plasma manipulation technique can reduce processing time, power consumption and gas-flow levels. It was found that as much as

2.4 minutes of processing time per chamber clean can be saved with 95% of gas utilization efficiency.

5.2 Recommendations for Future Work

The usage of inductively coupled plasma as a primary plasma source for fluorine radical restoration reduces the ion bombardment of the chamber walls. Indeed, the ICP discharge has much lower plasma potential with respect to CCP discharge. The ion bombardment can be a major concern associated with high-density plasma sources such as ICP sources where parasitic capacitive coupling (radial electric field) can cause sputtering of the applicator tube and subsequent contamination of the deposition chamber. The prevention of ion acceleration towards the wall could be achieved with proper studies of ICP source. Such studies are not possible without a self-consistent model of electromagnetic problem.

The recent studies show that the presence of helium in the discharge can essentially reduce the power consumption. The benefit especially seen when helium and argon are used together in selected proportions. While helium has a good heat transfer properties and therefore cannot be considered in high-density ICP discharge, it still could be used in CCP discharge. Studies in this direction could produce information for the optimization of power consumption in CCP discharge.

Of course, present work can be continued with further optimization investigation. For example, the investigation of optimization in power consumption with helium addition should be studied. Also, because pure fluorine (F_2) is a direct source of fluorine

radicals it could act as a drop-in solution for NF_3. An additional advantage is the absence of any other accompanying atoms. However, F_2 has not yet been an option as CVD cleaning gas in the semiconductor industry due to filling weight restrictions for F_2-cylinders (based on the health and safety regulations). Recently, the on-site generation of F_2 has become an interesting alternative way of supply, as it is already state-of-the-art in other industries and has been evaluated by some major semiconductor Original equipment Manufacturers. This new approach could possibly lead to a gas cost reduction in CVD cleaning greater than 50%. Concerns regarding the implementation are still local health and safety requirements, limited CVD process experiences with F_2, generator reliability and F_2 gas quality. Resolving these open issues, on-site generated F_2 could become a serious option in CVD cleaning in particular for future semiconductor fabrications.

LIST OF REFERENCES

1. Sze SM. Semiconductor Physics and Technology, John Wiley & Sons, New York 1985.

2. Raoux S, Tanaka T, Bhan M, Ponnekanti H, Seamons M, Deacon T, Xia LQ, Pham F, Silvetti D, Cheung D, Fairbairn K, Jonhson A, Pierce R, Langan J, Remote microwave plasma source for cleaning CVD chambers – A Technology to reduce global warming gas emissions. Submitted for publication in J. Vac. Sci. Technol.

3. Raoux S, Cheung D, Fodor M, Taylor N, Fairbairn K. Plasma Sources Sci. Technol. 1997;6:405.

4. Meeks E, Larson RS, Vosen SR, Shon JW. J. Electrochem. Soc. 1997;144:1.

5. Kastenmeier BE, Matsuo PJ, Oehrein GS, Langan JG. J. Vac. Sci. Technol. A. 1998;16:2047.

6. Kastenmeier BE, Oehrein GS, Langan JG, Entley WR. J. Vac. Sci. Technol. A. 2000;18:2102.

7. Gelb A, Kim SK. J.Chem.Phys., Vol 1971;55:10.

8. Vincenti WC, Kruger CH. Introduction to Physical Gas Dynamics. Wiley, New York 1967.

9. Christman K, Schaber O, Ertl G, Neumann M. J. Chem. Phys. 1974;60:4528.

10. Jumper EJ, Ultee CJ, Dorko EA. A Model of Fluorine Atom Recombination on a Nickel Surface. J. Phys. Chem. 1980;84:41.

11. Emmett PH. Catalysis: Vol. I, Fundamental Principles, Part I. Reinhold, New York 1954.

12. Glasstone S, Laidler JJ, Eyring H. Theory of Rate Processes. McGraw-Hill, New York 1941.

13. Von der Ziel A. Solid State Physical Electronics. Prentice-Hall, Englewood Cliffs, NJ 1957.

14. Lennard-Jones JE. Trans. Faraday Soc. 1932;28:334.

15. Mavroyannis C. Mol. Phys. 1963;6:593.

16. Bardeen J. Phys. Rev. 1940;58:727.

17. Margenau H, Pollard WG. Phys. Rev. 1941;60:128.

18. Logan RM, Keck JC. J. Chem. Phys. 1968;49:860.

19. Modak AT, Pagni PJ. J. Chem. Phys. 1973;59:2019.

20. Fischer CF. Atomic Data. 1972;4:301.

21. Lillis JR, Wright A. Air Force Weapons Laboratory, Albuquerque, NM 87117.

22. Ultee CJ. The homogeneous recombination rate constant of F atoms at room temperature. Chem. Phys. Lett. 1977;46:366.

23. Stueber GJ, Clarke SA, Bernstein ER. On the Production of Fluorine Containing Molecular Species in Plasma Atomic F Flows. To be published.

24. Meeks E, Ho P, Ting A, Buss RJ. J. Vac. Sci. Technol. A 1998;16:2227.

25. Meeks E, Larson RS, Ho P, Apblett C, Han SM, Edelberg E, Aydil ES. J. Vac. Sci. Technol. A 1998;16:544.

26. Kushner M, Collision W, Grapperhaus M, Holland J, Barnes M. J. Appl. Phys. 1996;80:1337.

27. Bukowski JD, Graves DB, Vitello P. J. Appl. Phys. 1996;80:2614.

28. Kortshagen U, Heil BG. IEEE Trans. on Plasma Sci. 1999;27:1297.

29. Raizer P. Physics of Gas Discharge 1987.

30. Suh S, Girshick S, Kortshagen U, Zachariah M. Modeling Gas-Phase Nucleation in Inductively-Coupled Silane-Oxygen Plasmas. Draft by SMS: revised by UK January 2002.

31. Cartwright DC, Hay PJ, Trajmar S. Chem Physics 1991;153:219.

32. Ultee CJ. Chem. Phys. Lett. 1977;46:366.

33. Ganguli PS. Kaufman M. Chem. Phys. Lett. 1974;25:221.

34. Meeks E, Larson RS, Vosen SR, Shon J, Electrochem J. Soc. 1997;144:357.

35. Arutyunov VS, Popov LS, Chaikin AM. Kinet. Catal. 1976;17:251.

36. Duman EL, Tishchenko NP, Shmatov IP. Dokl. Phys. Chem. 1987;295:5.

37. Beenakker CI, van Dommelen JH, Dieleman J. 157th Meeting, Electrochem. Soc. 1980;80:330.

38. Donelly VM, Flamm DL. J. Appl. Phys. 1980;10:5273.

39. Flamm DL, Mogab CJ, Sklaver ER. J. Appl. Phys. 1979;50:624.

40. Flamm DL, Donnelly VM, Mucha JA. J. Appl. Phys. 1981;52:5.

41. Horwath RH, Zarovin CB, Rosenberg R. 157th Meeting, Electrochem. Soc., 1980; 80:294.

42. Gudmundsson JT. Science Institute, University of Iceland, RH-25-99.

43. Lester MA. Semiconductor International, Newton 2001;24:44.

44. 3M Performance Chemicals and Fluids Division. Report 98-0212-0192-0 (HB) 1997.

45. Dutrow EA. A Partnership with the Semiconductor Industry for Reduction of PFC Emissions. SEMI Technical Program: SEMI, Mountain View, CA 1996:137.

46. Fraust C. World Semiconductor Council ESH Taskforce Update. SEMI Technical Program: A Partnership for PFC Reduction, SEMI, Mountain View, CA 1999:B1.

47. Pruette L, Karecki S, Reif R, Entley W, Langan J, Hazari V, Hines C. Electrochem, Solid-State Lett. 1999;2:592.

48. Pruette L, Karecki S, Reif R, Langan J, Rogers S, Ciotti R, Felker B. J. Vac. Sci. Tchnol. A 1998;16:1577.

49. Pruette L, Karecki S, Reif R, Tousignant L, Regan W, Keari S, Zassera L, Proc. Electrochem. Soc. 1999;99:20.

50. Allgood CC, Mocella MT, Chae H, Sawin HH. Submitted for publication 2003.

51. Aitchison K. SEMI Technical Program: Environmental Impact of Process Tools. SEMI: Mountain View CA, paper C 1999.

52. Presentation of these results was demonstrated for the PFC Seminar at SEMICON Southwest 2000.

APPENDIX A: PLASMA CHEMISTRY REACTIONS OF $NF_3/CF_4/C_2F_6$

Reactions $k = AT^{B} \exp(-E_a / RT)$	**A** [cm^3/mol-s, cm^6/mol^2-s];	**B**	**E_a** [cal/mol]
Ionization			
E+F=>F++2E	4.40E+11	0.9	100000.0
E+SIF3=>SIF3++2E	1.90E+14	0.4	60000.0
E+SIF3=>SIF2++F+2E	1.20E+14	0.5	90000.0
E+SIF3=>SIF++2F+2E	4.20E+11	0.7	90000.0
E+SIF3=>SI++2F+F+2E	1.10E+14	0.3	170000.0
E+SIF2=>SIF2++2E	1.60E+15	0.3	70000.0
E+SIF2=>SIF++F+2E	2.20E+11	1.0	80000.0
E+SIF2=>SI++2F+2E	4.80E+13	0.5	170000.0
E+SIF=>SI++F+2E	2.40E+14	0.4	80000.0
E+SIF=>SI+F++2E	4.80E+13	0.4	130000.0
E+SIF4=>SIF3++2E+F	1.40E+13	0.7	100000.0
E+SIF4=>SIF2++2F+2E	1.80E+13	0.5	130000.0
E+SIF4=>SIF++2F+F+2E	1.40E+10	1.1	150000.0
E+SIF4=>F++SIF3+2E	9.00E+10	0.9	200000.0
E+SIF=>SIF++2E	1.80E+15	0.3	45000.0
E+NF3=>NF3++2E	4.45E-10	5.0	75840.9
E+NF3=>NF2++2E+F	1.35E-13	6.5	68026.2
E+NF3=>NF++2E+2F	2.37E-39	11.0	79299.5
E+N2=>N2++2E	1.54E-19	7.1	62647.2
E+NF=>NF++2E	1.17E-18	6.8	66836.1
E+N2=>N2++2E	1.54E-19	7.1	62647.2
E+N=>N++2E	3.08E-13	5.8	94728.0
E+F2=>F2++2E	9.88E-21	7.3	65437.2
E+NF3*=>NF3++2E	4.45E-10	5.0	74527.5
E+NF3*=>NF2++2E+F	1.35E-16	6.5	66712.8
E+NF3*=>NF++2E+2F	2.37E-39	11.0	77986.1
E+NF3**=>NF3++2E	4.45E-10	5.0	72776.3
E+NF3**=>NF2++2E+F	1.35E-16	6.5	64961.6
E+NF3**=>NF++2E+2F	2.37E-39	11.0	76234.9
E+NF3***=>NF3++2E	4.45E-10	5.0	58985.6
E+NF3***=>NF2++2E+F	1.35E-16	6.5	51170.9
E+NF3***=>NF++2E+2F	2.37E-39	11.0	62444.2
E+O2=>O2++2E	8.40E+08	1.4	65490.0
E+O=>O++2E	1.40E+09	1.3	66500.0
E+C2F6=>CF3++CF3+2E	1.49E+12	0.9	163690.0
E+C2F6=>CF2++CF4+2E	1.98E+11	0.9	240820.0
E+CF4=>CF3++F+2E	6.96E+12	0.8	199310.0

E+CF4=>CF2++2F+2E	1.73E+13	0.5	264900.0
E+CF4=>CF++2F+F+2E	1.38E+10	1.1	313210.0
E+CF4=>F++CF3+2E	8.88E+10	0.9	402260.0
E+CF4=>F++CF3++3E	2.17E+07	1.4	396650.0
E+CF3=>CF3++2E	8.40E+12	0.6	113300.0
E+CF3=>CF2++F+2E	8.28E+13	0.4	198710.0
E+CF3=>CF++2F+2E	3.01E+13	0.5	245480.0
E+CF3=>F++CF2+2E	3.35E+14	0.3	333550.0
E+CF2=>CF2++2E	9.48E+12	0.6	112510.0
E+CF2=>CF++F+2E	1.47E+12	0.8	160190.0
E+CF2=>F++CF+2E	1.01E+15	0.3	444650.0
E+CF=>CF++2E	7.62E+10	1.0	102700.0
E+CO=>CO++2E	1.32E+17	0.0	276200.0
Dissociation by Electron Impact			
E+SIF3=>SIF2+F+E	7.20E+07	1.3	70000.0
E+SIF3=>SIF+2F+E	6.10E+07	1.2	110000.0
E+SIF4=>SIF4+E	2.80E+21	-1.4	2300.0
E+SIF4=>SIF3+F+E	1.40E+12	0.8	60000.0
E+SIF4=>SIF2+2F+E	6.30E+15	0.0	90000.0
E+SIF4=>SIF+3F+E	6.10E+07	1.2	110000.0
E+SIF2=>SIF+F+E	7.20E+07	1.3	70000.0
E+SIF=>SI+F+E	7.20E+15	1.3	70000.0
E+NF3=>NF2+F+E	1.24E+08	1.7	74175.3
E+NF3=>NF+2F+E	8.13E-07	4.5	68077.9
E+NF2=>NF+F+E	9.45E+07	1.8	54854.3
E+NF2=>N+2F+E	1.02E+03	3.0	74927.5
E+NF=>N+F+E	9.45E+07	1.8	54854.3
E+N2F2=>2N+2F+E	1.37E+07	1.7	72418.1
E+N2F4=>2N+4F+E	1.37E+07	1.7	72418.1
E+NF3*=>NF2+F+E	1.24E+07	1.7	72861.9
E+NF3*=>NF+2F+E	8.13E-07	4.5	66764.5
E+NF3**=>NF2+F+E	1.24E+07	1.7	71110.7
E+NF3**=>NF+2F+E	8.13E-07	4.5	65013.3
E+NF3***=>NF2+F+E	1.24E+07	1.7	57320.0
E+NF3***=>NF+2F+E	8.13E-07	4.5	51222.6
E+O2=>O+O+E	5.10E+08	1.1	75350.0
E+CF4=>CF3+F+E	7.14E+07	1.3	144650.0
E+CF4=>CF2+2F+E	4.66E+07	1.2	166300.0
E+CF4=>CF+2F+F+E	6.24E+07	1.2	220290.0
E+CF3=>CF2+F+E	2.50E+20	-0.9	130100.0
E+CF2=>CF+F+E	7.14E+07	1.3	144650.0
E+CF=>C+F+E	7.14E+07	1.3	144650.0
E+CO=>C+O+E	2.22E+12	0.7	125795.0
E+COF2=>COF+F+E	4.60E+11	0.0	0.0
E+CO2=>CO+O+E	4.60E+14	0.0	0.0
Excitation Reactions			

E+NF3=>NF3**+E	2.47E+15	0.2	66259.0
E+NF3=>NF3***+E	2.06E+03	2.5	3323.3
E+NF3=>NF3*+E	1.04E+12	0.0	6366.0
E+N2=>N2*+E	2.00E+14	0.0	0.0
Relaxation Reactions			
NF3*+M=>NF3+M	1.00E+10	0.0	0.0
NF3**+M=>NF3+M	1.00E+10	0.0	0.0
NF3***+M=>NF3+M	1.00E+10	0.0	0.0
N2*+M=>N2+M	1.00E+10	0.0	0.0
Recombination			
E+SIF3+=>SIF2+F	2.40E+16	0.0	0.0
E+SIF2+=>SIF+F	2.40E+16	0.0	0.0
E+SIF+=>SI+F	2.40E+16	0.0	0.0
F-+SIF3=>SIF4+E	2.40E+15	0.0	0.0
F-+SIF2=>SIF3+E	1.80E+14	0.0	0.0
F-+SIF=>SIF2+E	1.20E+14	0.0	0.0
F-+SI=>SIF+E	6.00E+13	0.0	0.0
E+F2+=>2F	1.35E+23	-2.0	0.0
E+F2+=>F2	1.35E+23	-2.0	0.0
E+F+=>F	1.35E+23	-2.0	0.0
E+N2+=>2N	1.35E+23	-2.0	0.0
E+N2+=>N2	1.35E+23	-2.0	0.0
E+N+=>N	1.35E+23	-2.0	0.0
E+O2+=>2O	2.40E+16	0.0	0.0
E+CF3+=>CF2+F	2.40E+14	0.0	0.0
E+CF2+=>CF+F	2.40E+14	0.0	0.0
E+CF+=>C+F	2.40E+14	0.0	0.0
E+CO+=>C+O	2.40E+14	0.0	0.0
E+E+F+=>F+E	7.00E+32	0.0	0.0
E+E+F2+=>F2+E	3.00E+32	0.0	0.0
E+E+NF3+=>NF3+E	3.00E+32	0.0	0.0
E+E+NF2+=>NF2+E	3.00E+32	0.0	0.0
E+E+NF+=>NF+E	3.00E+32	0.0	0.0
E+E+N+=>N+E	7.00E+32	0.0	0.0
E+E+N2+=>N2+E	7.00E+32	0.0	0.0
F-+CF3=>CF4+E	2.40E+14	0.0	0.0
F-+CF2=>CF3+E	1.80E+14	0.0	0.0
F-+CF=>CF2+E	1.20E+14	0.0	0.0
F-+C=>CF+E	6.00E+13	0.0	0.0
F-+O=>F+O+E	6.00E+13	0.0	0.0
F-+F=>2F+E	6.00E+13	0.0	0.0
Ion-Ion Recombination			
F-+SI+=>F+SI	2.40E+17	-0.5	0.0
F-+SIF+=>F+SIF	2.40E+17	-0.5	0.0
F-+SIF2+=>F+SIF+F	2.40E+17	-0.5	0.0
F-+SIF3+=>F+SIF2+F	2.40E+17	-0.5	0.0

F-+CF3+=>F+CF2+F	2.40E+17	-0.5	0.0
F-+CF2+=>F+CF2	2.40E+17	-0.5	0.0
F-+CF+=>F+C+F	2.40E+17	-0.5	0.0
F-+CO+=>F+CO	2.40E+17	-0.5	0.0
F-+O+=>F+O	2.40E+17	-0.5	0.0
F-+O2+=>F+O2	2.40E+17	-0.0	0.05
NF3++F-=>NF3+F	6.00E+16	0.0	0.0
NF2++F-=>NF3	6.00E+15	0.0	0.0
NF++F-=>NF2	6.00E+15	0.0	0.0
N++F-=>NF	6.00E+15	0.0	0.0
N2++F-=>N2+F	6.00E+15	0.0	0.0
F2++F-=>F2+F	6.00E+16	0.0	0.0
F-+F+=>F+F	2.40E+17	-0.5	0.0
Dissociative Attachment			
E+SIF3=>SIF2+F-	7.20E+15	-0.4	60000.0
E+SIF4=>SIF3+F-	7.20E+15	-0.4	60000.0
E+SIF2=>SIF+F-	7.20E+15	-0.4	60000.0
E+SIF=>SI+F-	7.40E+15	-0.4	60000.0
E+NF3=>NF2+F-	8.97E+15	-0.1	7464.5
E+F2=>F+F-	6.14E+18	-0.9	2153.2
E+NF3*=>NF2+F-	8.97E+15	-0.1	6151.1
E+NF3**=>NF2+F-	8.97E+15	-0.1	4399.9
E+NF3***=>NF2+F-	8.97E+15	-0.1	-9390.8
E+C2F6=>F-+CF2+CF3	1.51E+17	-0.7	-68466.0
E+CF4=>CF3+F-	1.42E+16	-0.5	58757.0
E+CF3=>CF2+F-	1.42E+16	-0.5	58757.0
E+CF2=>CF+F-	1.42E+16	-0.5	58757.0
E+CF=>C+F-	1.42E+16	-0.5	58757.0
E+CF4=>CF3+F-	1.42E+16	-0.5	58757.0
Reactions of Neutrals			
SIF+SIF4=>SIF2+SIF3	1.45E+13	0.0	0.0
SIF2+F2=>SIF3+F	2.83E+11	0.0	0.0
SI+SI+M=>SI2+M	2.47E+16	0.0	1178.0
F2+SIF=>SIF2+F	1.69E+13	0.0	0.0
F2+SI=>SIF+F	1.15E+14	0.0	0.0
F+SI=>SIF	3.01E+13	0.0	0.0
F+SIF=>SIF2	3.01E+14	0.0	0.0
F+SIF2=>SIF3	3.01E+11	0.0	0.0
F+SIF3=>SIF4	3.01E+15	0.0	0.0
NF2+F2=>NF3+F	1.66E+03	0.0	0.0
NF+NF=>N2+2F	6.40E+11	0.0	0.0
NF+NF=>N2+F2	2.41E+12	0.0	0.0
NF+NF2=>N2+F2+F	2.41E+12	0.0	0.0
NF+N2F2=>NF2+N2+F	1.20E+12	0.0	0.0
NF+NF2=>N2F2+F	1.21E+12	0.0	0.0
NF2+N=>2F+N2	6.14E+12	0.0	0.0

NF2+N=>2NF	1.81E+12	0.0	0.0
NF2+F+M=>NF3+M	3.73E+17	0.0	0.0
NF3+M=>NF2+F+M	5.22E-13	0.0	0.0
F+N3=>NF+N2	3.49E+13	0.0	0.0
N+N+M=>N2+M	7.20E+15	0.0	0.0
NF2+M=>NF+F+M	4.74E-23	0.0	0.0
NF2+NF2+M=>N2F4+M	5.43E+15	0.0	0.0
F+F+M=>F2+M	1.01E+14	0.0	0.0
O+NF2=>NF+OF	6.14E+17	0.0	0.0
O+NF=>NO+F	6.14E+17	0.0	0.0
2OF=>2F+O2	6.14E+17	0.0	0.0
O+OF=>O2+F	6.14E+17	0.0	0.0
N+N+N2=>N2+N2	4.96E-10	0.0	-500.0
N+N+N=>N2+N	1.40E-09	0.0	-500.0
N+NO=>N2+O	2.11E+13	0.0	49.8
N+O2=>NO+O	6.01E+12	0.0	3473.0
O+O+N2=>O2+N2	3.90E-11	0.0	-1039.0
O+O+N=>O2+N	3.90E-11	0.0	-1039.0
O+NO=>O2+N	2.53E+13	0.0	23200.0
CF3+CF3=>C2F6	4.30E+13	0.0	0.0
F+CF3=>CF4	1.20E+14	-7.7	1183.4
F+CF2=>CF3	5.00E+09	0.0	0.0
F+CF=>CF2	5.00E+14	0.0	0.0
F2+CF2=>CF3+F	2.70E+11	0.0	0.0
F2+CF3=>CF4+F	1.10E+10	0.0	0.0
COF+F=>COF2	1.60E+11	0.0	0.0
F+CO=>COF	2.40E+08	0.0	0.0
C+O2=>CO+O	1.80E+13	0.0	0.0
CF+O=>O+CF	1.20E+13	0.0	0.0
CF3+O=>COF2+F	1.80E+13	0.0	0.0
CF2+O=>COF+F	8.40E+12	0.0	0.0
CF2+O=>CO+F+F	2.40E+11	0.0	0.0
COF+O=>CO2+F	5.60E+13	0.0	0.0
COF+COF=>COF2+CO	6.00E+13	0.0	0.0
COF+CF2=>CF3+CO	1.80E+11	0.0	0.0
COF+CF2=>COF2+CF	1.80E+11	0.0	0.0
COF+CF3=>CF4+CO	6.00E+12	0.0	0.0
COF+CF3=>COF2+CF2	6.00E+12	0.0	0.0
Ion-Molecular Reactions			
F++N2=>N2++F	5.84E+14	0.0	0.0
O++O2=>O2++O	1.20E+13	0.0	0.0
F++O2=>O2++F	4.20E+14	0.0	0.0

APPENDIX B: COMPUTATIONAL CODE FOR CHEMISTRY MODELING IN A TRANSPORT TUBE

```
c  PROGRAM:  SURFCHEM: F, F2, Ar, surface recombination
c  PURPOSE:  user-defined code for surface reaction simulation in Fluent CFD
#include <udf.h>
#define max(a, b)  (((a) > (b)) ? (a) : (b))
#define min(a, b)  (((a) < (b)) ? (a) : (b))
#define BOUND(x,lo,hi) (((x)>(lo)) ? ( ((x)<(hi)) ? (x):(hi)) : (lo))
double GetArray(double dXCoord, int nArrayID);
void SetArray(double dXCoord, int nArrayID, double dValue);
double Rate(double dXCoord, double dVolFr, int ReactionID, int dDerFlag);
void PrintArray();
void Newton();
/*Array for temperature*/
#define MAX_XINDEX 300
#define MAX_XSIZE  0.3
/*Calculation control*/
#define MAX_EPS 1e-13
/*Array with grid points*/
double dXGrid[MAX_XINDEX];
/*Arrays*/
double dGlobalF2_Phys[MAX_XINDEX];
double dGlobalF2_Chem[MAX_XINDEX];
double dGlobalF_Phys[MAX_XINDEX];
double dGlobalF_Chem[MAX_XINDEX];
double dGlobalAr_Phys[MAX_XINDEX];
/*Volume Arrays*/
double dGlobalF_Vol[MAX_XINDEX];
double dGlobalF2_Vol[MAX_XINDEX];
double dGlobalAr_Vol[MAX_XINDEX];
double dDensity;        /* [kg/m3] */
double dTemperature; /* [K]      */
int nDebugMsg = -1;
DEFINE_ADJUST(Newton_On_Adjuct, d)
{
        Newton();
        Message("Newton\n");
}
DEFINE_ON_DEMAND(Print)
{
        Message("\n%s\n",VERSION);
        PrintArray();
}
DEFINE_ON_DEMAND(PrintVersion)
{
        Message("\n%s\n",VERSION);
}
/* Indexes of Species in Fluent sequences
F  - 0
F2 - 1
Ar - 2
```

```
yi[0] - mass fraction of F
yi[1] - mass fraction of F2
yi[2] - mass fraction of Ar  */

/* **********Surface Reactions************** */
DEFINE_SR_RATE(SurfChem,f,fthread,r,mw,yi,rr)
{
            real x[ND_ND];
            F_CENTROID(x,f,fthread);
            SetArray(x[0], 0, yi[0]);
            SetArray(x[0], 1, yi[1]);
            SetArray(x[0], 2, yi[2]);
  dDensity=C_R(F_C0(f,fthread),F_C0_THREAD(f,fthread));
  dTemperature=C_T(F_C0(f,fthread),F_C0_THREAD(f,fthread));
            /*F<->Fs*/
            if (!strcmp(r->name, "reaction-2"))
   {
                        *rr = Rate(x[0], yi[0], 1, 0) + Rate(x[0], yi[0], 2, 0);
                        if (nDebugMsg>0)
                        Message("%s Rate %e\n", r->name, *rr);
                        return;
   }
            /*F2<->F2s*/
            if (!strcmp(r->name, "reaction-3"))
   {
                        *rr = Rate(x[0], yi[1], 3, 0) + Rate(x[0], yi[1], 4, 0);
                        if (nDebugMsg>0)
                        Message("%s Rate %e\n",r->name, *rr);
                        return;
   }
            /*Ar<->Ars*/
            if (!strcmp(r->name, "reaction-4"))
   {
                        *rr = Rate(x[0], yi[2], 5, 0);
                         if (nDebugMsg>0)
                         Message("%s Rate %e\n",r->name, *rr);
                         return;
   }
            *rr = 0;
             return;
}
DEFINE_PROFILE(inlet_uv_parabolic, thread, np)
{
  face_t f;
  real x[ND_ND];
  begin_f_loop (f,thread)
    {
     F_CENTROID(x,f,thread);
 /*function that returns the coordinates of the middle point (x) on the specified face*/
     F_PROFILE(f,thread,np) = 0.4155- 1437.716*x[1]*x[1];
   }
  end_f_loop (f,thread)
}
DEFINE_PROFILE(inlet_new, thread, np)
{
  face_t f;
```

```
  real x[ND_ND];
  begin_f_loop (f,thread)
    {
     F_CENTROID(x,f,thread);
 /*function that returns the coordinates of the middle point (x) on the specified face*/
             F_PROFILE(f,thread,np) = 0.425*(1-SQR(x[1]/0.017));
    }
  end_f_loop (f,thread)
}
  return area;
}
/* SURFACE CHEMISTRY
ReactionID 1,2,3,4,5
when ReactionID  3,4 => dVolFr is for F2
when ReactionID  1,2 => dVolFr is for F
when ReactionID  5   => dVolFr is for Ar  */
double Rate(double dXCoord, double dVolFr, int ReactionID, int dDerFlag/*=0*/)
{
        double P = 266.6; /* Pa   */
        double T = 300;   /* [K]  */
        double S = 1;     /* [m2] */
        double V = 1;     /* [m3] */
        double Nf, Nf2, Nar;
        double sigma,theta;
        theta = GetArray(dXCoord, 1)+
                        GetArray(dXCoord, 2)+
                        GetArray(dXCoord, 3)+
                        GetArray(dXCoord, 4)+
                        GetArray(dXCoord, 5);
        switch (ReactionID)
        {
                /* %F - chemical bonding / y(1) in mole fractions */
        case 1:
                Nf=158*dVolFr*P*4.277e-04;
                sigma=5e+05*T*exp(-9137.68/T);
                if(dDerFlag==1)
                return (0.08*Nf-sigma-0.018*Nf)*S;
                        else
                return (0.08*Nf*(1-theta)-sigma*GetArray(dXCoord, 1)-
                      0.018*Nf*GetArray(dXCoord,1))*S;
                break;
                /* % F - physical bonding / y(2) in mole fractions */
        case 2:
                Nf=158*dVolFr*P*4.277e-04;
                sigma=5e+05*T*exp(-1000/T);
                if(dDerFlag==1)
                        return (0.27*Nf-sigma-0.018*Nf)*S;
                else
                        return (0.27*Nf*(1-theta)-sigma*GetArray(dXCoord, 2)-
                    0.018*Nf*GetArray(dXCoord,2))*S;
                break;
                /* % F2 - chemical bonding / y(3) in mole fractions */
        case 3:
                Nf2=111.75*dVolFr*P*4.277e-04;
                sigma=5e+05*T*exp(-8804.35/T);
                if(dDerFlag==1)
```

```
                        return (0.08*Nf2-sigma)*S;
                else
                        return (0.08*Nf2*(1-theta)-sigma*GetArray(dXCoord,3))*S;
                break;
                /* % F2 - physical bonding / y(4) in mole fractions */
        case 4:
                Nf2=111.75*dVolFr*P*4.277e-04;
                sigma=5e+05*T*exp(-962.32/T);
                if(dDerFlag)
                        return  (0.1*Nf2-sigma)*S;
                else
                        return  (0.1*Nf2*(1-theta)-sigma*GetArray(dXCoord,4))*S;
                break;
                /* % Ar - physical bonding / y(5) in mole fractions */
        case 5:
                Nar=110*dVolFr*P*4.277e-04;
                sigma=5e+05*T*exp(-1049.27/T);
                if(dDerFlag)
                        return (0.08*Nar-sigma)*S;
                else
                        return (0.08*Nar*(1-theta)-sigma*GetArray(dXCoord,5))*S;
                break;
                       default:
                return 0;
                break;
                }
}
void Newton()
{
        double dRelax = 0.01;
        double dXCoord;
        double dR;
        double dN;
        int i;
        for (i=0; i<MAX_XINDEX; i++)
        {
                dXCoord = (i+0.5)*MAX_XSIZE/MAX_XINDEX;
                /*F chem*/
                dR      = Rate(dXCoord, dGlobalF_Vol[i], 1, 1);
                if (fabs(dR)>MAX_EPS)
        dGlobalF_Chem[i] -=dRelax*Rate(dXCoord, dGlobalF_Vol[i], 1, 0)/dR;
        dGlobalF_Chem[i] = BOUND(dGlobalF_Chem[i], 0, 1);
                /*F phys*/
                dR      = Rate(dXCoord, dGlobalF_Vol[i], 2, 1);
                if (dR>MAX_EPS)
        dGlobalF_Phys[i] -= dRelax*Rate(dXCoord, dGlobalF_Vol[i], 2, 0)/dR;
        dGlobalF_Phys[i] = BOUND(dGlobalF_Phys[i], 0, 1);
                /*F2 chem*/
                dR      = Rate(dXCoord, dGlobalF2_Vol[i], 3, 1);
                if (fabs(dR)>MAX_EPS)
        dGlobalF2_Chem[i] -=dRelax*Rate(dXCoord, dGlobalF2_Vol[i], 3, 0)/dR;
      dGlobalF2_Chem[i] = BOUND(dGlobalF2_Chem[i], 0, 1);
                /*F2 Phys*/
                dR      = Rate(dXCoord, dGlobalF2_Vol[i], 4, 1);
                if (fabs(dR)>MAX_EPS)
        dGlobalF2_Phys[i] -=dRelax*Rate(dXCoord, dGlobalF2_Vol[i], 4, 0)/dR;
```

```
          dGlobalF2_Phys[i] = BOUND(dGlobalF2_Phys[i], 0, 1);
                    /*Ar Phys*/
                    dR      = Rate(dXCoord, dGlobalAr_Vol[i], 5, 1);
                    if (fabs(dR)>MAX_EPS)
            dGlobalAr_Phys[i] -=dRelax*Rate(dXCoord, dGlobalAr_Vol[i], 5, 0)/dR;
            dGlobalAr_Phys[i] = BOUND(dGlobalAr_Phys[i], 0, 1);
            }
}
void PrintArray()
{
            int i;
            Message("\n");
            Message("F  Chem:");
            for (i=0; i<MAX_XINDEX; i++)
                    Message("%5e  ", dGlobalF_Chem[i]);
            Message("\n");
            Message("F  Phys:");
            for (i=0; i<MAX_XINDEX; i++)
                    Message("%5e  ", dGlobalF_Phys[i]);
            Message("\n");
            Message("F2 Chem:");
            for (i=0; i<MAX_XINDEX; i++)
                    Message("%5e  ", dGlobalF2_Chem[i]);
            Message("\n");
            Message("F2 Phys:");
            for (i=0; i<MAX_XINDEX; i++)
                    Message("%5e  ", dGlobalF2_Phys[i]);
            Message("\n");
            Message("Ar Phys:");
            for (i=0; i<MAX_XINDEX; i++)
                    Message("%5e  ", dGlobalAr_Phys[i]);
            Message("\n");
}
double GetArray(double dXCoord, int nArrayID)
{
            int i =  dXCoord*MAX_XINDEX/MAX_XSIZE;

            if (i<0 || i>=MAX_XINDEX)
                    return 0;
            switch(nArrayID)
            {
                    case 1: return dGlobalF_Chem[i]; break;
                    case 2: return dGlobalF_Phys[i]; break;
                    case 3: return dGlobalF2_Chem[i]; break;
                    case 4: return dGlobalF2_Phys[i]; break;
                    case 5: return dGlobalAr_Phys[i]; break;
                    default: return 0; break;
            }
}
void SetArray(double dXCoord, int nArrayID, double dValue)
{
            int i =  dXCoord*MAX_XINDEX/MAX_XSIZE;
            if (i<0 || i>=MAX_XINDEX)
                    return;
            switch(nArrayID)
            {
```

```
                case 1: dGlobalF_Vol[i]  = dValue; break;
                case 2: dGlobalF2_Vol[i] = dValue; break;
                case 3: dGlobalAr_Vol[i] = dValue; break;
                default: return; break;
        }
}
```

APPENDIX C: COMPUTATIONAL CODE FOR HDP-CVD MODELING

```
c  PROGRAM:  Plasma Mode
c  PURPOSE:    user-defined code for plasma-chemistry simulation in Fluent CFD

#include <udf.h>
DEFINE_VR_RATE(vol_reac_rate, c, t, r, wk, yk, rate, rr)
{
  real ci, prod;
  int i;
  static int nFlag = 0;
  if (nFlag <10)
  {
            Message("%s - reactants %d\n", r->name, r->n_reactants);
            nFlag++;
  }
/* Calculation of Arrhenius reaction rate */
  prod = 1.;
  for (i = 0; i < r->n_reactants; i++)
    {
             // C_R(c,t)-density
             // C_T(c,t)-temperature
      ci     = C_R(c,t) * yk[r->reactant[i]] / wk[r->reactant[i]];
      prod  *= pow(ci, r->exp_reactant[i]);
    }
  *rate = r->A * exp( - r->E / (UNIVERSAL_GAS_CONSTANT * C_T(c,t))) *
                              pow(C_T(c,t), r->b) * prod;
  *rr = *rate;
            if ( THREAD_ID(t)!=5 )
            {
                      if(!strcmp(r->name, "reaction-1"))
                      {
                                *rate = 0;  *rr = 0;
                      }
            }
            if ( THREAD_ID(t)==5 )
            {
                      if(!strcmp(r->name, "reaction-3"))
                      {
                                *rate = 0;  *rr = 0;
                      }
            }
            if ( THREAD_ID(t)==26 && THREAD_ID(t)==31 )
            {
                      if(!strcmp(r->name, "reaction-2"))
                      {
                                *rate = 0;  *rr = 0;
                      }
            }
            // User_Defined Memory
            if(!strcmp(r->name, "reaction-1"))
            {
```

```
			C_UDMI(c, t, 0) = *rate;
		}
		if(!strcmp(r->name, "reaction-2"))
		{
			C_UDMI(c, t, 1) = *rate;
		}
		if(!strcmp(r->name, "reaction-3"))
		{
			C_UDMI(c, t, 2) = *rate;
		}
	}
```

VITA

Kamilla Iskenderova was born on March 28, 1977 in Kiev, Ukraine. She received her B.S. degree in Applied Physics and Mathematics from Moscow Institute of Physics and Technology, Moscow, Russia in 1999. In the summer of 2000 she graduated from University of Rochester, Rochester, NY with M.S. degree in Mechanical Engineering. At the same time she joined plasma group at the University of Illinois at Chicago led by Professor Alexander Fridman. In August 2002 she moved with the entire group to Drexel University where she continued to work on her doctoral program. Kamilla's research interests mainly include low temperature plasma physics, chemistry and plasma processing, chemical kinetics, reacting flows, surface chemistry, etching and cleaning in chemical vapor deposition reactors.